

JADES: Evolution of nitrogen abundances in star-forming galaxies from $z \sim 1.5 - 7$

Alex J. Cameron,^{1,2,3*} Courtney Carreira,⁴ Charlotte Simmonds,⁵ Andrew J. Bunker,³ Aayush Saxena,^{3,6} Stefano Carniani,⁷ Stéphane Charlot,⁸ Jacopo Chevallard,³ Emma Curtis-Lake,⁹ Kevin Hainline,¹⁰ Ryan Hausen,¹¹ Xihan Ji,^{12,13} Zhiyuan Ji,¹⁰ Benjamin D. Johnson,¹⁴ Pierluigi Rinaldi,¹⁵ Brant Robertson,⁴ Jan Scholtz,^{12,13} Maddie S. Silcock,⁹ Sandro Tacchella,^{12,13} James A. A. Trussler,¹⁴ Hannah Übler,¹⁶ Christina C. Williams,¹⁷ Christopher N. A. Willmer,¹⁰ Chris Willott,¹⁸ Joris Witstok,^{1,2}

¹Cosmic Dawn Center (DAWN), Copenhagen, Denmark

²Niels Bohr Institute, University of Copenhagen, Jagtvej 128, DK-2200, Copenhagen, Denmark

³Department of Physics, University of Oxford, Denys Wilkinson Building, Keble Road, Oxford, OX1 3RH, UK

⁴Department of Astronomy and Astrophysics University of California, Santa Cruz, 1156 High Street, Santa Cruz CA 95054, USA

⁵Departamento de Astronomía, Universidad de Chile, Camino El Observatorio 1515, Las Condes, Santiago, Chile

⁶Department of Physics and Astronomy, University College London, Gower Street, London WC1E 6BT, UK

⁷Scuola Normale Superiore, Piazza dei Cavalieri 7, I-56126 Pisa, Italy

⁸Sorbonne Université, CNRS, UMR 7095, Institut d’Astrophysique de Paris, 98 bis bd Arago, 75014 Paris, France

⁹Centre for Astrophysics Research, Department of Physics, Astronomy and Mathematics, University of Hertfordshire, Hatfield AL10 9AB, UK

¹⁰Steward Observatory, University of Arizona, 933 N. Cherry Avenue, Tucson, AZ 85721, USA

¹¹Department of Physics and Astronomy, The Johns Hopkins University, 3400 N. Charles St., Baltimore, MD 21218

¹²Kavli Institute for Cosmology, University of Cambridge, Madingley Road, Cambridge, CB3 OHA, UK

¹³Cavendish Laboratory - Astrophysics Group, University of Cambridge, 19 JJ Thomson Avenue, Cambridge, CB3 OHE, UK

¹⁴Center for Astrophysics | Harvard & Smithsonian, 60 Garden St., Cambridge MA 02138 USA

¹⁵Space Telescope Science Institute, 3700 San Martin Drive, Baltimore, Maryland 21218, USA

¹⁶Max-Planck-Institut für extraterrestrische Physik (MPE), Gießenbachstraße 1, 85748 Garching, Germany

¹⁷NSF National Optical-Infrared Astronomy Research Laboratory, 950 North Cherry Avenue, Tucson, AZ 85719, USA

¹⁸NRC Herzberg, 5071 West Saanich Rd, Victoria, BC V9E 2E7, Canada

Accepted XXX. Received YYY; in original form ZZZ

ABSTRACT

We present nitrogen abundance measurements based on the low-ionisation [N II] $\lambda 6583$ emission line for 588 galaxies between $1.5 < z < 7.0$ from the JWST Advanced Deep Extragalactic Survey (JADES). We detect the temperature-sensitive [O III] $\lambda 4363$ auroral line in 40 galaxies in our sample, affording T_e -based abundances for this subset. We find that the average N/O abundance ratio in our low-metallicity sample is at least 0.1 dex higher than $z \sim 0$ samples. In particular, we find significant scatter toward high N/O, with five galaxies being identified with enhanced nitrogen abundances ($\log(\text{N/O}) > -1.1$) at low-metallicity ($12 + \log(\text{O/H}) < 8.0$) from T_e -based measurements. Meanwhile, applying strong-line abundance measurements to the remainder of our sample reveals a further 14 candidate galaxies passing these abundance cuts, implying that around 13 % of $12 + \log(\text{O/H}) < 8.0$ galaxies at these redshifts are nitrogen-enhanced at this level. We find that N/O abundance in low-metallicity systems correlates with SFR, Σ_{SFR} , and Σ_{M_*} at high redshift, while only in high-metallicity systems does a correlation with M_* emerge. Despite healthy representation of these ‘moderately nitrogen-enhanced’ galaxies ($-1.1 < \log(\text{N/O}) \leq -0.6$), no galaxies in our low-metallicity sample are identified as having $\log(\text{N/O}) > -0.6$, abundances that are typical of high-redshift N III]- and N IV]-emitters. This demonstrates that the extreme nitrogen enhancements seen in some N III]- and N IV]-emitters are only attained during the most extreme starbursts. This suggests that these elevated abundances are caused by enrichment from young massive stars in extreme environments and that the impact of this enrichment pathway is milder, though still important, for high-redshift systems on the star-forming main sequence.

Key words: galaxies: abundances – galaxies: evolution – galaxies: high-redshift – galaxies: ISM – ISM: abundances

1 INTRODUCTION

Chemical abundances within the interstellar medium (ISM) of galaxies depend on many processes, including nucleosynthesis, gas mix-

ing, outflows, depletion and dilution (e.g., [Matteucci 2012](#); [Maiolino & Mannucci 2019](#)). In particular, since different sources of nucleosynthesis operate over different timescales with different chemical yields, ratios of abundances of different metals are a powerful constraint on star formation histories and the properties of current and

* E-mail: alex.cameron@nbi.ku.dk

previous generations of stellar populations (Izotov & Thuan 1999; Berg et al. 2019; Kobayashi et al. 2020; Kobayashi & Taylor 2023).

Core-collapse supernovae (CCSNe), arising from stars with initial masses $\sim 8 - 25 M_{\odot}$, are an important chemical enrichment mechanism, producing large quantities of α -elements on relatively short timescales after the onset of star formation (e.g. Nomoto et al. 2013). Indeed, oxygen, the Universe's most abundant metal, is primarily synthesised via this channel (Kobayashi & Taylor 2023).

Nitrogen is an interesting element since, as an odd-numbered element, it is only produced in modest amounts by CCSNe (Nomoto et al. 2013; Limongi & Chieffi 2018). Among $z \sim 0$ galaxies, the nitrogen-to-oxygen abundance ratio (N/O) has been shown to have no correlation with gas-phase oxygen abundance (O/H) at low oxygen abundances ($12 + \log(O/H) \lesssim 8.0$; Izotov & Thuan 1999; Pérez-Montero & Contini 2009; Berg et al. 2019; Arellano-Córdova et al. 2025a; Scholte et al. 2026), but rises steeply with higher oxygen abundances (Vila-Costas & Edmunds 1993; Pilyugin et al. 2012; Berg et al. 2020), greatly exceeding the N/O ratio from pure CCSNe yields. At high-metallicity, this is typically attributed to secondary enrichment during the asymptotic giant branch (AGB) phase of intermediate mass ($\sim 4 - 7 M_{\odot}$) stars (Kobayashi et al. 2011; Romano 2022), which occurs on timescales of > 100 Myr (Vincenzo & Kobayashi 2018). Meanwhile the level of (and scatter about) the plateau at low oxygen abundance is thought to comprise contributions from both CCSNe yields and pre-supernovae winds of massive stars (e.g. López-Sánchez & Esteban 2010; Roy et al. 2021).

Prior to *JWST*, ground-based studies exploring the N/O – O/H relation out to $z \sim 2$ were largely limited to relatively metal-enriched galaxies, finding no significant evolution in this relation (Strom et al. 2018; Hayden-Pawson et al. 2022). However, *JWST*/NIRSpec spectroscopy of low metallicity galaxies at higher redshifts has begun to change this picture.

In Cameron et al. (2023a), it was shown that the strong rest-frame ultraviolet N III] $\lambda\lambda 1750$ and N IV] $\lambda\lambda 1483, 1486$ emission lines in the spectrum of the $z = 10.6$ galaxy GN-z11 (Bunker et al. 2023b) implied that the N/O abundance was at least a factor of ~ 4 higher than the solar N/O, despite the sub-solar O/H abundance. Independent studies have since confirmed this super-solar N/O measurement (e.g., Senchyna et al. 2023; Martinez et al. 2025). Subsequent studies have identified many more of these highly nitrogen enhanced systems feature strong N III] and/or N IV] emission implying highly enhanced N/O at low O/H (Isobe et al. 2023; Marques-Chaves et al. 2023; Castellano et al. 2024; Ji et al. 2024, 2026; Topping et al. 2024; Schaefer et al. 2024; Berg et al. 2025; Naidu et al. 2025; Napolitano et al. 2025; Morel et al. 2025). In addition to high-ionisation emission lines with high-equivalent widths, these systems are typically observed to be compact, with high electron densities ($n_e \gtrsim 10^5 \text{ cm}^{-3}$; Senchyna et al. 2023; Maiolino et al. 2024; Topping et al. 2025) and high star-formation rates (SFR; Marques-Chaves et al. 2023; Schaefer et al. 2024) commonly inferred. The strong deviation of these systems from what is observed in $z \sim 0$ samples suggests differences either in the enrichment mechanisms or the metal-mixing in these systems.

Many studies have subsequently explored models that can reconcile such high nitrogen abundances at low O/H. On the one hand, enrichment from winds of Wolf-Rayet stars (Kobayashi & Ferrara 2024; Bekki & Tsujimoto 2023; Watanabe et al. 2024; Berg et al. 2025) and very massive stars ($100 - 500 M_{\odot}$; Vink 2023; Higgins et al. 2025) have been invoked as viable sources of strong nitrogen enrichment, as have as yet unobserved supermassive stars ($\geq 1000 M_{\odot}$) formed in dense environments (Cameron et al. 2023a; Charbonnel et al. 2023; Nagele & Umeda 2023; Ji et al. 2024; Nandal et al. 2025).

On the other hand, other studies have shown that galactic winds with strong oxygen-loading (Rizzuti et al. 2025) or the formation of stars from pre-processed nitrogen-rich molecular gas (McClymont et al. 2025) can result in the required abundance patterns without invoking a strong contribution from massive star winds.

Although these are clearly interesting systems, at the depths available in most *JWST*/NIRSpec $z \gtrsim 3$ spectroscopic programs, nitrogen abundances measured from these N III] and N IV] features can rarely be obtained for systems with sub-solar N/O (Zhu et al. 2025; Martinez et al. 2025). As a result, measurements of the full distribution of nitrogen abundances across the high-redshift population are limited. Conversely, nitrogen abundances measured from the optical [N II] $\lambda 6583 / [\text{O II}] \lambda\lambda 3726, 3729$ ratio are sensitive down to low N/O ratios in systems on the star-forming main sequence, and are a mainstay of previously mentioned $z \sim 0$ studies. Despite this, relatively few [N II]-based abundance studies have been performed at high-redshift (Arellano-Córdova et al. 2025b; Stiavelli et al. 2025; Zhang et al. 2025; Cataldi et al. 2025a; Schaefer et al. 2026), with no consensus yet on the behaviour of N/O at low O/H in galaxies more representative of the star-forming main sequence.

In this work, we perform a systematic survey of nitrogen abundances based on this low-ionisation [N II] line using data from the *JWST* Advanced Deep Extragalactic Survey (JADES; Eisenstein et al. 2023a). This allows us to be sensitive to much lower N/O abundances ($\log(\text{N/O}) \lesssim -1.6$), across galaxies with a more diverse range of ionisation conditions. The paper is structured as follows: the data sets and analysis techniques used are outlined in Section 2. Section 3 then describes our chemical abundances measurements and associated uncertainties. We present the key results in Section 4 before presenting a discussion of the implications of these in Section 5. We provide a summary of the work in Section 6.

2 DATA & METHODS

2.1 Observations & sample assembly

We draw our sample from the spectroscopic component of the *JWST* Advanced Deep Extragalactic Survey (JADES; Eisenstein et al. 2023a). A detailed description of the planning and execution of JADES spectroscopic observations can be found in the JADES NIRSpec data release papers (Bunker et al. 2023a; D'Eugenio et al. 2025; Curtis-Lake et al. 2025; Scholtz et al. 2025a), however, here we briefly review the main aspects as relevant to this work.

The JADES spectroscopic sample was compiled from over 30 different pointings observed with the NIRSpec/MOS mode (Jakobsen et al. 2022; Ferruit et al. 2022) across the GOODS-South and GOODS-North legacy fields. All pointings are observed in the low-resolution Prism/CLEAR mode and all three medium resolution ($R \sim 1000$) gratings: G140M/F070LP, G235M/F170LP, and G395M/F290LP, which have observed wavelength ranges of $0.70 - 2.20 \mu\text{m}$, $1.66 - 4.00 \mu\text{m}$, and $2.87 - 5.48 \mu\text{m}$, respectively.

Since this work hinges on measurements of the [N II] $\lambda 6583$ emission line, which is significantly blended with H α at Prism resolution, our analysis focuses on the $R \sim 1000$ spectroscopy. We note that during target assignment, low-priority targets are removed from grating observations if their spectra overlap with protected higher priority targets, meaning around 8 % of the full JADES sample is only observed with Prism.

JADES observations were split into two main tiers: ‘deep’ and

'medium'¹, with the former obtaining deeper observations for a smaller sample. In practice, the difference in depth between the two primarily relates to Prism observations, since for 'deep', the Prism integrations were four times longer than the grating integrations, while for 'medium' these were approximately equal. In fact, because individual targets in the medium tiers could be observed in multiple overlapping pointings, there is no great difference in depth between these tiers in the $R \sim 1000$ spectroscopy relevant to this study. All targets in our sample are observed with at least $t_{\text{exp}} = 0.57$ h per grating, but the median depth is $t_{\text{exp}} = 2.3$ h, and the deepest spectra in our sample reach $t_{\text{exp}} = 6.9$ h.

The two main sub-samples within JADES target prioritisation scheme were: (1) m_{UV} -selected galaxies at $z > 5.7$ and (2) m_{F444W} -selected galaxies at $1.5 < z \leq 5.7$ (approximating a stellar mass based selection). Given the wavelength coverage of the NIRSpec $R \sim 1000$ gratings does not extend much past $5 \mu\text{m}$, our $[\text{N II}]$ -based study is limited to galaxies at $z < 7$. We further impose a lower bound of $z > 1.5$ for this analysis to align with the cutoff for the JADES m_{F444W} -based selection.

Figure 1 shows the distribution of m_{F444W} as a function of redshift for the JADES spectroscopic sample. The parent sample, shown in grey, includes filler targets not selected within our main target allocation scheme, but which were added at a lower priority. The m_{F444W} cuts employed for the main sample are shown by the black dotted lines – the fainter $m_{\text{F444W}} < 27.5$ cut corresponds to the 'deep' tiers, while $m_{\text{F444W}} < 27.0$ was employed for the 'medium' tiers which dominate the number counts here. In the end, many of our filler targets returned robust redshifts (green points).

We take our initial sample as anything with a confirmed spectroscopic redshift $1.5 < z_{\text{spec}} < 7.0$ for which we have coverage of each of $[\text{O II}] \lambda\lambda 3727, \text{H}\beta, [\text{O III}] \lambda 5007, \text{H}\alpha$, and $[\text{N II}] \lambda 6583$, meaning that some objects are discarded from our sample due to one or more of these lines falling within the detector chip gap.

A brief note on JADES target nomenclature: given that our sample spans multiple JADES tiers, and ID numbers can be duplicated across tiers, we identify individual galaxies by listing both their tier and ID number. The tier name has three components: [field]-[depth][hst/jwst], which, respectively, indicate (1) whether the pointing is in GOODS-S or GOODS-N, (2) whether the pointing was observed at 'medium' or 'deep' depth, and (3) whether the target selection was performed from catalogues based on primarily *HST*- or *JWST*-based imaging (see [Curtis-Lake et al. 2025](#) for details). Throughout this paper we interchangeably refer to tier names in their full form, or in shorthand, where the field name is shortened to 'gs' or 'gn' and single character designations are used for depth ('m' or 'd') and selection ('h' or 'j'). For example, goods-s-mediumjwst is used interchangeably with 'gsmj'.

Throughout this paper we use 1D and 2D spectra reduced by the JADES pipeline, as described in [Scholtz et al. \(2025a\)](#). All our JADES observations employ a 3-point nodding scheme, and our default approach is to perform local background subtraction using this 3-point scheme. Many of the targets in this paper are spatially extended, and thus we default to using 1D extractions from the full shutter open area.

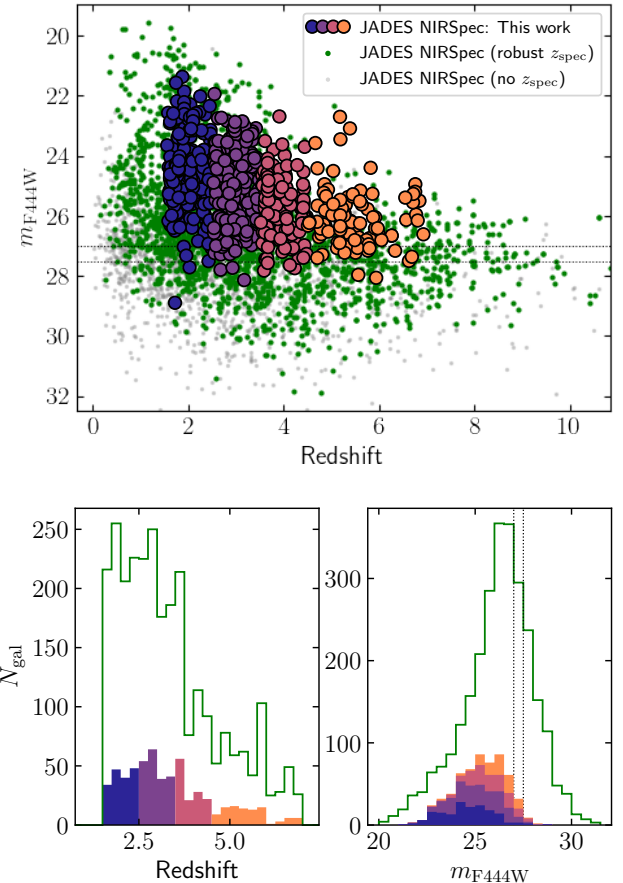


Figure 1. *Upper panel:* m_{F444W} vs. redshift for JADES NIRSpec galaxies entering into this sample. Large circles show the galaxies making it into our final sample (see Section 2) with colours denoting redshift. Green points show the distribution of all JADES galaxies with robust spectroscopic redshifts, while grey points show the portion of the JADES sample for which no reliable redshift was obtained (with the point location given by the photometric redshift). *Lower left:* Redshift distribution of final sample (colours) vs. all JADES galaxies with a robust spectroscopic redshift and $1.5 < z \leq 7$. *Lower right:* As for lower left, except showing the m_{F444W} distribution. Black dashed lines at $m_{\text{F444W}} = 27.0$ and 27.5 show the magnitude cuts for the m_{F444W} -limited portion of the JADES NIRSpec selection for Medium/JWST and Deep/JWST respectively (see [Curtis-Lake et al. 2025](#) for details).

2.2 Emission line fitting

The continuum is generally at least marginally detected in the $R \sim 1000$ spectra. To fit the continuum, we begin by masking out any spectral regions with prominent emission lines. We then drew 1000 perturbed spectra where each spectral pixel was adjusted randomly from a normal distribution centered on the measured flux with a standard deviation of the $1-\sigma$ uncertainty output by the pipeline. To each realisation, we fit the continuum with a univariate spline. Our best-fit continuum was taken by combining the median at each spectral pixel across all 1000 fits, while we adopt the standard deviation at each spectral pixel as the uncertainty on the continuum fit. We visually confirm that this results in a reasonable fit and then subtract this continuum from the 1D spectrum before performing emission line fits.

We model the emission lines with single-component Gaussian profiles. The $\text{H}\alpha + [\text{N II}] \lambda\lambda 6548, 6583 + [\text{S II}] \lambda\lambda 6716, 6731$ complex

¹ JADES also included an 'ultradeep' tier, but we exclude that from this study as it did not observe in the G235M/F170LP grating.

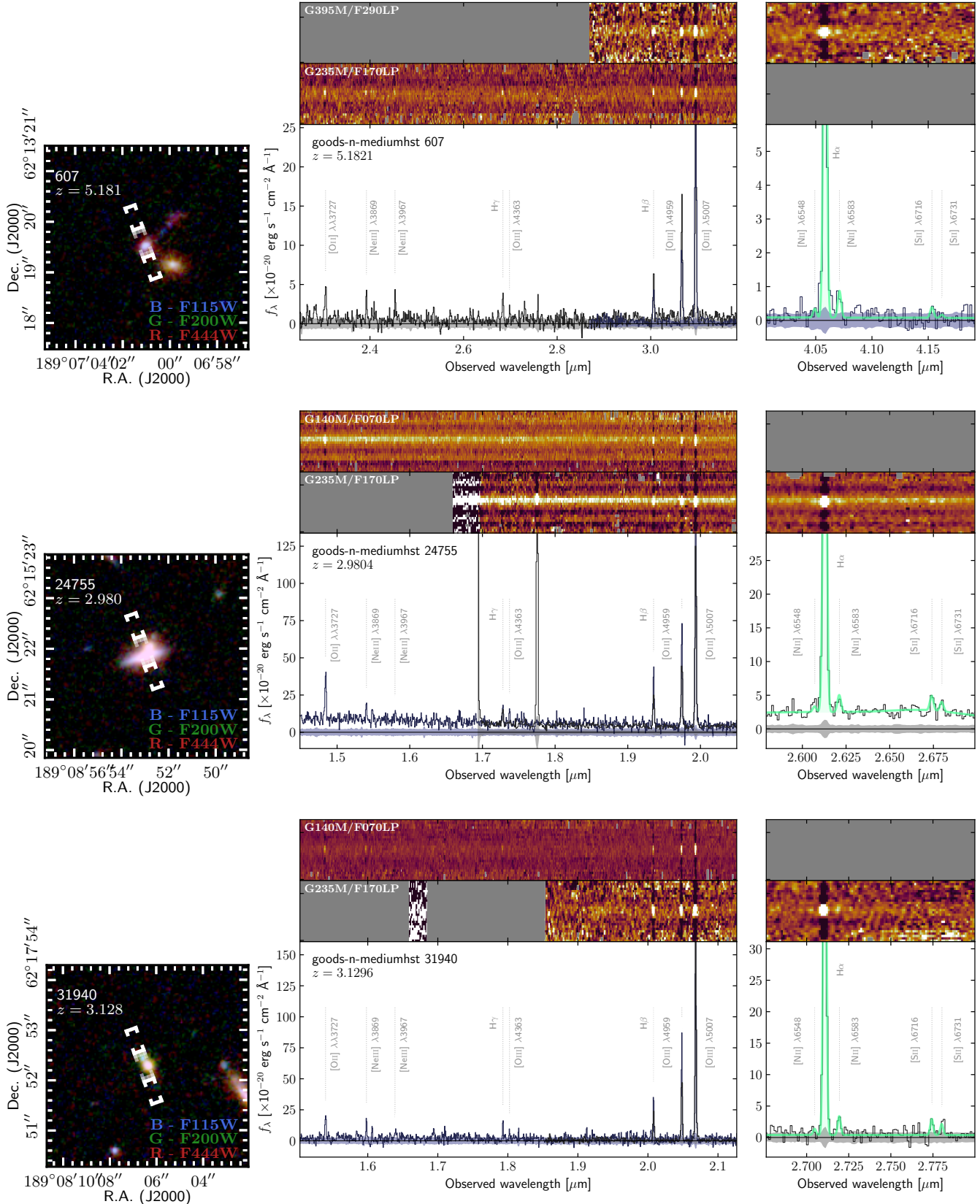


Figure 2. Example spectra of three galaxies in the T_e -based sample. *Left:* RGB thumbnail showing the location of the three-shutter slitlet. *Middle:* Section of the NIRSpec spectrum in which key rest-frame optical emission lines from [O II] $\lambda\lambda 3726, 3729$ to [O III] $\lambda 5007$ are observed. *Right:* Section of the NIRSpec spectrum surrounding H α , [N II] $\lambda 6583$, and [S II] $\lambda\lambda 6716, 6731$. Our best-fit model to this complex is shown in green. There is generally overlapping wavelength coverage between different gratings. Across both plot regions, the top panel shows the 2D spectrum from either G140M/F070LP or G395M/F290LP (see label), while the second panel shows the 2D spectrum from G235M/F170LP. In the 1D spectrum, G235M/F170LP is in black and other gratings are in blue. MNRAS **000**, 1–41 (2026)

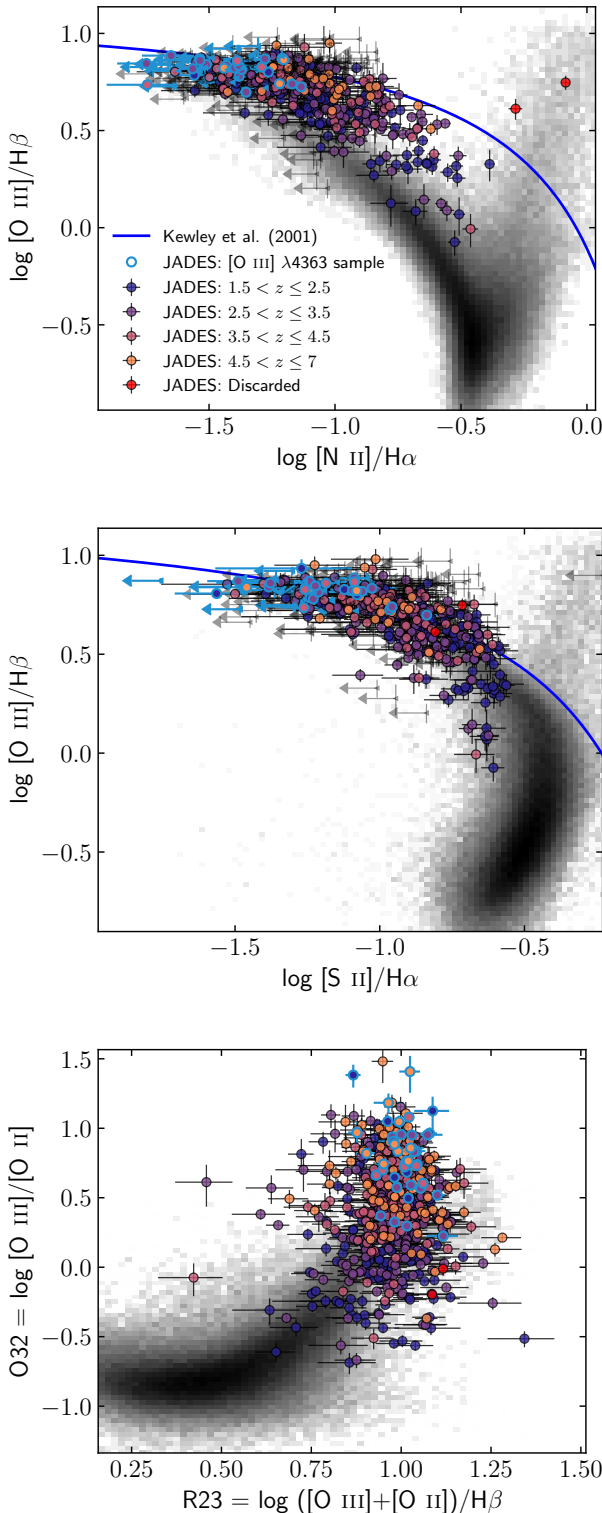


Figure 3. Diagnostic diagrams showing the location of galaxies in our sample in emission line ratio space compared to $z \sim 0$ galaxies from SDSS (Aihara et al. 2011, grey 2D histogram). Red points show the galaxies that we discard from our sample due to significant AGN contamination, while the other colours indicate the approximate redshift of each source. The Kewley et al. (2001) AGN-SF demarcation line is shown in blue.

was fit simultaneously, with the line widths and redshift being tied. The flux ratio of $[\text{N II}]\lambda 6583/\lambda 6548$ was fixed to 3.0, but the total flux of this $[\text{N II}]$ doublet was allowed to vary freely, as were the fluxes of $\text{H}\alpha$ and each of the two $[\text{S II}]$ lines. Examples of our $\text{H}\alpha + [\text{N II}] + [\text{S II}]$ fitting are shown in the right panels of Figure 2. Note that, throughout this paper, mentions of ‘ $[\text{N II}]$ flux’ refer to the flux of only the $[\text{N II}]\lambda 6583$ component, not the combined doublet. All other emission lines were fit individually with the line width and redshift allowed to vary within a small buffer range. The fitted lines relevant for this study include $[\text{O II}]\lambda\lambda 3727$, $[\text{Ne III}]\lambda\lambda 3869$, $\text{H}\gamma$, $[\text{O III}]\lambda 4363$, $\text{H}\beta$, $[\text{O III}]\lambda 4959$, $[\text{O III}]\lambda 5007$, in addition to the $\text{H}\alpha + [\text{N II}] + [\text{S II}]$ complex.²

We adopt the integrated flux of the best-fit profile as the line flux and the formal uncertainty from the fit as the uncertainty. If this results in a signal-to-noise ratio of $S/N < 3$ then we consider the line undetected and adopt a 3σ upper limit by integrating the variance spectrum across five spectral pixels centered on the expected line centroid.

We correct the emission lines ratios for dust reddening using the measured $\text{H}\alpha/\text{H}\beta$ ratios, assuming an intrinsic ratio of 2.79 (assuming case B recombination with $T_e = 15,000$ K and $n_e = 100 \text{ cm}^{-3}$; calculated with PYNEB Luridiana et al. 2015) and adopting the SMC dust law from (Gordon et al. 2003). Throughout the rest of this paper we work with these dust-corrected emission line values.

While the vast majority of this paper focuses on these fits to the medium resolution spectra, we do consider the low-resolution prism spectra for the purpose of measuring the equivalent width of $\text{H}\alpha$ since the improved continuum sensitivity makes for a more reliable measurement of this quantity. The prism continuum was fit in the same way as described above for the medium-resolution spectra. Given the lower resolution, the $\text{H}\alpha + [\text{N II}]$ complex is blended, and we simply fit this with a single Gaussian component. For galaxies in which we detect $[\text{N II}]\lambda 6583$ in the medium resolution spectrum, we use the $[\text{N II}]/\text{H}\alpha$ ratio to account for the $[\text{N II}]$ contribution to this component when calculating the $\text{H}\alpha$ equivalent width, while for galaxies without a detection of $[\text{N II}]$, we simply adopt the combined flux of this component as the $\text{H}\alpha$ flux, noting that the upper limits on $[\text{N II}]$ generally imply a maximum contribution of less than 5–10% (see top panel of Figure 3). The resulting equivalent width values are only used in Section 4.3.

2.3 Final sample

From our sample of JADES galaxies with emission line fits, we applied a signal-to-noise cut on $\text{H}\beta$ of $S/N_{\text{H}\beta} > 5$.

We use the BPT diagram (Figure 3, top panel) to discard galaxies which are clearly contaminated with significant emission powered by an active galactic nucleus (AGN). We note that it has been widely reported that AGN-SF demarcation lines – such as the Kewley et al. (2001) line shown in blue – may not be reliable for separating these populations at high-redshift (e.g. Scholtz et al. 2025b). In short, this is partly because the harder ionising fields of lower metallicity stellar populations at $z \gtrsim 2$ drive an offset from the $z \sim 0$ BPT sequence (e.g. Kewley et al. 2013; Steidel et al. 2014) – an effect which is

² We note that the redshift range of our sample limits our ability to observe the $\text{N III}\lambda\lambda 1750$ complex and the $\text{N IV}\lambda\lambda 1483, 1486$ doublet. These are unobservable for most of our sample and even where they are covered by the G140M/F070LP grating, the relatively shallow observations in that grating mean that these are not viably detected unless nitrogen abundances are extremely enhanced.

clearly seen for the locus of our sample in Figure 3, relative to $z \sim 0$ galaxies from SDSS (Aihara et al. 2011). This effect is compounded by the fact that, at low-metallicity, AGN tend to shift toward lower values of $[\text{N II}]/\text{H}\alpha$ (e.g. Groves et al. 2006), an effect which has been observed in high-redshift AGN observed with *JWST* (Übler et al. 2023). Given that our abundance analysis relies heavily on the $[\text{N II}]\lambda 6583$ line, we do not discard galaxies with $\log [\text{N II}]/\text{H}\alpha < -0.5$, even if they exceed the Kewley et al. (2001) demarcation, so as not to bias ourselves against selecting galaxies with enhanced nitrogen abundances. In the end, we discard only two galaxies as being clearly AGN-contaminated based on the BPT diagram which both were above this demarcation line and had $N2 > -0.5$ (shown as red points in Figure 3).

In the S2-VO7 diagram (middle panel) and R23-O32 diagram (bottom panel), we find that our sample largely follows the extension of the $z \sim 0$ star-forming sequence, consistent with other high-redshift samples reported from *JWST* observations (e.g. Cameron et al. 2023b; Cataldi et al. 2025a).

We also discard any objects with broad emission lines. This is partly in order to remove broad-line AGN from our sample (e.g., Maiolino et al. 2023). However, even for objects where the broad component also appears in the forbidden lines (i.e. galaxies with strong outflows; Carniani et al. 2024), we remove these from our sample since a significant broad component can confuse the fitting of $[\text{N II}]$ and $\text{H}\alpha$.

Applying these extra sample selection constraints, we arrive at a final sample of 588 galaxies, of which 40 have $[\text{O III}]\lambda 4363$ detections. In the next sections, we outline our SED and morphological fitting, which are based on NIRCam imaging. Only 484 (including 31 with $[\text{O III}]\lambda 4363$) of these 588 galaxies have robust galaxy properties measured from SED and morphological fitting, limiting some of our analyses to this subset. The coloured points and histograms in Figure 1 show the redshift and magnitude distributions of our final sample compared to the distributions of all JADES galaxies with $1.5 < z_{\text{spec}} < 7.0$. The redshift distribution of our final sample approximately mimics that of the parent sample. In the bottom right panel of Figure 1, we see that the number counts in our final sample level off at $m_{\text{F444W}} \approx 25.5$, around a magnitude brighter than in the parent sample. However, we do retain some objects even fainter than the $m_{\text{F444W}} = 27$ and 27.5 survey cuts.

2.4 SED fitting

To derive basic galaxy properties, we perform SED fitting to *JWST*/NIRCam photometry with PROSPECTOR (Johnson et al. 2019, 2021) following the procedure outlined in Simmonds et al. (2024). We use photometric fluxes from the JADES (Eisenstein et al. 2023a; Rieke et al. 2023) catalog.

For any given galaxy, we fit using all available photometric bands. In the best cases, this amounts to *JWST*/NIRCam photometry in F090W, F115W, F150W, F162M, F182M, F200W, F210M, F250M, F277W, F300M, F335M, F356W, F410M, F430M, F444W, F460M, and F480M as well as photometry from *HST*/ACS (F435W, F606W, F775W, F814W, and F850LP) and *HST*/WFC3 (F105W, F125W, F140W, and F160W). These photometric data are derived from imaging based on numerous programs, including: JADES (Eisenstein et al. 2023a), JEMS (Williams et al. 2023), JOF (Eisenstein et al. 2023b), and FRESCO (Oesch et al. 2023).

Photometry is extracted using a consistent Kron convolved aperture across all bands, and photometric uncertainties are floored at 5% to account for residual systematic errors not captured by the data reduction pipelines or the SED modelling. Redshifts are fixed to

spectroscopic values from NIRSpec. The stellar population modelling follows Tacchella et al. (2022), adopting a Chabrier IMF (Chabrier 2003), stellar metallicities spanning 0.01–1, Z_{\odot} , and a two-component dust attenuation model that accounts for differential attenuation of young (< 10 Myr) stars and nebular emission (Kriek & Conroy 2013). The spectral energy distributions are generated using the FSPS code (Conroy & Gunn 2010), with nebular emission computed via CLOUDY and MIST stellar evolutionary tracks. We adopt a non-parametric star formation history (continuity SFH; Leja et al. 2019), in which the SFH is described by eight time bins whose amplitudes and ratios are allowed to vary following a Student's t -distribution with width 0.3, allowing for bursty behaviour when supported by the data. Intergalactic medium absorption is modelled using a flexible scaling of the Madau (1995) prescription. For further details of the SED-fitting methodology, we refer the reader to Simmonds et al. (2024).

2.5 Morphological fits

We compute sizes and other structural parameters for our sample using *pysersic* (Pasha & Miller 2023), a Bayesian inference framework for fitting surface brightness profiles to galaxies with robust uncertainty estimation made possible by implementing Markov chain Monte Carlo (MCMC) methods. We adopt sizes from the posterior distributions of the structural parameters for single-component Sérsic fits.

A detailed description of the procedure for fitting Sérsic profiles to galaxies in JADES, and the resulting structural parameters, can be found in Carreira et al. (2026). In brief, we obtain cutouts of sources from the JADES *JWST*/NIRCam F200W and F444W imaging mosaics, as described in Johnson et al. (2026) and Robertson et al. (2026). Additionally, we obtain cutouts of the uncertainty mosaic and segmentation map for the source, the latter of which indicates the assignment of pixels in the mosaic to a particular source. These cutouts, alongside a modeled PSF representative of the observational program in which a given source was primarily imaged, are provided to *pysersic*. We utilize the MCMC sampling mode, resulting in posterior distributions for 7 different parameters: centroid values, total flux, effective (half-light) radius, Sérsic index n , axis-ratio, and position angle. The median value of each posterior distribution is used as the best fit value of that parameter.

3 ABUNDANCE MEASUREMENTS

The gold-standard for extragalactic abundance studies is to measure abundances via the so-called ‘direct method’ which relies on directly constraining the electron temperature (T_e) with one or more faint, temperature-sensitive auroral lines. We detect the $[\text{O III}]\lambda 4363$ auroral line in 40 of our galaxies, allowing us to make temperature-based abundance measurements for only a fraction of our full sample of 588 galaxies. Thus, much of the analysis in this paper will focus on abundances derived from strong-line methods. Although strong-line methods have larger systematic uncertainties on a galaxy-by-galaxy basis, across a sufficiently large sample, they are still effective for studying trends between chemical abundances and galaxy properties (e.g. Sanders et al. 2020). However, we begin by exploring temperature-based abundance measurements, making use of our 40 $[\text{O III}]\lambda 4363$ detections.

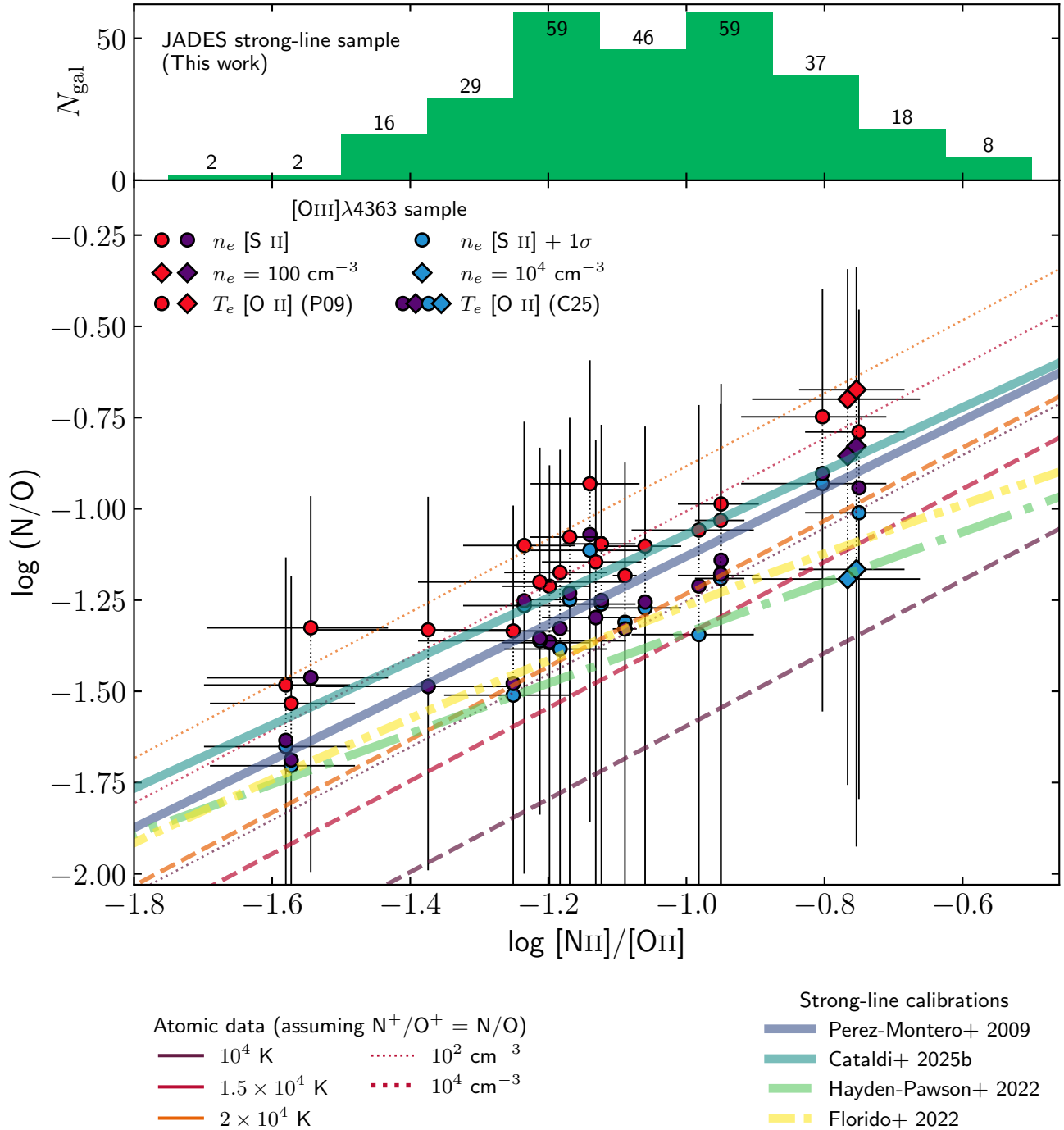


Figure 4. Main panel: JADES T_e -based N/O abundance measurements as a function of measured $[\text{N II}]\lambda 6583/[\text{O II}]\lambda\lambda 3726, 3729$ ratio under different T_e and n_e assumptions. All points have $T_e[\text{O III}]$ derived from $[\text{O III}]\lambda 4363/\lambda 5007$ measurements, comprising a sample of 22 galaxies. Purple points show abundances derived assuming the $T_e[\text{O III}]$ – $T_e[\text{O III}]$ relation of Cataldi et al. (2025a), while red points show how these change if Pilyugin et al. (2009) is adopted instead. Circles denote galaxies for which n_e is measured from the $[\text{S II}]\lambda\lambda 6716, 6731$ doublet, and the blue circles show how the purple points would shift if the $+1\sigma$ value was adopted instead of the best-fit n_e value. Diamonds denote galaxies without n_e constraints – purple and blue diamonds assume $n_e = 100$ & 10^4 cm^{-3} , respectively. Dotted and dashed lines show conversions of $[\text{N II}]/[\text{O III}]$ to N/O for different T_e and n_e values (assuming $\text{ICF}(\text{N}^+/\text{O}^+) = 1$). Dark blue solid, light blue solid, green dot-dash, and yellow double-dot-dash lines show the Pérez-Montero & Contini (2009), Cataldi et al. (2025b), Hayden-Pawson et al. (2022), and Florido et al. (2022) strong-line calibrations respectively. Top panel: The distribution of $[\text{N II}]\lambda 6583/[\text{O II}]\lambda\lambda 3726, 3729$ ratios among galaxies in which both lines are detected with $S/N > 3$ in our JADES strong-line sample.

Table 1. Nebular properties and chemical abundances derived for the 40 galaxies in our T_e -based sample. Columns 1 – 3 give unique identifiers and redshift. Columns 4 & 5 give the n_e derived from the $[\text{S II}]\lambda 6716/\lambda 6731$ ratio and T_e derived from the $[\text{O III}]\lambda 4363/\lambda 5007$ ratio. Column 6 gives the low-ionisation $T_e[\text{O II}]$ derived adopting the [C25](#) and [P09](#) relations, respectively. Columns 7 & 9 give $12 + \log(\text{O/H})$ and $\log(\text{N/O})$ derived using the [C25](#) relation, while Columns 8 & 10 indicate how these values change if the [P09](#) relation is adopted instead.

Tier	ID	z	n_e cm^{-3}	$T_e[\text{O III}]$ 10^4 K	$T_e[\text{O II}]$ 10^4 K	$12 + \log(\text{O/H})$ ($T_e[\text{O II}]$: C25 , P09 ,	$\Delta \log(\text{O/H})$ C25 , P09)	$\log(\text{N/O})$ C25 , P09)	
goods-s-deephst	18846	6.3349	...	$1.9^{+0.3}_{-0.3}$	1.4 – 1.9	$7.56^{+0.03}_{-0.03}$	-0.03	< -0.64	+0.15
goods-s-mediumhst	58850	6.2633	...	$1.7^{+0.3}_{-0.3}$	1.3 – 1.7	$7.78^{+0.03}_{-0.04}$	-0.01	< -0.41	+0.16
goods-s-deephst	22251	5.798	...	$2.6^{+0.5}_{-0.5}$	1.6 – 2.4	$7.39^{+0.03}_{-0.03}$	-0.04	< -0.93	+0.14
goods-s-mediumjwst	81034	5.3904	...	$2.6^{+0.5}_{-0.4}$	1.7 – 2.4	$7.41^{+0.02}_{-0.02}$	-0.02	< -0.97	+0.14
goods-n-mediumjwst	79349	5.1824	...	$2.1^{+0.3}_{-0.3}$	1.4 – 2.0	$7.58^{+0.03}_{-0.03}$	-0.03	< -0.94	+0.15
goods-n-mediumhst	607	5.1822	...	$1.8^{+0.3}_{-0.3}$	1.3 – 1.8	$7.79^{+0.04}_{-0.04}$	-0.04	$-0.83^{+0.56}_{-0.36}$	+0.16
goods-n-mediumjwst	70920	5.0356	< 1011	$2.1^{+0.2}_{-0.2}$	1.4 – 2.0	$7.63^{+0.03}_{-0.03}$	-0.04	< -1.27	+0.15
goods-s-mediumjwst	206035	4.7735	...	$1.9^{+0.3}_{-0.3}$	1.3 – 1.8	$7.64^{+0.03}_{-0.03}$	-0.04	$-0.83^{+0.76}_{-0.34}$	+0.15
goods-s-mediumhst	15325	4.7002	...	$2.5^{+0.5}_{-0.4}$	1.6 – 2.3	$7.42^{+0.04}_{-0.04}$	-0.01	< -0.69	+0.15
goods-n-mediumhst	3008	4.5345	1930^{+4029}_{-877}	$1.7^{+0.3}_{-0.3}$	1.2 – 1.7	$7.85^{+0.02}_{-0.02}$	-0.05	$-1.21^{+0.7}_{-0.34}$	+0.15
goods-n-mediumjwst	10000865	4.407	10^{+122}_{-10}	$1.5^{+0.2}_{-0.2}$	1.1 – 1.5	$8.06^{+0.02}_{-0.02}$	-0.06	$-1.36^{+0.84}_{-0.33}$	+0.15
goods-n-mediumjwst	16553	4.3822	< 100	$1.8^{+0.3}_{-0.3}$	1.3 – 1.8	$7.82^{+0.02}_{-0.03}$	-0.05	< -1.36	+0.16
goods-s-deephst	7892	4.2286	...	$3.0^{+0.9}_{-0.7}$	1.8 – 2.8	$7.26^{+0.03}_{-0.04}$	-0.04	< -0.93	+0.14
goods-s-deephst	4270	4.0224	< 100	$1.7^{+0.2}_{-0.2}$	1.2 – 1.7	$7.77^{+0.02}_{-0.02}$	-0.06	$-1.49^{+0.5}_{-0.36}$	+0.16
goods-s-mediumjwst	191576	3.7937	284^{+140}_{-65}	$1.3^{+0.1}_{-0.1}$	1.1 – 1.3	$8.14^{+0.01}_{-0.02}$	-0.05	$-1.18^{+1.08}_{-0.32}$	+0.15
goods-s-mediumjwst	88182	3.6505	...	$1.9^{+0.3}_{-0.3}$	1.4 – 1.9	$7.7^{+0.03}_{-0.03}$	-0.05	< -1.08	+0.15
goods-n-mediumjwst	42939	3.4671	470^{+1208}_{-56}	$1.5^{+0.2}_{-0.2}$	1.1 – 1.5	$7.98^{+0.02}_{-0.02}$	-0.03	$-0.94^{+0.78}_{-0.34}$	+0.15
goods-s-mediumhst	17366	3.4591	...	$1.7^{+0.2}_{-0.2}$	1.3 – 1.7	$7.84^{+0.03}_{-0.03}$	-0.04	< -1.09	+0.16
goods-s-mediumjwst	60310684	3.3467	< 165	$1.5^{+0.2}_{-0.2}$	1.2 – 1.6	$7.96^{+0.02}_{-0.02}$	-0.05	$-1.35^{+0.48}_{-0.37}$	+0.15
goods-s-mediumjwst	159438	3.2389	856^{+812}_{-343}	$1.6^{+0.1}_{-0.1}$	1.2 – 1.6	$7.88^{+0.01}_{-0.01}$	-0.04	$-1.14^{+0.87}_{-0.33}$	+0.15
goods-n-mediumhst	31940	3.1295	< 389	$1.7^{+0.3}_{-0.3}$	1.3 – 1.7	$7.76^{+0.03}_{-0.03}$	-0.03	$-0.9^{+0.62}_{-0.35}$	+0.16
goods-s-mediumjwst	54612	3.0833	315^{+182}_{-211}	$1.3^{+0.1}_{-0.1}$	1.0 – 1.3	$8.19^{+0.01}_{-0.01}$	-0.1	$-1.33^{+1.4}_{-0.31}$	+0.15
goods-s-mediumhst	8767	3.0633	1002^{+1198}_{-408}	$1.9^{+0.3}_{-0.3}$	1.3 – 1.8	$7.79^{+0.02}_{-0.02}$	-0.07	$-1.33^{+0.77}_{-0.34}$	+0.15
goods-s-mediumjwst	192837	3.0	< 100	$1.5^{+0.2}_{-0.2}$	1.1 – 1.5	$8.02^{+0.01}_{-0.02}$	-0.04	$-1.3^{+0.78}_{-0.34}$	+0.15
goods-n-mediumhst	24755	2.9803	10^{+585}_{-10}	$2.9^{+0.6}_{-0.5}$	1.8 – 2.7	$7.35^{+0.03}_{-0.03}$	-0.05	$-1.07^{+0.75}_{-0.34}$	+0.14
goods-n-mediumhst	33391	2.9016	475^{+233}_{-165}	$1.5^{+0.1}_{-0.1}$	1.1 – 1.5	$7.99^{+0.02}_{-0.02}$	-0.05	$-1.26^{+0.89}_{-0.33}$	+0.15
goods-s-mediumjwst	10012070	2.8105	10^{+252}_{-10}	$1.7^{+0.2}_{-0.2}$	1.2 – 1.7	$7.97^{+0.02}_{-0.02}$	-0.07	$-1.69^{+0.62}_{-0.35}$	+0.16
goods-s-mediumjwst	225349	2.7851	325^{+769}_{-10}	$2.7^{+0.7}_{-0.6}$	1.7 – 2.5	$7.37^{+0.05}_{-0.05}$	-0.02	< -1.0	+0.14
goods-s-mediumjwst	164658	2.6749	< 100	$3.0^{+0.9}_{-0.7}$	1.8 – 2.8	$7.48^{+0.04}_{-0.05}$	-0.08	$-1.46^{+0.53}_{-0.36}$	+0.14
goods-s-mediumjwst	176834	2.6699	369^{+225}_{-98}	$2.1^{+0.3}_{-0.3}$	1.4 – 2.0	$7.68^{+0.02}_{-0.02}$	-0.06	$-1.63^{+0.62}_{-0.35}$	+0.15
goods-s-mediumjwst	202446	2.6167	233^{+201}_{-17}	$2.0^{+0.4}_{-0.4}$	1.4 – 1.9	$7.72^{+0.02}_{-0.02}$	-0.1	$-1.23^{+0.91}_{-0.33}$	+0.15
goods-s-mediumjwst	167544	2.5762	76^{+151}_{-10}	$2.2^{+0.5}_{-0.4}$	1.5 – 2.1	$7.56^{+0.03}_{-0.03}$	-0.08	$-1.25^{+0.73}_{-0.34}$	+0.15
goods-n-mediumhst	29455	2.5309	...	$2.0^{+0.3}_{-0.3}$	1.4 – 1.9	$7.71^{+0.04}_{-0.05}$	-0.03	< -1.02	+0.15
goods-s-mediumjwst	51489	2.4561	< 864	$2.8^{+0.7}_{-0.6}$	1.7 – 2.6	$7.44^{+0.05}_{-0.06}$	-0.01	< -0.61	+0.14
goods-n-mediumhst	23638	2.4173	10^{+201}_{-10}	$2.2^{+0.4}_{-0.3}$	1.4 – 2.1	$7.62^{+0.02}_{-0.03}$	-0.05	< -1.44	+0.15
goods-s-mediumjwst	60309998	2.1989	...	$1.7^{+0.2}_{-0.2}$	1.2 – 1.7	$7.67^{+0.02}_{-0.03}$	-0.02	< -0.65	+0.16
goods-n-mediumhst	26751	2.1763	10^{+193}_{-10}	$1.6^{+0.2}_{-0.2}$	1.2 – 1.6	$7.93^{+0.02}_{-0.02}$	-0.08	$-1.25^{+0.92}_{-0.33}$	+0.15
goods-n-mediumhst	29849	1.8142	< 149	$1.6^{+0.2}_{-0.2}$	1.2 – 1.6	$7.8^{+0.02}_{-0.02}$	-0.03	< -1.05	+0.16
goods-n-mediumhst	25451	1.676	...	$1.8^{+0.3}_{-0.2}$	1.3 – 1.7	$7.85^{+0.02}_{-0.03}$	-0.03	< -0.99	+0.16
goods-n-mediumhst	25771	1.675	10^{+438}_{-10}	$1.2^{+0.1}_{-0.2}$	1.0 – 1.3	$8.17^{+0.01}_{-0.02}$	-0.06	$-1.48^{+0.69}_{-0.34}$	+0.14

3.1 Temperature-based oxygen abundances

For our 40 galaxies with $[\text{O III}]\lambda 4363$ auroral line detections (' T_e -based sample' hereafter), we derive the oxygen abundance (O/H) following the methodology outlined in Cameron et al. (2023a). Briefly, we assume the total oxygen abundance is the sum of singly- and doubly-ionised oxygen ($\text{O/H} = \text{O}^+/\text{H}^+ + \text{O}^{2+}/\text{H}^+$), deriving each ionic abundance from the $[\text{O III}]\lambda\lambda 5007/\text{H}\beta$ and $[\text{O II}]\lambda\lambda 3727/\text{H}\beta$ line ratios respectively, using emissivities calculated with pyneb (Luridiana et al. 2015).

Where available, we use n_e measured from the $[\text{S II}]\lambda\lambda 6716/\lambda 6731$ ratio for the emissivity calculation. For 17 galaxies in our T_e -based sample, detections of the $[\text{S II}]$ lines afford a n_e measurement with values ranging up to $n_e \approx 2000 \text{ cm}^{-3}$, although the majority are below $n_e \lesssim 500 \text{ cm}^{-3}$ (Table 1). For a further 9 galaxies we can only place an upper limit on the n_e , and for these we adopt a density of $n_e = 100 \text{ cm}^{-3}$ for our emissivity calculation. The remaining 14 galaxies lack a detection of $[\text{S II}]$ altogether. For these, we also adopt $n_e = 100 \text{ cm}^{-3}$ as our fiducial assumption, but also consider the effect of assuming a higher density of $n_e = 10^4 \text{ cm}^{-3}$ (see discussion below).

We use the $[\text{O III}]\lambda 4363 / [\text{O III}]\lambda 5007$ ratio to derive $T_e[\text{O III}]$, which we adopt as the temperature of the high-ionisation zone. Given that none of these galaxies exhibits a detection of any low-ionisation auroral lines, such as $[\text{O II}]\lambda\lambda 7320, 7330$ or $[\text{N II}]\lambda 5755$, we must rely on an empirical calibration to derive $T_e[\text{O II}]$ from $T_e[\text{O III}]$.

Many such $T_e[\text{O II}] - T_e[\text{O III}]$ calibrations exist (e.g. Campbell et al. 1986; Garnett 1992; Pilyugin et al. 2009), but this approach suffers from significant intrinsic scatter observed around this relation (e.g. Berg et al. 2020; Yates et al. 2020; Méndez-Delgado et al. 2023). Furthermore, little is yet known about the evolution of these relations toward higher redshift and lower metallicity as existing data sets in these regimes are still relatively small (e.g. Strom et al. 2023; Rogers et al. 2023; Hamel-Bravo et al. 2025), and exhibit significant scatter (e.g. Cataldi et al. 2025a; Sanders et al. 2025). For this analysis, we adopt two temperature calibrations: those of Pilyugin et al. (2009) (P09 hereafter) and Cataldi et al. (2025a) (C25 hereafter). The P09 relation is fairly steep and predicts $T_e[\text{O II}] \approx T_e[\text{O III}]$, while the C25 relation is much shallower and predicts that $T_e[\text{O II}]$ rarely exceeds $\sim 15,000 \text{ K}$. In this work we do not explore which of these two scenarios better represents our sample, but rather consider both to bracket the range of likely values.

Columns 7 & 8 of Table 1 give the derived 12+log(O/H) values assuming the C25 relation, and then the difference from that value that adopting P09 would lead to. The P09 relation results in oxygen abundances that are systematically lower (owing to the higher $[\text{O II}]$ temperature), but the difference is only mild (≤ 0.1).

3.2 Nitrogen abundance measurement

Because we do not observe higher ionisation states of nitrogen (i.e. N^{2+} or N^{3+}) in this sample, in addition to the T_e - and n_e -dependence, we must also consider the impact of the 'ionisation correction factor' (ICF), which corrects for these unseen ionisation states, in our N/O abundance determination. The ICF of N^+/O^+ is often assumed to be unity (i.e. $\text{N}^+/\text{O}^+ = \text{N/O}$) (e.g. Peimbert & Costero 1969; Arellano-Córdova et al. 2025a) due to the similar ionisation potentials of these species. Amayo et al. (2021) derived an ICF based on photoionisation models which does suggest a non-zero ICF, albeit with a very modest value of $\log(\text{N/O}) \approx \log(\text{N}^+/\text{O}^+) + 0.1$. Modeling in Martinez et al. (2025) found similar ICFs when low density ($n_e = 10^2 \text{ cm}^{-3}$) was assumed, although they found that, at higher

densities, N^+/O^+ begins to overestimate N/O, with ICFs of around $\log(\text{N/O}) \approx \log(\text{N}^+/\text{O}^+) - 0.1$ at $n_e = 10^5 \text{ cm}^{-3}$. As outlined above, where we are able to measure densities in our sample, we find them to be low, albeit acknowledging that $n_e([\text{S II}])$ can underestimate density in the presence of high-density gas (Martinez et al. 2025). As a result, throughout this work, we adopt $\text{N}^+/\text{O}^+ = \text{N/O}$, noting that adopting a non-zero ICF would generally push total N/O abundances higher by $\lesssim 0.1$ dex in systems with $\sim 10^2 \text{ cm}^{-3}$, and would move total N/O abundances down by similar amounts toward higher densities.

Figure 4 shows how the T_e - and n_e -dependence of the $[\text{N II}]\lambda 6583$ and $[\text{O II}]\lambda\lambda 3726, 3729$ emissivities are each responsible for around 0.3 dex of systematic uncertainty in the final N/O abundance if not well constrained. The dotted and dashed lines in Figure 4 show the conversion from line ratio to ionic abundance for $n_e = 100$ and 10^4 cm^{-3} , respectively. At higher densities, the same $[\text{N II}]/[\text{O II}]$ ratio corresponds to an abundance ratio that is around 0.3 dex lower. Meanwhile, T_e values of 10^4 K (shown in purple) also result in systematically lower N/O values than if $T_e \geq 1.5 \times 10^4 \text{ K}$ is assumed.

From our T_e -based sample, 22 galaxies exhibit detections of both $[\text{N II}]\lambda 6583$ and $[\text{O II}]\lambda\lambda 3727$, allowing us to derive the N/O ratio as

$$\frac{\text{N}}{\text{O}} \approx \frac{\text{N}^+}{\text{O}^+} = \frac{f_{[\text{N II}]\lambda 6583}}{f_{[\text{O II}]\lambda\lambda 3726, 3729}} \times \frac{\epsilon_{[\text{O II}]\lambda\lambda 3726, 3729}}{\epsilon_{[\text{N II}]\lambda 6583}}, \quad (1)$$

where ϵ is the emissivity, dependent on both T_e and n_e . The remaining 18 galaxies have detections of $[\text{O II}]$, but only an upper-limit on $[\text{N II}]$, resulting in an upper limit on the N/O ratio.

Of course, the required temperature for this calculation is the low-ionisation temperature which is not measured in any of our sample. As discussed above, obtaining $T_e[\text{O II}]$ via a calibration can result in significantly different values depending on which relation is adopted. Columns 9 & 10 of Table 1 give the log(N/O) values derived assuming the two $T_e[\text{O II}] - T_e[\text{O III}]$ relations. The shallower C25 relation results in log(N/O) values which are ~ 0.15 dex lower than the P09 relation. Note that the difference is more pronounced than that seen in the total oxygen abundance. These differences are also shown in Figure 4, with the red points showing the higher derived N/O at fixed $[\text{N II}]/[\text{O II}]$ ratio resulting from adopting the P09 relation compared to the C25 relation (purple points).

The majority of these galaxies (20/22) have a measurement or an upper limit placed on the density from the $[\text{S II}]\lambda\lambda 6716, 6731$ doublet, indicated by the circle markers in Figure 4. We explore the effect of n_e on the derived N/O abundance by showing (as blue circles) the measured N/O if the $+1\sigma$ upper limit of the measured n_e is adopted instead of the best-fit n_e value. In most cases, this results in negligible difference (median difference of -0.02 dex), but the most significant cases can result in abundances that are 0.13 dex lower.

For the two galaxies in this sample which have a $[\text{N II}]$ detection but no constraint on n_e from $[\text{S II}]$, we adopt two values: 100 cm^{-3} (purple diamonds) and 10^4 cm^{-3} (blue diamonds). Changing the assumed density between these values results in a far more significant change of 0.33 dex to the derived N/O. This upper density value is higher than any of our measured values in this sample and higher also than the majority of low-ionisation density measurements at high-redshift (e.g. Harikane et al. 2025, and references therein), albeit not unprecedented (e.g. Berg et al. 2025). However, Martinez et al. (2025) showed that $[\text{S II}]$ -based n_e measurements are always biased low when the density is not homogeneous, suggesting that some systems with measured $n_e([\text{S II}]) \approx 10^3 \text{ cm}^{-3}$ could still host significant quantity of $n_e \gtrsim 10^4 \text{ cm}^{-3}$ gas. Thus, while we do not have direct evidence for high-density gas in any of our systems, we cannot rule

out its presence, and, as shown by the blue diamonds in Figure 4, this would impact the N/O abundances derived. Obtaining density measurements from density tracers such as C III] $\lambda 1907/\lambda 1909$ or [Ar IV] $\lambda 4714/\lambda 4742$, which are sensitive to higher densities, would help elucidate the presence or absence of high-density gas, but are unfortunately not detected at the depth of this data set.

3.2.1 Nitrogen-to-oxygen strong-line calibration

In Figure 4 we show several strong-line calibrations for mapping [N II]/[O II] to N/O. Three of these were derived from T_e -based abundances from H II regions and star-forming galaxies at $z \sim 0$ (Pérez-Montero & Contini 2009, Hayden-Pawson et al. 2022, and Florido et al. 2022; blue solid, green dot-dashed, yellow dot-dot-dashed lines, respectively). We also show the recent calibration from Cataldi et al. (2025b, light blue solid line) which was determined based on $z > 1$ JWST/NIRSpec spectroscopy. These calibrations all return very similar values for $\log([N\,II]/[O\,II]) \lesssim -1.5$, but Pérez-Montero & Contini (2009) and Cataldi et al. (2025b) gradually diverge to yield ~ 0.3 dex higher N/O at $\log([N\,II]/[O\,II]) \gtrsim -0.8$.

Our sample with density measurements (circles), clearly align better with the Pérez-Montero & Contini (2009) and Cataldi et al. (2025b) calibrations. This is true even when adopting the C25 temperature relation, while adopting the P09 relation shifts the majority of our sample well above these calibrations. The two galaxies without density constraints have among the highest [N II]/[O III] ratios in our sample. Regardless of the adopted T_e relation, these only yield N/O values consistent with the the Hayden-Pawson et al. (2022) and Florido et al. (2022) relations if $n_e = 10^4 \text{ cm}^{-3}$ is assumed. Even in these cases, they fall right on the relation, and adopting the steeper P09 T_e relation or a positive ICF would push these measurements above these two shallower strong-line calibrations. Thus, it is clear that our sample favours the steeper calibrations.

A plausible explanation is that the offset toward high N/O values is driven by higher temperatures, seen, for example, in the atomic data lines in Figure 4. The Hayden-Pawson et al. (2022) calibration is based on stacks of SDSS spectra, the vast majority of which have $12 + \log(O/H) \gtrsim 8$, and the Florido et al. (2022) calibration is based on H II regions with similarly high metallicities. These metallicities are higher than the bulk of our our JADES T_e -based sample. As a result, one might expect that the electron temperature in these calibration samples will be much lower than our sample ($T_e \gtrsim 1.5 \times 10^4 \text{ K}$ for all our individual [O III] measurements, in line with previous studies at high redshift; e.g. Laseter et al. 2023; Sanders et al. 2023, 2025).

Meanwhile, the calibration from Cataldi et al. (2025b) is based on galaxies with $7.3 \lesssim 12 + \log(O/H) \lesssim 8.3$. Similarly, the calibration sample in Pérez-Montero & Contini (2009) has a significant number of objects with $12 + \log(O/H) \lesssim 8$. In their Figure 10, one can see that the ‘H II galaxies’ (which are generally low metallicity) in their sample prefer a calibration with a higher normalisation, while if the sample had been limited to ‘Giant Extragalactic H II Regions’ (which have metallicities comparable to the Hayden-Pawson et al. 2022 and Florido et al. 2022 calibration samples), a flatter calibration more in line with those works would have been derived. As a result, we adopt the Pérez-Montero & Contini (2009) calibration as our default N/O strong-line calibration.

3.3 Strong-line oxygen abundances

To support our strong-line N/O measurements, outlined above, we make strong-line oxygen abundance measurements across our sample, following the methodology outlined in Curti et al. (2023). In

short, we adopt the strong-line calibrations of Sanders et al. (2025) measuring the metallicity from multiple strong-line ratios and performing a weighted average of these metallicity measurements to determine the best-fit $12 + \log(O/H)$ value for the galaxy in question. Since we ultimately want to explore how nitrogen abundance correlates with oxygen abundance, we only consider ratios of O, Ne, and H lines in these calculations. Namely, we consider $R3 = \log([O\,III]/H\beta)$, $R2 = \log([O\,II]/H\beta)$, $O32 = \log([O\,III]/[O\,II])$, $Ne3O2 = \log([Ne\,III]/[O\,II])$, and $R23 = \log(([O\,III]+[O\,II])/H\beta)$. These strong-line calibrations are quoted by Sanders et al. (2025) as being valid over the range $7.3 \leq 12 + \log(O/H) \leq 8.6$. Without strictly enforcing this validity range in our fitting, we find that all but nine of our 548 strong-line metallicities fall within this range. Eight galaxies in our sample marginally exceed this, with all returning $12 + \log(O/H) < 8.74$, while one galaxy returns a best-fit abundance of $12 + \log(O/H) = 7.06^{+0.07}_{-0.06}$. The main function of our O/H measurements throughout this paper is to differentiate between nitrogen enrichment at ‘low-metallicity’ ($12 + \log(O/H) \lesssim 8.0$) and ‘high-metallicity’, since nitrogen abundances at high-metallicity are widely accepted to be driven by different enrichment sources (see Section 1). Thus, these minor extrapolations should not impact our results, and we leave these extrapolated abundances as derived.

4 RESULTS

4.1 Nitrogen abundance variation with oxygen abundance

4.1.1 Temperature-based abundances

Figure 5 shows the N/O abundance ratio as a function of O/H from our JADES T_e -based sample (diamonds). As discussed in Section 3.1, deriving T_e [O II] values from a temperature calibration leads to a > 0.1 dex uncertainty in the measured N/O, and a somewhat smaller uncertainty in O/H. The salmon arrows in Figure 5 show how these measured abundances shift if the adopted relation is changed from C25 (which is shown by the location of the points) to P09 (head of salmon arrows). For galaxies which lack a n_e constraint from [S II], or has one which has a large uncertainty, the effect of increasing the adopted n_e is shown by the purple arrows.

Comparing to the sample of H II regions at $z \sim 0$ (Pilyugin et al. 2012, Berg et al. 2020; green circles and diamonds respectively) and the $z \sim 0$ abundance scalings presented in Nicholls et al. (2017), Cataldi et al. (2025b), and Scholte et al. (2026), our T_e -based sample appears to deviate to higher N/O values. Our sample is limited to low metallicities $12 + \log(O/H) < 8.2$ and those with [N II] $\lambda 6583$ detections have a median value of $\log(N/O) = -1.25$ and a weighted mean of $\log(N/O) = -1.26 \pm 0.03$. This is notably higher than the low-metallicity N/O plateau of $\log(N/O) = -1.391 \pm 0.003$ derived by Scholte et al. (2026) from a sample of almost 50,000 T_e -based abundances in $z \sim 0$ galaxies observed with the Dark Energy Spectroscopic Instrument (DESI; DESI Collaboration et al. 2024), and also than the weighted average of $\log(N/O) = -1.41 \pm 0.09$ found for $z \sim 0$ dwarf galaxies in Berg et al. (2019) (purple dashed line), and for metal-poor galaxies from Izotov & Thuan (1999) ($\log(N/O) = -1.46 \pm 0.14$).

Green squares show galaxies from the CLASSY survey, which have high SFRs for $z \sim 0$ and span a large range of O/H (Berg et al. 2022; Arellano-Córdova et al. 2025a). These have a median $\log(N/O)$ of -1.36 which, while somewhat higher than the other $z \sim 0$ samples, is still at least 0.10 dex lower than ours. We note that abundances in that work were derived assuming the T_e calibration of Garnett (1992) which lies between the two considered in this

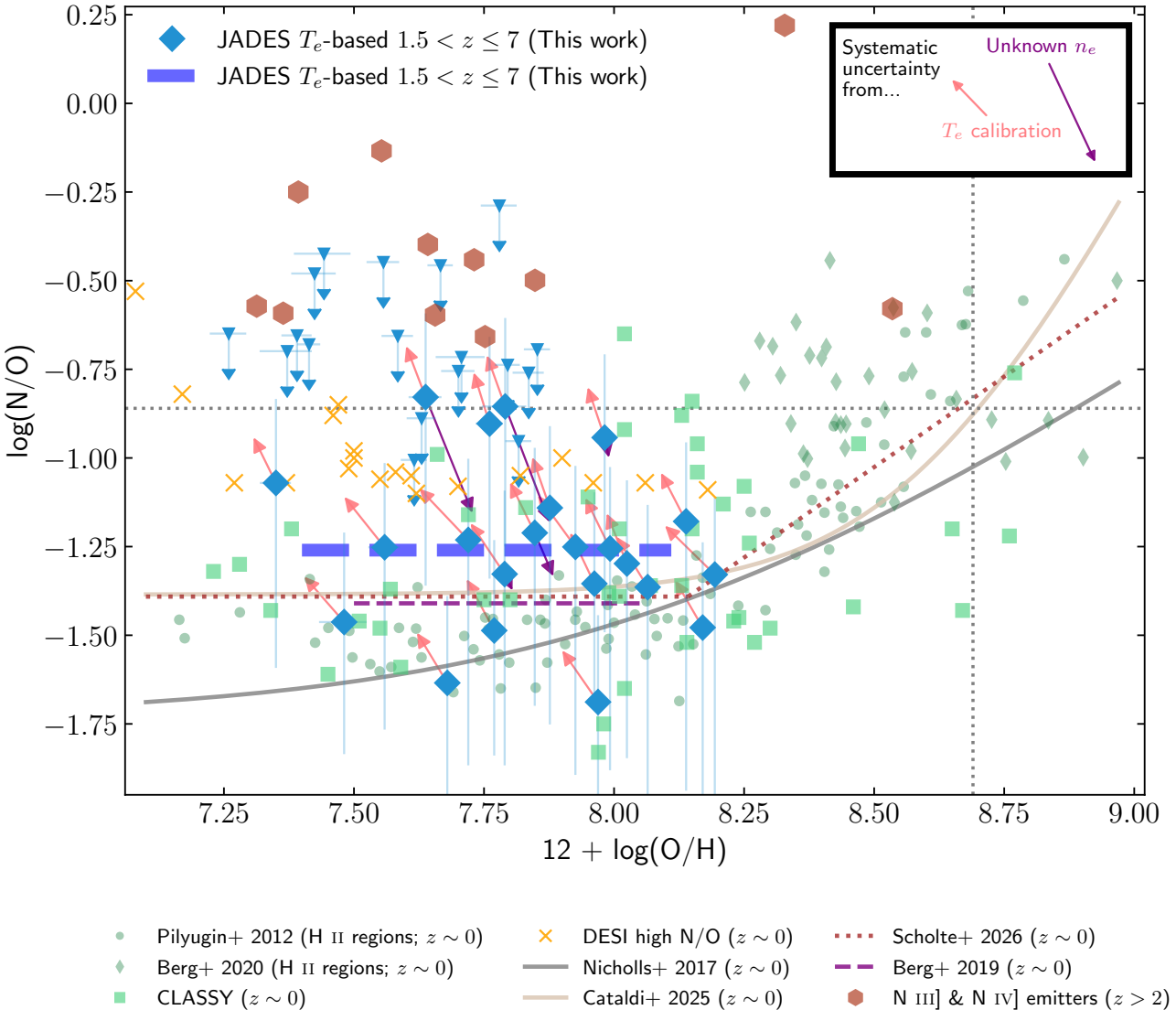


Figure 5. Nitrogen-to-oxygen abundance ratio as a function of oxygen abundance for our JADES T_e -based sample (blue diamonds). The blue dashed line shows the weighted average N/O for this $12 + \log(\text{O/H}) < 8.2$ sample. Salmon arrows show how these points would shift if the P09 $T_e[\text{O II}] - T_e[\text{O III}]$ calibration was used instead of the C25 adopted for the fiducial values. Purple arrows show the systematic uncertainty arising from a weak or absent n_e constraint (see Section 3.2 for details). Green circles and diamonds show $z \sim 0$ H II regions (Pilyugin et al. 2012; Berg et al. 2020). Green squares show $z \sim 0$ star-forming galaxies from the CLASSY survey (Arellano-Córdova et al. 2025a). Orange ‘ \times ’ marks show the high-N/O-selected subsample of DESI galaxies from Bhattacharya & Kobayashi (2025). High-redshift N III]- and N IV]-emitters are shown by the brown hexagons, compiled from (Isobe et al. 2023; Marques-Chaves et al. 2023; Castellano et al. 2024; Schaefer et al. 2024; Martinez et al. 2025; Naidu et al. 2025). The grey solid, beige solid, and brown dotted lines show the N/O – O/H scaling from Nicholls et al. (2017), Cataldi et al. (2025b), and Scholte et al. (2026) respectively, while the purple dashed line shows the average N/O value derived for $z \sim 0$ metal-poor dwarf galaxies in Berg et al. (2019). The faint dotted lines show the solar ratios of each abundance.

work, and results in $T_e[\text{O II}]$ values that are $\sim 10 - 20$ % higher than those from the C25 relation, indicating that the true offset between our $\log(\text{N/O})$ values and those of (Arellano-Córdova et al. 2025a) would be even higher than the 0.10 dex quoted.

Our result is consistent with a recent analysis of T_e -based abundances in a $z \approx 2 - 3.5$ from Schaefer et al. (2026) which found a mean of $\log(\text{N/O}) = -1.29^{+0.25}_{-0.21}$, although that sample extends to higher metallicity, ranging up to $12 + \log(\text{O/H}) = 8.44$.

Even adopting the ‘high n_e ’ assumption (purple arrows), the median value of our sample only drops marginally to $\log(\text{N/O}) = -1.28$, and if we would have adopted the P09 relation as our default, we

would recover a median value of $\log(\text{N/O}) = -1.10$. We note that a further 10 galaxies in this redshift range did not have [N II] detected for which we can only place a relatively weak upper limit on the N/O. However, given these upper limits are all well above the median value, there is no suggestion that deeper data to obtain the [N II] line would push the sample median lower.

4.1.2 Strong-line abundances

In Figure 6, we expand our focus to show the strong-line abundance measurements, spanning our full sample. We have divided this into

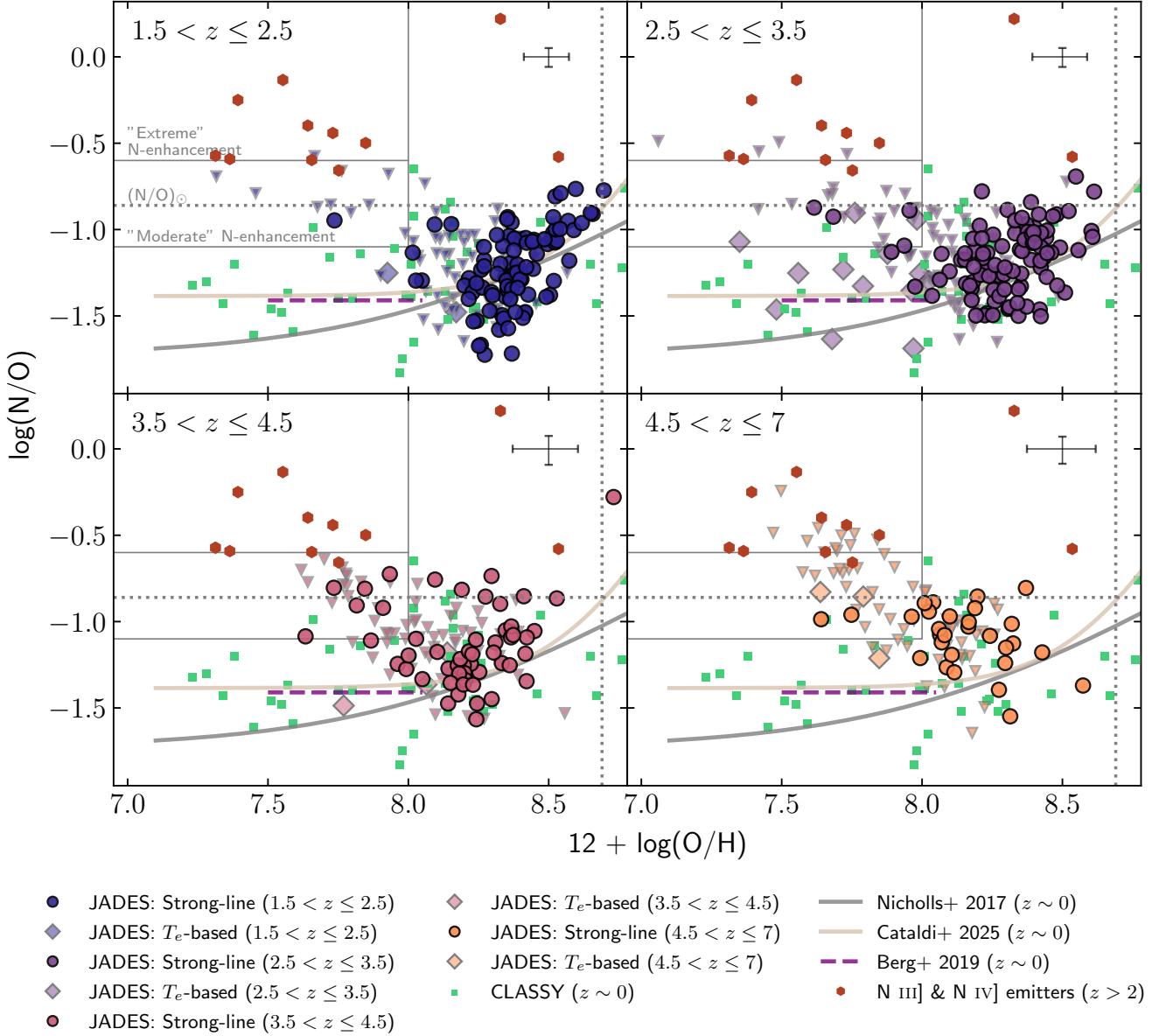


Figure 6. Nitrogen-to-oxygen abundance ratio as a function of oxygen abundance for our JADES strong-line sample, divided into four redshift bins. Circles show our strong-line abundance measurements, while triangles show galaxies for which we only have an upper limit on $\log(\text{N}/\text{O})$. The black errorbars in the upper right corner show the median measurement uncertainties for the strong-line sample. Diamond markers show T_e -based abundances, carried over from Figure 5. We include demarcation lines for our ‘moderate’ and ‘extreme’ nitrogen-enhancement selection criteria as a visual aid (see Section 4.2). Green squares and brown hexagons are as in Figure 5, as are the grey, beige, and purple lines. Faint dotted lines show the solar ratios of each abundance.

four panels showing different redshift slices from $z = 1.5 - 7$ for visual clarity. While strong-line oxygen abundance measurements are known to be less reliable than T_e -based measurements, the overall trends across a sample this large are likely robust (e.g. Sanders et al. 2020).

Around 50 % of our sample has $7.9 \lesssim 12 + \log(\text{O}/\text{H}) \lesssim 8.3$, and we see at least an order of magnitude of spread in the nitrogen abundance distribution within this range, from $-1.72 \leq \log(\text{N}/\text{O}) \leq -0.72$, with some upper limits even suggesting values that might be lower still. The median value in this metallicity range is $\log(\text{N}/\text{O}) = -1.2$, comparable to what we found in our auroral line sample extending to lower metallicity. At higher metallicities, we begin to observe a

high fraction of the galaxies with much higher N/O , in line with the $\text{N}/\text{O} - \text{O}/\text{H}$ trend that is observed locally (e.g., Pilyugin et al. 2012; Hayden-Pawson et al. 2022).

Computing the Kendall’s τ coefficient between $\log(\text{N}/\text{O})$ and $12 + \log(\text{O}/\text{H})$ across the full sample (all redshifts and all metallicities), we find a weak correlation ($\tau = 0.10$) at high significance ($p = 0.002$). Of course, the $\text{N}/\text{O} - \text{O}/\text{H}$ relation is well-established to have little correlation at low metallicity, with a much stronger correlation at higher metallicity, where secondary nitrogen enrichment becomes much more significant. Splitting the sample at the median metallicity, the high metallicity ($12 + \log(\text{O}/\text{H}) > 8.20$) returns a much stronger correlation ($\tau = 0.24$, $p < 10^{-4}$). Considering only

the low metallicity sample ($12 + \log(\text{O/H}) \leq 8.0$) in isolation, we find no evidence for any correlation, and instead obtain a *negative* τ value at low significance ($\tau = -0.07, p = 0.14$).

Although there is a tentative visual shift towards higher N/O values in the higher redshift panels of Figure 6, a τ test shows that this is not significant, yielding $\tau = 0.05$ with $p = 0.11$ for the correlation between $\log(\text{N/O})$ and z across the full sample, with high- and low-metallicity sub-samples returning very similar values. This suggests that while there does seem to be a general trend of galaxies having higher N/O at fixed O/H toward higher redshift, this is more likely driven by another parameter whose redshift evolution may drive this trend.

4.2 Nitrogen-enhanced galaxies at low metallicity

To explore the enhancement of N/O at high redshift, we begin by considering the most nitrogen-enhanced galaxies in our sample. Throughout this section we consider a galaxy ‘nitrogen-enhanced’ if it has $\log(\text{N/O}) > -1.1$, corresponding to a factor of two above the $\log(\text{N/O})_{\text{plateau}} \approx -1.4$ typically found at $z \sim 0$ (Berg et al. 2019; Scholte et al. 2026). For this section, we limit our focus to galaxies with metallicity below $12 + \log(\text{O/H}) < 8.0$.

In addition to the [N II]-based abundances introduced in the previous section, Figures 5 & 6 also show a compilation of abundances derived for high-ionisation N III] and N IV] emitters at $z \gtrsim 2$. We primarily use values from Martinez et al. (2025), where available, as these were derived using a custom treatment of the high n_e regions identified in many of these systems (e.g. Senchyna et al. 2023; Topping et al. 2025; Berg et al. 2025), but the overall finding that these galaxies have highly enhanced N/O abundances has now been demonstrated by numerous studies (Cameron et al. 2023a; Isobe et al. 2023; Marques-Chaves et al. 2023; Castellano et al. 2024; Topping et al. 2024; Schaefer et al. 2024; Naidu et al. 2025; Morel et al. 2025).

Immediately we can note that, despite the enhanced average N/O of our sample relative to $z \sim 0$ samples, even the highest measured values are still considerably lower than what is measured for the N III] and N IV] emitters, which typically have $\log(\text{N/O}) > -0.6$ (labelled as ‘extreme N-enhancement’ in Figure 6). This holds for both the T_e -based and the strong-line sample (Figures 5 & 6). While we identify five nitrogen-enhanced galaxies in our T_e -based samples (Table 3), all of these have abundances of $\log(\text{N/O}) < -0.8$, well below this ‘extreme N-enhancement’ threshold.

We note that the two most nitrogen-rich galaxies (gnmh_607 and gsmj_206035), all also lack n_e constraints from [S II]. If these galaxies have densities comparable with the remainder of our sample ($n_e \lesssim 10^3 \text{ cm}^{-3}$), they would be confirmed as nitrogen-enhanced systems, but adopting a density of $n_e = 10^4 \text{ cm}^{-3}$ would move them below our $\log(\text{N/O}) > -1.1$ cut. That said, gsmj_206035 was identified by Morel et al. (2025) as a nitrogen-enhanced galaxy based on UV nitrogen lines detected in low-resolution prism spectroscopy, which are far less n_e -sensitive when deriving abundances (Cameron et al. 2023a; Martinez et al. 2025). Nonetheless, this highlights that while n_e uncertainty does not significantly affect our derived value for the low-metallicity plateau, it’s clear that our inference on the fraction of galaxies with enhanced N/O abundance ratios can be impacted by the electron density.

We additionally identify 14 candidate nitrogen-enhanced galaxies from our strong-line sample. As seen in Figure 6 and Table 2, we again find that none of this sample reaches the ‘extreme nitrogen-enhancement’ ($\log(\text{N/O}) > -0.6$) found in N III] and N IV] emitters, with the highest abundance being gsmj_203994 with $\log(\text{N/O}) =$

-0.72. The spectra of all nitrogen-enhanced candidates from the strong-line sample are shown in Figures B2 – B6.

Figure 7 shows the M_* and SFR measurements for these nitrogen-enhanced galaxies relative to our full sample and the NIRCam-based sample from Simmonds et al. (2025) (see Section 2.4 for details)³. In this figure, we can see the effect of our $\text{H}\beta$ signal-to-noise requirement – essentially mimicking a SFR cut – with very few galaxies below $\text{SFR}_{10} \approx 1 M_\odot \text{ yr}^{-1}$ entering our sample. Comparing to the NIRCam-based sample from Simmonds et al. (2025) (grey points), we see that above $\log(M_*/M_\odot) > 9$, the star-forming main sequence (SFMS) is well-sampled, while at lower masses we are biased toward galaxies above the main sequence. Here we can see our nitrogen-enhanced galaxies tend to lie on or above the SFMS, however there is no obvious trend that emerges, and most galaxies that lie above the SFMS are not nitrogen-enhanced.

The total of 19 nitrogen-enhanced galaxies is drawn from a parent sample of 151 galaxies across our combined sample with $12 + \log(\text{O/H}) < 8.0$, equating to a nitrogen-enhanced fraction of 13 % at this metallicity. If nitrogen-enhancements tend to occur in highly star-forming systems, our sample should be more complete in selecting for these systems than ‘nitrogen-normal’ systems, in which case this fraction of 13 % would represent an upper limit.

A recent study by Cataldi et al. (2025b) examined [N II]-based N/O abundances across a sample of $z > 1$ galaxies compiled from the JWST/NIRSpec MARTA program (PID 1879; PI Curti), additional JWST observations obtained from the DAWN JWST Archive (DJA; Valentino et al. 2025), and ground-based data sets including MOSDEF (Kriek et al. 2015) and KLEVER (Curti et al. 2020). Among their sample, Cataldi et al. (2025b) also found that a significant fraction had $\log(\text{N/O}) > -1.1$ at low oxygen abundance, but likewise identified very few galaxies with [N II]-based abundances exceeding $\log(\text{N/O}) > -0.6$.

Comparing to low-redshift samples, we again see evidence for a shift toward more nitrogen-rich systems at higher redshift. Bhattacharya & Kobayashi (2025) searched the DESI data release 1 to find the most extreme N/O galaxies with $12 + \log(\text{O/H}) < 8.2$ (orange crosses in Figure 5). Scholte et al. (2026) identified 139 galaxies with $\log(\text{N/O}) > -0.75$ and $12 + \log(\text{O/H}) < 8.0$, but these were drawn from a sample of almost 50,000 galaxies with T_e -based abundances, and the vast majority of low-metallicity galaxies have N/O below our ‘N-enhanced’ threshold. While our sample is admittedly small in comparison (40 T_e -based abundances, drawn from fewer than six thousand total JADES spectra), if a nitrogen-enhanced fraction of ~13 % is confirmed in larger samples, this would indicate that the fraction of nitrogen enhancement is higher at $z > 1.5$ compared to $z \sim 0$.

We note that $z \sim 0$ galaxies with $12 + \log(\text{O/H}) \lesssim 7.3$ – so called extremely metal poor galaxies (XMPs) – are seen to exhibit a much larger scatter in N/O, not unlike what is observed in our high-redshift sample (Breneman et al. 2025). However, XMPs are at lower metallicity than the bulk of our sample. Only 6 of the JADES galaxies in this work have $12 + \log(\text{O/H}) < 7.4$. Furthermore, XMPs at $z \sim 0$ typically have stellar masses $\log(M_*/M_\odot) \lesssim 6 - 7$ (Izotov et al. 2019; Breneman et al. 2025), whereas 94 % of our JADES sample has $\log(M_*/M_\odot) \geq 8$. Thus, the link between nitrogen enhancement in XMPs at $z \sim 0$ and star-forming galaxies observed with JWST at $z > 2$ is unclear, though intriguing.

³ We adopt star-formation rate values from SED fitting rather than $\text{H}\alpha$ measurements to reflect the ‘global’ SFR since, in many cases, the NIRSpec/MSA shutter does not capture the full extent of the galaxy.

Table 2. Nitrogen-enhanced galaxies from the JADES strong-line sample, based on our criteria of $\log(\text{N/O}) > -1.1$ and $12 + \log(\text{O/H}) < 8.0$.

Tier	ID	z_{spec}	$12 + \log(\text{O/H})$	$\log([\text{N II}]/[\text{O II}])$	$\log(\text{N/O})$
goods-n-mediumhst	920	4.885	$7.75^{+0.28}_{-0.23}$	$0.15^{+0.05}_{-0.05}$	$-0.96^{+0.12}_{-0.16}$
goods-s-mediumhst	58656	4.780	$7.96^{+0.11}_{-0.13}$	$0.15^{+0.03}_{-0.03}$	$-0.97^{+0.08}_{-0.1}$
goods-n-mediumhst	946	4.695	$7.64^{+0.16}_{-0.14}$	$0.14^{+0.05}_{-0.05}$	$-0.99^{+0.12}_{-0.17}$
goods-s-mediumjwst	209839	4.468	$7.85^{+0.2}_{-0.17}$	$0.22^{+0.08}_{-0.08}$	$-0.81^{+0.12}_{-0.17}$
goods-s-mediumjwst	51102	4.230	$7.82^{+0.15}_{-0.14}$	$0.17^{+0.06}_{-0.06}$	$-0.91^{+0.12}_{-0.18}$
goods-s-mediumjwst	203994	4.044	$7.93^{+0.22}_{-0.23}$	$0.27^{+0.1}_{-0.1}$	$-0.72^{+0.12}_{-0.18}$
goods-s-mediumjwst	179198	3.831	$7.91^{+0.12}_{-0.13}$	$0.17^{+0.02}_{-0.02}$	$-0.92^{+0.05}_{-0.06}$
goods-s-mediumjwst	10009453	3.705	$7.73^{+0.14}_{-0.14}$	$0.22^{+0.05}_{-0.05}$	$-0.8^{+0.08}_{-0.09}$
goods-s-mediumjwst	50234	3.700	$7.63^{+0.14}_{-0.13}$	$0.11^{+0.04}_{-0.04}$	$-1.09^{+0.11}_{-0.16}$
goods-s-mediumhst	17349	3.491	$7.62^{+0.14}_{-0.12}$	$0.19^{+0.06}_{-0.06}$	$-0.87^{+0.12}_{-0.16}$
goods-s-mediumjwst	51204	3.472	$7.94^{+0.12}_{-0.13}$	$0.11^{+0.04}_{-0.04}$	$-1.09^{+0.13}_{-0.19}$
goods-s-mediumjwst	63722	3.060	$7.96^{+0.12}_{-0.13}$	$0.18^{+0.03}_{-0.03}$	$-0.89^{+0.06}_{-0.07}$
goods-n-mediumhst	23873	2.941	$7.68^{+0.18}_{-0.15}$	$0.17^{+0.05}_{-0.05}$	$-0.93^{+0.1}_{-0.13}$
goods-s-mediumjwst	282381	2.107	$7.74^{+0.14}_{-0.13}$	$0.16^{+0.05}_{-0.05}$	$-0.95^{+0.11}_{-0.16}$

Table 3. Nitrogen-enhanced galaxies from the JADES T_e -based sample, based on our criteria of $\log(\text{N/O}) > -1.1$ and $12 + \log(\text{O/H}) < 8.0$. Abundance measurements can be found in Table 1.

Tier	ID	z_{spec}
goods-n-mediumhst	607	5.1822
goods-s-mediumjwst	206035	4.7735
goods-n-mediumjwst	42939	3.4671
goods-n-mediumhst	31940	3.1295
goods-n-mediumhst	24755	2.9803

4.3 Relationship with galaxy properties

We now turn our attention to exploring whether there exists any correlation between N/O and galaxy properties. Figure 8 shows N/O abundance ratios of our JADES sample as a function of stellar mass (M_*), star formation rate (SFR), the surface density of each of these properties (Σ_{M_*} & Σ_{SFR}), specific star formation rate (sSFR), and the $\text{H}\alpha$ equivalent width. We divide our sample into $12 + \log(\text{O/H}) \leq 8.16$ (purple) and $12 + \log(\text{O/H}) > 8.16$ (pink), with that cut being set as the median metallicity, to explore how trends may differ in each of these metallicity regimes. In addition to our JADES T_e -based and strong-line sample (diamonds and circles, respectively), we also show a selection of N III]- and N IV]-emitters compiled from the literature (hexagons) and $z \sim 0$ CLASSY galaxies from Arellano-Córdova et al. (2025a) (squares).

To explore which properties correlate more strongly with N/O, we calculate Kendall's τ coefficients, allowing for upper limits as described in Isobe et al. (1986) and implemented by Flury et al. (2022) and Herenz et al. (2025)⁴.

Considering just the T_e -based $z > 1$ measurements, we find the strongest correlation with Σ_{SFR} ($\tau_{\Sigma_{\text{SFR}}} = 0.45$; $p = 10^{-4}$), while SFR and Σ_{M_*} also return clear correlations ($\tau_{\text{SFR}} = 0.36$; $p = 0.002$ and $\tau_{\Sigma_{M_*}} = 0.35$, $p = 0.004$). A weaker correlation is observed for sSFR ($\tau_{\text{sSFR}} = 0.26$; $p = 0.03$), while we find no correlation with M_* ($\tau_{M_*} = -0.04$; $p = 0.71$).

This T_e -based sample is heavily biased toward galaxies with low

metallicity ($12 + \log(\text{O/H}) \lesssim 8.0$). A great strength of our strong-line analysis is our ability to extend to much higher metallicities. Revisiting these correlations, instead for our full sample of JADES strong-line measurements, we find the correlations with SFR, Σ_{SFR} , and Σ_{M_*} are much milder; $\tau_{\text{SFR}} = 0.20$ ($p < 10^{-6}$), $\tau_{\Sigma_{\text{SFR}}} = 0.11$ ($p < 10^{-3}$), and $\tau_{\Sigma_{M_*}} = 0.14$, $p < 10^{-4}$, respectively. On the other hand, the correlation with mass ($\tau_{M_*} = 0.20$, $p < 10^{-6}$) becomes much more significant. Meanwhile, we do not find any correlation with either sSFR or $EW_0(\text{H}\alpha)$ in our strong-line sample ($\tau_{\text{sSFR}} = 0.01$, $p = 0.71$; $\tau_{EW(\text{H}\alpha)} = 0.00$, $p = 0.86$).

One take-home message arising here is that, considering the full sample, N/O abundances correlate with each of M_* , SFR, Σ_{M_*} , and Σ_{SFR} . However, the fact that the correlation with M_* emerged much more significantly for the full JADES strong-line sample, which extends the sample to much higher metallicities, suggests the correlation with mass is driven by these most metal rich systems. Indeed, considering only the high-metallicity sample ($12 + \log(\text{O/H}) > 8.16$), we find the strongest correlation with stellar mass $\tau_{M_*} = 0.34$, compared to 0.33, 0.21, and 0.20 for SFR, Σ_{SFR} , and Σ_{M_*} , respectively, albeit highly significant ($p < 10^{-5}$) in all cases. This suggests that the nitrogen enrichment in the evolved, chemically-mature portion of our sample is dominated by older stars. This is consistent with the $z \sim 0$ picture (e.g. Romano 2022), suggesting secondary enrichment from AGB stars has already taken over as the dominant source of nitrogen for galaxies with $Z \gtrsim 0.3 Z_\odot$ at $z \sim 2 - 7$. However, the diversity of N/O abundance ratios found among low-metallicity systems correlates more strongly with SFR and Σ_{SFR} , suggesting that enhanced nitrogen abundances at these low metallicities are driven by properties of the young stellar populations during strong starburst events.

In Figure 9, we recast this slightly by showing how the fraction of nitrogen-enhanced galaxies in our sample changes in bins of these same galaxy properties. Employing the same $12 + \log(\text{O/H}) = 8.16$ cut, we divide our high- and low-metallicity samples into five equally-population bins of (a) stellar mass, (b) SFR, (c) Σ_{M_*} , and (d) Σ_{SFR} . The low-metallicity sample has total of 268 galaxies and the high-metallicity sample has 269, resulting in 53 – 54 galaxies per bin. We calculate the ‘enhanced-N/O fraction’ simply as the number of

⁴ <https://github.com/Knusper/kendall>

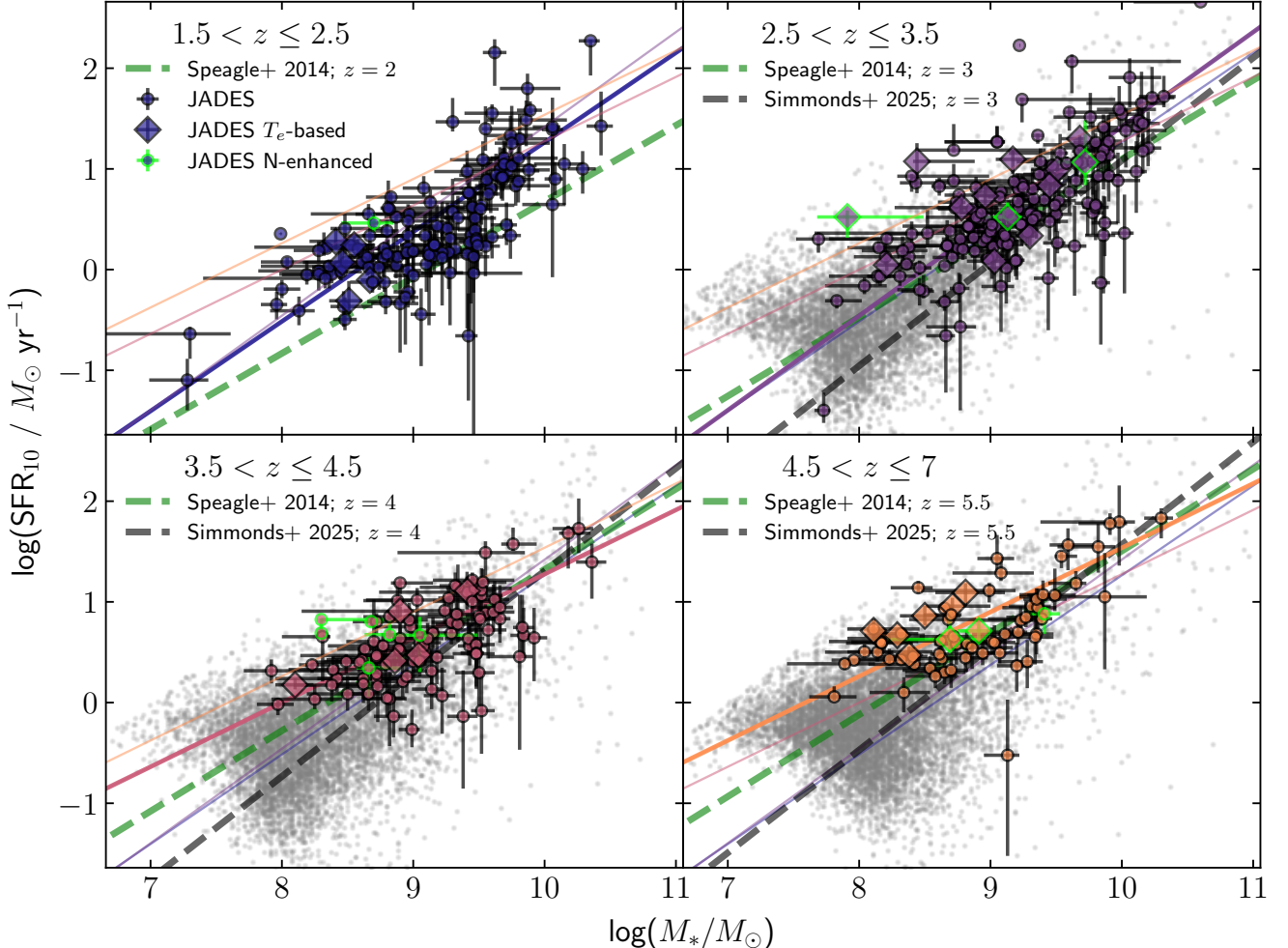


Figure 7. Stellar mass vs. star formation rate derived from SED fitting for our JADES sample in bins of redshift. Points with green outlines are nitrogen-enhanced galaxies (see Section 4.2). Solid lines are carried across all panels and show the best fit relation to each of the four sub-samples. The green and black dashed lines show the evolving star-forming main sequence fits from Speagle et al. (2014) and Simmonds et al. (2025) respectively. The sample from Simmonds et al. (2025) are shown as grey points with a $m_{F444W} < 29$ cut applied.

galaxies in that bin that have a [N II] detection that puts $\log(\text{N}/\text{O}) > -1.1$ divided by the total number of galaxies in that bin.

The [N II] line is well-detected across much of our sample, especially in our high-metallicity sample and our high stellar mass bins, although we note that for approximately 44 % of our sample, we only have an upper limit on [N II] (and, by extension, $\log(\text{N}/\text{O})$). The majority of these upper limits are sufficiently constraining to be able to confirm $\log(\text{N}/\text{O}) < -1.1$. However, for 15 % of the total strong-line sample, we cannot conclusively identify the galaxy as ‘nitrogen-enhanced’ or not, with these being particularly prominent in the low mass and low SFR bins of the low-metallicity sample. The vertical errorbars in Figure 9 quantify the contribution of these galaxies which lack a strong constraint on $\log(\text{N}/\text{O})$. The upper extent of the errorbar shows the fraction that would be obtained if half of the ‘indeterminate’ cases proved to fall in the enhanced-N/O category.

We again find clear evidence for a strong correlation between N/O and stellar mass in the high-metallicity sample. Almost no nitrogen-enhanced galaxies are found below $\log(M_*/M_\odot) < 9.5$, but the fraction rapidly increases above this threshold, with over 60 % of the galaxies in the highest mass bin exceeding our N/O cut.

The interpretation of the low-metallicity sample is hampered by the much larger fraction for which we cannot determine whether the galaxy is nitrogen-enhanced. The N-enhanced galaxies that we do identify tend have higher masses and star-formation rates, although it is only in the highest bins that the fraction ever rises above 20 %. This suggests that while galaxies with $\log(\text{N}/\text{O}) > -1.1$ arise naturally as galaxies grow in mass and metallicity, their existence below $12 + \log(\text{O}/\text{H}) \lesssim 8.16$ tends to be reserved for only systems going through particularly strong starbursts. Deeper data pushing the detection limit to lower values of $\log(\text{N}/\text{O})$, would shed more light onto this picture.

4.4 Relationship with electron density

Arellano-Córdova et al. (2025a) found a correlation between electron density from the [S II] doublet (n_e [S II]) and $\log(\text{N}/\text{O})$ for $z \sim 0$ galaxies from the CLASSY survey. It is particularly pertinent for us to test for a correlation in our strong-line sample since electron density is an important factor in the conversion from [N II]/[O II] to N/O (see Figure 4 and discussion in Section 3.2).

Figure 10 shows all our JADES galaxies for which we have a

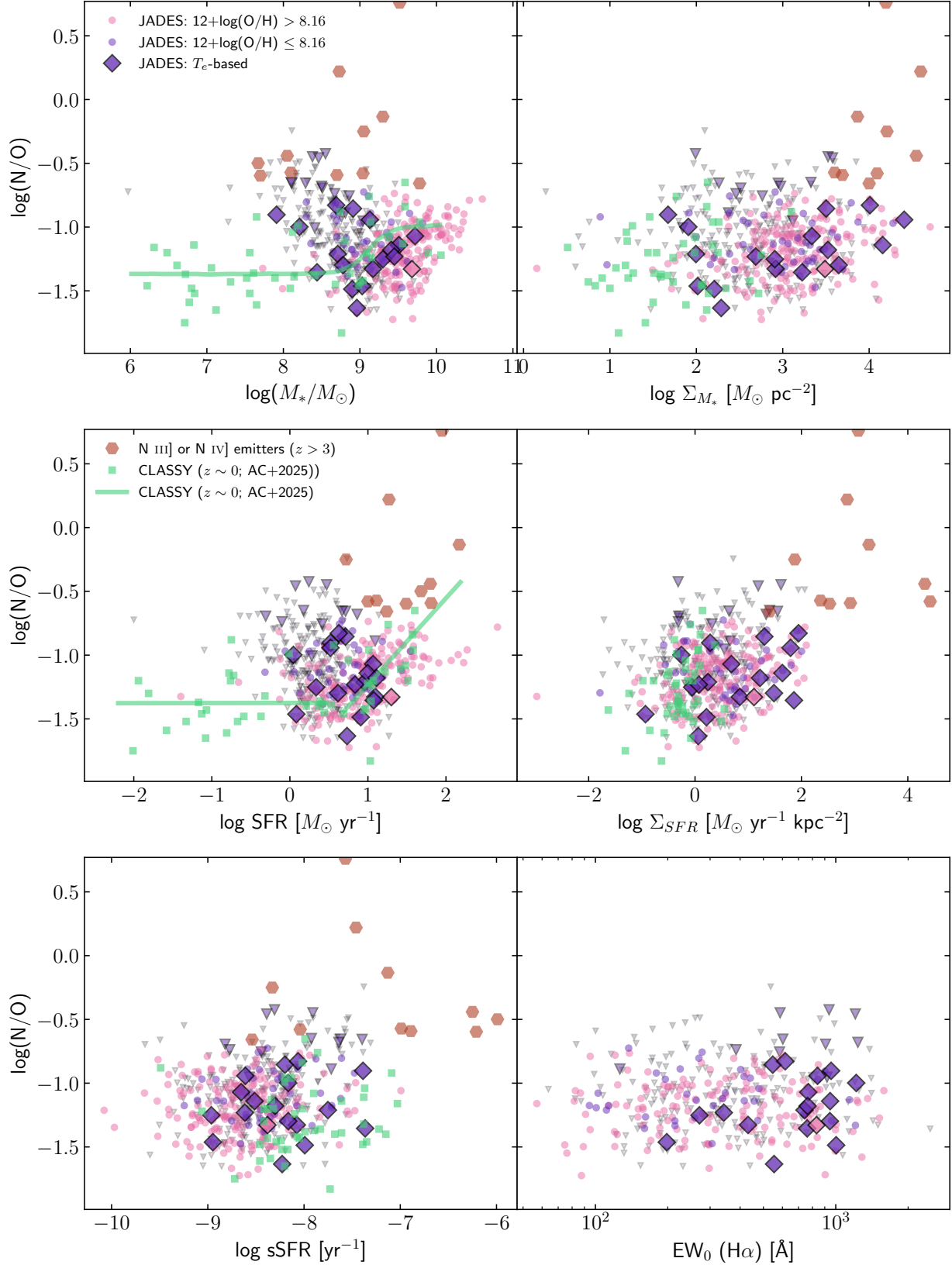


Figure 8. N/O abundances as a function of galaxy properties. From left-to-right, top-to-bottom, these properties are: stellar mass, stellar mass surface density, star formation rate, star formation rate surface density, specific star formation rate, and equivalent width of $\text{H}\alpha$. In each panel, we show our T_e -based measurements (diamonds) alongside strong-line measurements (circles), each divided into $12 + \log(\text{O}/\text{H}) \leq 8.16$ (purple) and $12 + \log(\text{O}/\text{H}) > 8.16$ (pink) sub-samples. Upper limits are denoted by triangles. High-redshift N III] - and N IV] -emitters are shown as brown hexagons (Martinez et al. 2025), while green squares show $z \sim 0$ galaxies from CLASSY (Arellano-C  rdova et al. 2025a) for reference.

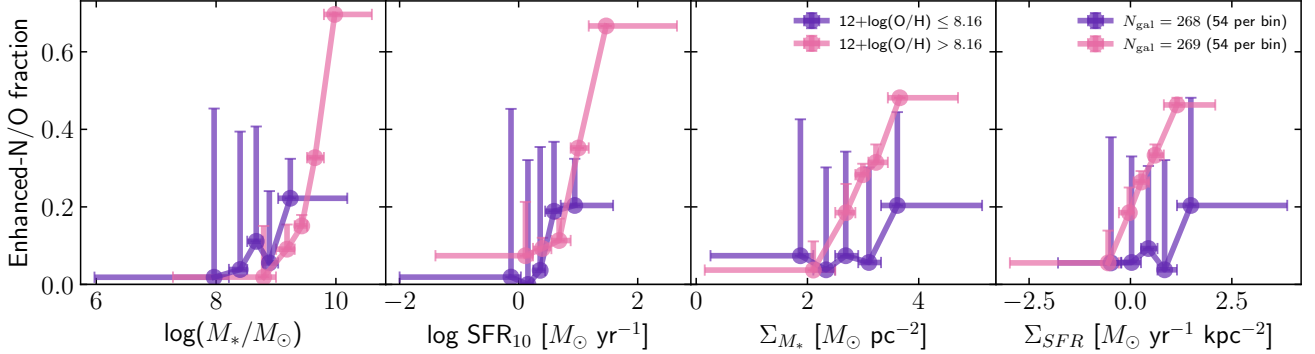


Figure 9. Fraction of galaxies with $\log(\text{N/O}) > -1.1$ for each of the $12 + \log(\text{O/H}) \leq 8.16$ (purple) and $12 + \log(\text{O/H}) > 8.16$ (pink) sub-samples of our JADES sample in equally-populated bins of (a) stellar mass, (b) star formation rate, (c) stellar mass surface density, and (d) star formation rate surface density.

constraint on both $\log(\text{N/O})$ and n_e . In our T_e -based abundance measurements, we derive $\log(\text{N/O})$ using the density constraint that we have, removing the systematic uncertainty we might have due to density. For this sample (diamonds), we find no correlation between $\log(\text{N/O})$ and n_e ($\tau = 0.03$, $p = 0.87$).

For our strong-line sample, 268 galaxies have a detection of at least one [S II] line, allowing us to place a constraint on the n_e . These galaxies (pink and purple circles) also show no correlation between $\log(\text{N/O})$ and n_e ($\tau = -0.01$, $p = 0.78$). As shown in Figure 4, an increase in density from $n_e = 100 \text{ cm}^{-3}$ to 10^4 cm^{-3} increases the [N II]/[O II] ratio by approximately 0.3 dex at fixed N/O abundance. Inverting this, the same density change can cause $\log(\text{N/O})$ to be overestimated by 0.3 dex if not taken into account. This uncertainty is much smaller than the dynamic range of $\log(\text{N/O})$ values spanned by our sample. Moreover, the relation fit by Arellano-Córdova et al. (2025a) implies that $\log(\text{N/O})$ changes by ~ 0.9 dex over a 2 dex range in n_e in their sample. This is larger than the overall spread in $\log(\text{N/O})$ in our sample, suggesting that whatever drives this effect within the CLASSY sample is not strongly affecting our JADES sample at high redshift.

In 171 galaxies in the strong-line sample, we do not have any n_e [S II] constraint. This is typically due to a non-detection of [S II], but in some cases the [S II] doublet is not within the spectral coverage. For the majority of these (143/171), this is simply a case of a low signal-to-noise spectrum as these also only have an upper limit on [N II] (and by extension $\log(\text{N/O})$). In the middle panel of Figure 10, we plot the distribution of $\log(\text{N/O})$ values obtained for the remaining 28 of these cases, compared to the full sample. We see that this subsample has a slightly higher median value: -1.10 , rather than -1.18 for the full strong-line sample.

One interpretation could be that deeper data would reveal these galaxies to have higher densities. If this were the case, the elevated [N II]/[O II] ratios we observe, which here are being interpreted as elevated N/O abundance ratios, could in fact be due to an elevated n_e . This interpretation would imply that this fraction of our sample might be biased high by ~ 0.1 dex. Alternatively, this could simply represent the fact that the majority of cases where we have no [S II] detection are lower signal-to-noise spectra and the fact that we've limited this histogram to detections of [N II] implicitly biases them to only including galaxies with high N/O, where [N II] is therefore sufficiently strong so as to be detected.

In the bottom panel of Figure 10 we then show the distribution

of signal-to-noise on the H β line for each of these sub-samples. The sample with [S II] non-detections is clearly biased to lower S/N (median=9.5, rather than 13.7 for the full sample). Furthermore, none of these galaxies have $S/N_{H\beta} > 25$. Combined with the fact that actually most of the [S II] non-detections are also [N II] non-detections (143/171), we conclude that the effect we're seeing here is primarily a signal-to-noise effect.

That said, we note that the [S II] doublet is only sensitive at densities below $n_e \lesssim 10^4 \text{ cm}^{-3}$ and will underestimate the average density in an inhomogeneous system, especially if a significant quantity of gas with $n_e \gtrsim 10^4 \text{ cm}^{-3}$ is present (Martinez et al. 2025). We cannot rule out that this trend may look different if we revisited the relationship between N/O and density using deeper data with access to diagnostics such as C III] $\lambda 1907/\lambda 1909$ or [Ar IV] $\lambda 4714/\lambda 4742$ which are sensitive to higher densities.

In summary, we find no evidence that our strong-line N/O measurements are strongly biased by not accounting for n_e , due to the lack of any correlation among galaxies that do have measurements of n_e , and from the distribution of $\log(\text{N/O})$ values derived for galaxies that do not have n_e constraints. Furthermore, the correlation reported by Arellano-Córdova et al. (2025a) is sufficiently steep that its presence would outweigh the n_e -induced systematic uncertainty. The fact that we find no such correlation in our sample suggests that the nitrogen enrichment mechanisms in our $z > 1.5$ sample differ from those in the CLASSY sample.

5 DISCUSSION

5.1 Why are [N II]-enhancements milder than N III]- and N IV]-enhancements?

Perhaps the most significant finding in this work is that while 13 % of our $12 + \log(\text{O/H}) < 8.0$ sample has $\log(\text{N/O}) > -1.1$ ('moderately nitrogen-enhanced' hereafter), we do not identify any galaxies across our sample with [N II]-based abundances exceeding $\log(\text{N/O}) > -0.6$, typical of the extreme N III] and N IV] emitters identified with *JWST* ('extremely nitrogen-enhanced' hereafter). There is consensus now that the strong rest-frame UV nitrogen emission found at high-redshift generally does represent highly enhanced N/O (e.g. Cameron et al. 2023a; Senchyna et al. 2023; Martinez et al. 2025; Zhu et al. 2025). Hayes et al. (2025) showed that, for their emission line ratios derived from stacked spectra, assuming a high density

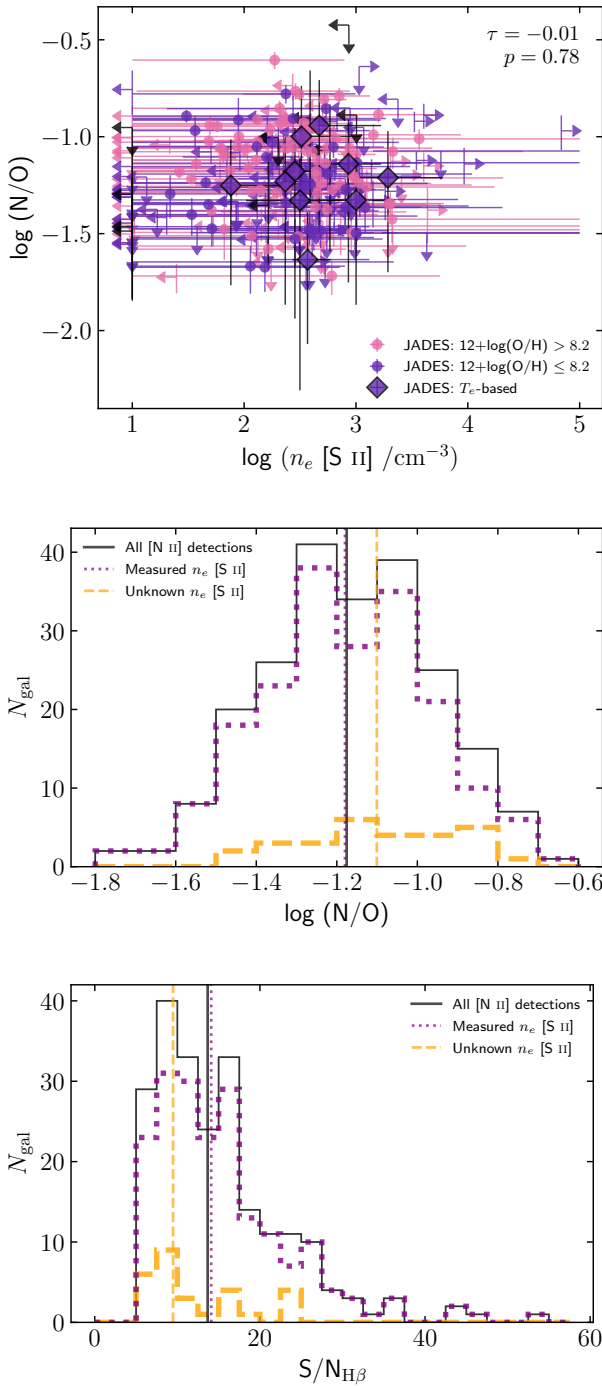


Figure 10. *Top:* Relation between $\log(N/O)$ and electron density (n_e) for all galaxies in our strong-line and T_e -based samples for which we can derive n_e constraints from the [S II] doublet. *Middle:* Histogram of $\log(N/O)$ values for all galaxies in the strong-line sample with [N II] detections (black; i.e. not including upper limits on $\log(N/O)$). The purple dotted histogram shows the subset of these with an n_e constraint from [S II] (either measured value or upper- or lower-limit). The orange dashed histogram shows the subset without any n_e constraint, due to a non-detection of [S II]. Vertical lines show the median values of each of these samples. *Bottom:* Histogram of signal-to-noise ratio on the $H\beta$ emission line for the same sub-samples as shown in the middle panel.

(10^6 cm^{-3}) resulted in a higher derived O/H, which may move otherwise discrepant N/O values much closer to the high metallicity end of the $z \sim 0$ N/O–O/H relation. However, the multi-phase modeling presented in Martinez et al. (2025) found that the majority of known strong N III]- and N IV]-emitters remained in the $12 + \log(\text{O/H}) \lesssim 8.0$ regime.

As discussed in Section 3, assuming hotter low-ionisation temperatures (T_e [O II]) would increase N/O abundances in our low-metallicity [N II]-based sample, but not enough to reconcile them with the N III]- and N IV]-emitting sample (see Figure 5). Meanwhile, adopting higher densities, perhaps under the assumption that n_e ([S II]) is underestimating the average density, would instead decrease the derived N/O abundances. This rules out that the difference in abundances between [N II]-based and UV-based N/O determinations is caused by systematic uncertainties impacting the accuracy of the abundance measurements.

Therefore, two possible explanations for the lack of galaxies with $\log(N/O) > -0.6$ in our [N II]-based sample could be: (1) galaxies are chemically stratified, and the most extreme N/O enhancements are only observed in central, highly-ionised zones, or (2) this reflects a sample selection effect, and extreme values of $\log(N/O) > -0.6$ are only observed in the most extreme starburst systems which are not adequately represented in our JADES [N II] sample.

5.1.1 Chemically stratified galaxies?

Although many of the N III]- and N IV]-emitters lack spectra with a detection of [N II]⁵, several examples now exist that bridge this divide. Berg et al. (2025) measured [N II]-based abundance for the lensed N IV]-emitter RXCJ2248 at $z = 6.1$, finding $\log(N/O)_{\text{N}^+} = -0.502$. While this is marginally lower than the N/O abundances inferred from the higher ionisation states, it is still highly super-solar, and more nitrogen-enhanced than anything in our JADES sample. Similarly, the [N II]-based abundance observed in the Sunburst Arc – another lensed galaxy – was found to be significantly enhanced ($\log(N/O) = -0.65^{+0.16}_{-0.25}$, Welch et al. 2025), albeit somewhat lower than that observed from N III] measurements ($\log(N/O) \approx -0.24$; Pascale et al. 2023). One nitrogen-enhanced galaxy in our sample (gsmj_206035) overlapped with the N III]- and N IV]-selected sample from Morel et al. (2025), again suggesting that the high- and low-ionisation abundances can be in good agreement. On the other hand, Ji et al. (2024) showed that the [N II]-based abundance was more than 1.0 dex lower than the N IV]-based abundance in GS_3073, a galaxy observed to host a broad-line AGN (Übler et al. 2023), suggesting a stratified structure with heterogeneous chemical enrichment across the different ionisation zones.

Expanding the sample of galaxies which have high signal-to-noise measurements of all of [N II], N III], and N IV] would clearly shed more light onto what fraction of galaxies exhibit any kind of chemical stratification. Nonetheless, while the evidence here is mixed, it is clear that at least some N IV]-emitting galaxies are not chemically stratified and can have $\log(N/O) > -0.6$ as measured from [N II], which raises the question of why our JADES sample does not identify any galaxies with abundances in this range.

⁵ In many cases, this is because they are $z > 7$ and [N II] $\lambda 6583$ cannot be observed with *JWST*/NIRSpec, or they lack $R \gtrsim 1000$ spectroscopy, and [N II] $\lambda 6583$ cannot be deblended from H α . In some cases, it is simply that this line is undetected, due to insufficient depth.

5.1.2 Impact of sample selection

We now turn our attention to how our JADES sample selection might contribute to the lack of extremely nitrogen-enhanced galaxies in this work. The majority of our JADES $1.5 < z < 5.7$ parent sample comes from a m_{F444W} -based pre-selection, approximating a mass-based cut (see [Curtis-Lake et al. 2025](#) and Section 2). We then applied an emission line signal-to-noise cut, essentially setting a minimum SFR for our sample, albeit a fairly permissive one, with the star-forming main sequence well sampled down to at least $\log(M_*/M_\odot) \approx 9.0$ (see Figure 7). At higher redshifts ($z > 5.7$), where most N III]- and N IV]-emitters are found, spectroscopic sample selections typically rely more on m_{UV} -based selections (since the rest-frame optical is progressively less available to *JWST*/NIRCam imaging), which is more akin to a SFR-based selection.

With this in mind, the low fraction of extremely nitrogen-enhanced galaxies compared to higher redshifts could reflect that much more of our sample comes from a mass-based selection, sampling the star-forming main sequence, and that the extremely nitrogen-enhanced galaxies identified at higher redshift give us a biased picture.

Another possibility is that the absence of extremely nitrogen-enhanced galaxies from our sample simply reflects that these extreme emitters are either too highly ionised or have too high n_e to be picked up in our sample. If the [N II] $\lambda 6583$ and [O II] $\lambda\lambda 3726, 3729$ lines are too weak, owing to a low N⁺ and O⁺ abundance (i.e., too highly ionised) or the collisional suppression of these lines (expected at $n_e \gtrsim 10^5 \text{ cm}^{-3}$), we might simply miss these galaxies. Note that this differs from the chemically stratified scenario – in this scenario, the low-ionisation ([N II]-emitting) gas is still highly N/O enhanced, but we do not detect the low-ionisation lines at the depth of this study. In the case of RXCJ2248 ([Topping et al. 2024](#); [Berg et al. 2025](#)), it's clear that shallower spectroscopy would still identify the N/O enhancement based on N IV], but it is only with exceptionally deep spectroscopy that [N II] can be accurately measured.

Instead, at moderate spectroscopic depths, [N II]-based samples such as this work are representative of ‘typical’ star-forming conditions, where a significant fraction of the emission comes from low-ionisation gas. Several other studies exploring [N II]-based abundances in low metallicity galaxies at $z \gtrsim 2$ have similarly identified ample moderately nitrogen-enhanced systems, but very few extremely nitrogen-enhanced objects ([Cataldi et al. 2025b](#); [Zhang et al. 2025](#); [Stiavelli et al. 2025](#)). This suggests that the absence of extreme nitrogen-enhancements in our sample is not simply an effect of the way JADES galaxies are selected, but rather reflects that systems with extreme nitrogen-enhancements have very weak low-ionisation lines.

5.2 What sources drive nitrogen enhancement at low metallicity?

We now turn our attention to how these findings relate to the mechanisms that drive nitrogen-enhancement at high-redshift. Identifying the dominant sources of nitrogen enrichment requires first establishing whether nitrogen-enhancements represent enrichment from previous generations (and that we are witnessing stars forming from nitrogen-enhanced gas), or whether they reflect enrichment from the current generation of stars, with young massive stars directly enriching the H II regions.

Our finding that the most extreme nitrogen-enhancements are limited to the most extreme starbursts supports the latter scenario. If nitrogen-enhancement arose from properties of previous generations of stars or from dilution, outflows, and gas-mixing effects then we

would expect to see such enhancements across a diverse range of star-formation conditions, implying a stronger representation in this sample.

Instead, the fact that [N II]-based studies do not seem to identify extreme N/O-enhancements supports the scenario in which the enrichment is driven by the young stars that are also responsible for powering the emission. This then raises the question of what, if any, connection there is between the extreme nitrogen-enhancements seen in UV-based studies, and the mild nitrogen-enhancements seen in the [N II]-based studies, such as this work.

Many explanations have been put forward that explain the observed nitrogen enhancement in the context of prompt enrichment from massive stars ($\gtrsim 50 M_\odot$). Enrichment from Wolf-Rayet (WR) stars, expected to have progenitor masses $\gtrsim 40 M_\odot$ at SMC metallicity and below ([Shenar et al. 2020](#)), is believed to be an important source of nitrogen at low metallicity ([Limongi & Chieffi 2018](#)) and has been invoked in many models of nitrogen-enhanced systems ([Bekki & Tsujimoto 2023](#); [Kobayashi & Ferrara 2024](#); [Zhang et al. 2025](#)). Conventional WR models overproduce carbon relative to what is observed in extremely nitrogen-enhanced galaxies, prompting some studies to instead invoke winds of rotating massive stars without WR enrichment (e.g. [Tapia et al. 2024](#)), VMS winds ([Vink 2023](#)), or SMS winds (e.g. [Charbonnel et al. 2023](#); [Nagele & Umeda 2023](#)). On the other hand, [Berg et al. \(2025\)](#) argued that abundances can be reconciled by extrapolating the observed increase in WN/WC ratio from the Milky Way to the SMC down to even lower metallicity, an argument supported by recent observations of low metallicity stars that may be evolving directly from WN to WO stars, skipping the WC phase ([Sander et al. 2025](#)).

The relative lack of extremely [N II]-enhanced systems found here could indicate that our moderately nitrogen-enhanced galaxies are an extension of these massive-star-based scenarios toward slightly less extreme star formation rates. If milder star-formation events are not always capable of fully populating the upper regions of the stellar IMF ($\gtrsim 50 - 200 M_\odot$, as variously invoked aforementioned studies) it might naturally follow that these systems do not attain the extreme nitrogen-enhancements seen for more intense starbursts. Moreover, the existence of a significant population of moderately nitrogen-enhanced objects suggests that extremely nitrogen-enhanced galaxies are not a discrete population, but rather the upper-most extension of a broad distribution. This may favour explanations invoking enrichment from a distributed population of objects (e.g. many $\sim 50 - 200 M_\odot$ stars) over solutions involving a single monolithic source (e.g. a $> 1000 M_\odot$ SMS).

However, an alternative explanation is that these moderately nitrogen-enhanced systems might reflect the remnants of extremely nitrogen-enhanced galaxies after a short-lived phase. If a softening radiation field resulting from an aging population (leading to an increased [N II]/N IV] ratio), is mirrored by a decreasing N/O abundances due to increased oxygen enrichment from CCSNe, the result could be a galaxy that appears closer to the star-forming main sequence and maintains an abundance pattern similar to the moderately nitrogen-enhanced galaxies identified in this study.

Ultimately, more detailed studies of nitrogen-enhanced galaxies are needed to accurately determine the properties of the sources responsible for this enrichment. One promising approach is to directly search for stellar features in the spectra of these galaxies. From deep $R \sim 1000$ spectroscopy, [Berg et al. \(2025\)](#) identified Wolf-Rayet wind features in the spectrum of RXCJ2248. Meanwhile [Zhang et al. \(2025\)](#) also found tentative evidence for Wolf-Rayet features in a moderately nitrogen-enhanced system. This provides compelling evidence that massive stars in this brief evolutionary phase are at least

part of the solution. It is also worth noting that the wind features of Wolf-Rayet stars may not be as prominent at low metallicity, and the absence of Wolf-Rayet features in an integrated spectrum does not necessarily confirm their absence (González-Torà et al. 2025).

Given these massive stars impact on very local scales, detailed spatially resolved data will also be very insightful. Gravitational lensing is, of course, very appealing in this endeavour. Many studies have explored enrichment in the Sunburst Arc on small scales (Pascale et al. 2023; Choe et al. 2025; Rivera-Thorsen et al. 2025; Welch et al. 2025). While $z > 1.5$ galaxies in blank fields cannot be studied on parsec spatial scales, it is worth noting that many of the galaxies in this study show extended and/or clumpy morphologies. An example of this is gnmh_31940, which has two clumps which, given the slit alignment, are resolvable along the spatial direction (Figure 2, bottom row). The global spectrum resulted in a N-rich abundance pattern of $\log(\text{N/O}) = -0.90^{+0.62}_{-0.35}$, but extracting 1D spectra for each clump separately, we tentatively obtain an even higher N/O abundance in the central clump ($\log(\text{N/O}) \approx -0.72$; see Appendix A). This further highlights that nitrogen enhancement likely arises from processes happening on very small scales, and detailed studies with high spatial resolution will be an important component of establishing a complete picture. Revisiting correlations between nitrogen abundances and physical properties on a spatially-resolved scale is beyond the scope of this paper, but may reveal important new insights.

6 CONCLUSIONS

We have presented a systematic analysis of nitrogen abundances based on measurements of the [N II] $\lambda 6583$ emission line in galaxies at redshifts $1.5 < z < 7.0$ from the JADES survey. Arising from singly-ionised nitrogen, this line is sensitive to nitrogen abundances across galaxies with a wider range of ISM conditions than the rest-frame UV N III] and N IV] lines that have been widely studied at high redshift.

After removing AGN and employing a cut of $\text{S/N}_{H\beta} > 5$, we assembled a sample of 588 galaxies, of which 40 had $> 3\sigma$ detections of the [O III] $\lambda 4363$ auroral line, affording temperature-based abundance measurements. We find that our T_e -based N/O measurements have a significant dependence on the adopted calibration between the high-ionisation T_e [O III] and the low-ionisation T_e [O II], with the final N/O abundance changing by more than 0.14 dex depending on which relation is adopted. Poorly constrained n_e can give rise to over 0.3 dex of systematic uncertainty, however for over half of our sample we are able to place adequate constraints on n_e [S II] to alleviate this uncertainty. Furthermore, we find no correlation between electron density and derived N/O, suggesting our measurements are not systematically biased by density variations.

Comparing our T_e -based abundances to strong-line calibrations from the literature, we find that our sample is in good agreement with the calibrations of Pérez-Montero & Contini (2009) and Cataldi et al. (2025b), favouring a steeper relation than is derived from higher metallicity samples in Hayden-Pawson et al. (2022) or Florido et al. (2022).

Our [N II]-based nitrogen abundance measurements are sensitive to much lower N/O values than N III]- and N IV]-based measurements, with individual measurements from our T_e -based sample probing as low as $\log(\text{N/O}) \approx -1.63$, below typical N/O abundances in local metal-poor dwarf galaxies (e.g. Berg et al. 2019), allowing us to probe the primary plateau at high-redshift. Under conservative assumptions around T_e - and n_e -structure, we find that our low-metallicity (i.e., $12 + \log(\text{O/H}) < 8.2$) T_e -based sample has an average N/O value of

$\log(\text{N/O}) = -1.26 \pm 0.03$, at least 0.1 dex higher than values found at $z \approx 0$ (e.g. Scholte et al. 2026). Furthermore, we identify six galaxies for which we measure $\log(\text{N/O}) > -1.1$, a threshold which is very rarely exceeded in the same O/H range at $z \approx 0$ (Bhattacharya & Kobayashi 2025). Applying strong-line measurements to the remainder of our sample, we find an additional 14 candidate galaxies with $12 + \log(\text{O/H}) < 8.0$ and $\log(\text{N/O}) > -1.1$, suggesting that as many as 13 % of star-forming galaxies at $1.5 < z < 7$ may be ‘nitrogen-enhanced’.

Despite the presence of many ‘moderately nitrogen-enhanced’ ($\log(\text{N/O}) > -1.1$) galaxies in our sample, we find a notable absence of [N II]-based abundances exceeding $\log(\text{N/O}) > -0.6$, values which are typical of the $z > 3$ N III]- and N IV]-emitters. This suggests that these most extreme N/O ratios are only reached during the most extreme starburst phases, and not during mild star-formation activity, which our sample is much more heavily weighted towards. Indeed, we find N/O abundance among low-metallicity systems at $z > 1.5$ to correlate with Σ_{SFR} , SFR, and Σ_{M_*} , further highlighting that the strongest nitrogen enhancements are found in the most extreme systems.

This favours an interpretation in which the nitrogen enrichment in low-metallicity systems observed at high-redshift is dominated by young massive stars from the present generation of star formation, rather than scenarios in which a star cluster is formed from nitrogen-rich gas. If nitrogen-enhanced galaxies represent a brief phase of a galaxy’s evolution, the lower typical nitrogen enhancements from our [N II]-based sample could reflect the fact that, in milder bursts of star formation, the impact from these massive stars is reduced. Alternatively, our [N II]-based sample might tend to pick up milder systems that are the remnants of extreme N III]- and N IV]-emitters as they are in the process of evolved down to more typical N/O abundances.

Meanwhile, for the high metallicity portion of our sample ($12 + \log(\text{O/H}) > 8.0$), we find that N/O correlates strongly with M_* . This is in line with the chemical evolution picture at $z \sim 0$, suggesting that, even at $z \sim 1.5-7$, nitrogen enrichment of more massive, chemically-mature systems is dominated by secondary nitrogen enrichment from intermediate-mass AGB stars.

It is clear now that the extreme nitrogen abundances observed in N III]- and N IV]-emitting galaxies do not represent a discrete population of unusual systems, but rather are the extreme end of a distribution of nitrogen abundances observed in low metallicity systems at high redshift. Better characterising the properties of the stars responsible for this enrichment and how they might impact other galaxy properties, such as feedback budget, ionising photon output, and mass-to-light ratios, will be greatly aided by detailed analyses of deep spectroscopy capable of spatially and spectrally resolving key features of massive stars.

ACKNOWLEDGEMENTS

The authors wish to thank Danielle Berg and Karla Arellano-Córdova for helpful discussions in relation to this work. This work is based on observations made with the NASA/ESA/CSA James Webb Space Telescope. The data were obtained from the Mikulski Archive for Space Telescopes at the Space Telescope Science Institute, which is operated by the Association of Universities for Research in Astronomy, Inc., under NASA contract NAS 5-03127 for JWST. AJC & JW gratefully acknowledges support from the Cosmic Dawn Center through the DAWN Fellowship. The Cosmic Dawn Center (DAWN) is funded by the Danish National Research Foundation under grant

No. 140. AJC, AJB, JC & AS acknowledge funding from the "First-Galaxies" Advanced Grant from the European Research Council (ERC) under the European Union's Horizon 2020 research and innovation programme (Grant agreement No. 789056). CC, ZJ, BDI, BER & CNAW acknowledge support from the JWST/NIRCam Science Team contract to the University of Arizona, NAS5-02105. CC, BER & JAAT acknowledge support from JWST Program 3215. Support for program 3215 was provided by NASA through a grant from the Space Telescope Science Institute, which is operated by the Association of Universities for Research in Astronomy, Inc., under NASA contract NAS 5-03127. JAAT also acknowledges support from the Simons Foundation. CS, XJ & JS acknowledge support from the Science and Technology Facilities Council (STFC). CS, XJ & JS acknowledge support by the ERC through Advanced Grant 695671 "QUENCH". CS & XJ acknowledge support by the UKRI Frontier Research grant RISEandFALL. SC acknowledges support by European Union's HE ERC Starting Grant No. 101040227 - WINGS. ECL acknowledges support of an STFC Webb Fellowship (ST/W001438/1). Some funding for this research was provided by the Johns Hopkins University, Institute for Data Intensive Engineering and Science (IDIES). MSS acknowledges support by the Science and Technology Facilities Council (STFC) grant ST/V506709/1. ST acknowledges support by the Royal Society Research Grant G125142. HÜ acknowledges funding by the European Union (ERC APEX, 101164796). Views and opinions expressed are however those of the authors only and do not necessarily reflect those of the European Union or the European Research Council Executive Agency. Neither the European Union nor the granting authority can be held responsible for them. The research of CCW is supported by NOIRLab, which is managed by the Association of Universities for Research in Astronomy (AURA) under a cooperative agreement with the National Science Foundation.

SOFTWARE

In addition to software packages referenced directly in the text, this work made use of the following Python packages: Astropy (Astropy Collaboration et al. 2022), CMasher (van der Velden 2020), LMFIT (Newville et al. 2014), Matplotlib (Hunter 2007), NumPy (Harris et al. 2020), PyNeb (Luridiana et al. 2015), and SciPy (Virtanen et al. 2020).

DATA AVAILABILITY

This study primarily makes use of data from JADES (Eisenstein et al. 2023a). The spectroscopic data are available for direct download⁶ or by querying the JADES database⁷ and have been described in detail in Bunker et al. (2023a), D'Eugenio et al. (2025), Curtis-Lake et al. (2025), and Scholtz et al. (2025a). The imaging has been described in Rieke et al. (2023), Johnson et al. (2026) and Robertson et al. (2026).

REFERENCES

Aihara H., et al., 2011, *ApJS*, **193**, 29

Amayo A., Delgado-Ingla G., Stasińska G., 2021, *MNRAS*, **505**, 2361

Arellano-Córdova K. Z., et al., 2025a, *arXiv e-prints*, p. arXiv:2507.11658

⁶ <https://jades-survey.github.io/scientists/data.html>

⁷ <https://jades.herts.ac.uk/search/>

Arellano-Córdova K. Z., et al., 2025b, *MNRAS*, **540**, 2991

Astropy Collaboration et al., 2022, *ApJ*, **935**, 167

Bekki K., Tsujimoto T., 2023, *MNRAS*, **526**, L26

Berg D. A., Erb D. K., Henry R. B. C., Skillman E. D., McQuinn K. B. W., 2019, *ApJ*, **874**, 93

Berg D. A., Pogge R. W., Skillman E. D., Croxall K. V., Moustakas J., Rogers N. S. J., Sun J., 2020, *ApJ*, **893**, 96

Berg D. A., et al., 2022, *ApJS*, **261**, 31

Berg D. A., et al., 2025, *arXiv e-prints*, p. arXiv:2511.13591

Bhattacharya S., Kobayashi C., 2025, *arXiv e-prints*, p. arXiv:2508.11998

Breneman J. A., McQuinn K. B. W., Menchaca A., Berg D. A., Telford O. G., Newman M. J. B., Dolphin A., Zeimann G. R., 2025, *ApJ*, **991**, 191

Bunker A. J., et al., 2023a, *arXiv e-prints*, p. arXiv:2306.02467

Bunker A. J., et al., 2023b, *A&A*, **677**, A88

Cameron A. J., Katz H., Rey M. P., Saxena A., 2023a, *MNRAS*, **523**, 3516

Cameron A. J., et al., 2023b, *A&A*, **677**, A115

Campbell A., Terlevich R., Melnick J., 1986, *MNRAS*, **223**, 811

Carniani S., et al., 2024, *A&A*, **685**, A99

Castellano M., et al., 2024, *ApJ*, **972**, 143

Cataldi E., et al., 2025a, *arXiv e-prints*, p. arXiv:2504.03839

Cataldi E., et al., 2025b, *arXiv e-prints*, p. arXiv:2512.07955

Chabrier G., 2003, *PASP*, **115**, 763

Charbonnel C., Schaefer D., Prantzos N., Ramírez-Galeano L., Fragoz T., Kuruvanthodhi A., Marques-Chaves R., Gieles M., 2023, *A&A*, **673**, L7

Choe S., et al., 2025, *A&A*, **698**, A16

Conroy C., Gunn J. E., 2010, FSPS: Flexible Stellar Population Synthesis, Astrophysics Source Code Library, record ascl:1010.043 (ascl:1010.043)

Curti M., et al., 2020, *MNRAS*, **492**, 821

Curti M., et al., 2023, *arXiv e-prints*, p. arXiv:2304.08516

Curtis-Lake E., et al., 2025, *arXiv e-prints*, p. arXiv:2510.01033

DESI Collaboration et al., 2024, *AJ*, **167**, 62

D'Eugenio F., et al., 2025, *ApJS*, **277**, 4

Eisenstein D. J., et al., 2023a, *arXiv e-prints*, p. arXiv:2306.02465

Eisenstein D. J., et al., 2023b, *arXiv e-prints*, p. arXiv:2310.12340

Ferruit P., et al., 2022, *A&A*, **661**, A81

Florido E., Zurita A., Pérez-Montero E., 2022, *MNRAS*, **513**, 2006

Flury S. R., et al., 2022, *ApJ*, **930**, 126

Garnett D. R., 1992, *AJ*, **103**, 1330

González-Torà G., et al., 2025, *arXiv e-prints*, p. arXiv:2511.16323

Gordon K. D., Clayton G. C., Misselt K. A., Landolt A. U., Wolff M. J., 2003, *ApJ*, **594**, 279

Groves B. A., Heckman T. M., Kauffmann G., 2006, *MNRAS*, **371**, 1559

Hamel-Bravo M. J., et al., 2025, *MNRAS*, **543**, 1322

Harikane Y., et al., 2025, *ApJ*, **993**, 204

Harris C. R., et al., 2020, *Nature*, **585**, 357

Hayden-Pawson C., et al., 2022, *MNRAS*, **512**, 2867

Hayes M. J., Saldana-Lopez A., Citro A., James B. L., Mingozi M., Scarlata C., Martinez Z., Berg D. A., 2025, *ApJ*, **982**, 14

Herenz E. C., et al., 2025, *A&A*, **693**, A252

Higgins E. R., Vink J. S., Hirschi R., Laird A. M., Sabhahit G., 2025, *A&A*, **699**, A71

Hunter J. D., 2007, *Computing in Science & Engineering*, **9**, 90

Isobe T., Feigelson E. D., Nelson P. I., 1986, *ApJ*, **306**, 490

Isobe Y., et al., 2023, *ApJ*, **959**, 100

Izotov Y. I., Thuan T. X., 1999, *ApJ*, **511**, 639

Izotov Y. I., Guseva N. G., Fricke K. J., Henkel C., 2019, *A&A*, **623**, A40

Jakobsen P., et al., 2022, *A&A*, **661**, A80

Ji X., et al., 2024, *MNRAS*, **535**, 881

Ji X., Belokurov V., Maiolino R., Monty S., Isobe Y., Kravtsov A., McClymont W., Übler H., 2026, *MNRAS*, **545**, staf2110

Johnson B. D., Leja J. L., Conroy C., Speagle J. S., 2019, Prospector: Stellar population inference from spectra and SEDs, Astrophysics Source Code Library, record ascl:1905.025

Johnson B. D., Leja J., Conroy C., Speagle J. S., 2021, *ApJS*, **254**, 22

Kewley L. J., Dopita M. A., Sutherland R. S., Heisler C. A., Trevena J., 2001, *ApJ*, **556**, 121

Kewley L. J., Dopita M. A., Leitherer C., Davé R., Yuan T., Allen M., Groves B., Sutherland R., 2013, *ApJ*, **774**, 100

Kobayashi C., Ferrara A., 2024, *ApJ*, **962**, L6

Kobayashi C., Taylor P., 2023, *arXiv e-prints*, p. arXiv:2302.07255

Kobayashi C., Karakas A. I., Umeda H., 2011, *MNRAS*, **414**, 3231

Kobayashi C., Karakas A. I., Lugaro M., 2020, *ApJ*, **900**, 179

Kriek M., Conroy C., 2013, *ApJ*, **775**, L16

Kriek M., et al., 2015, *ApJS*, **218**, 15

Laseter I. H., et al., 2023, *arXiv e-prints*, p. arXiv:2306.03120

Leja J., Carnall A. C., Johnson B. D., Conroy C., Speagle J. S., 2019, *ApJ*, **876**, 3

Limongi M., Chieffi A., 2018, *ApJS*, **237**, 13

López-Sánchez Á. R., Esteban C., 2010, *A&A*, **517**, A85

Luridiana V., Morisset C., Shaw R. A., 2015, *A&A*, **573**, A42

Madau P., 1995, *ApJ*, **441**, 18

Maiolino R., Mannucci F., 2019, *A&ARv*, **27**, 3

Maiolino R., et al., 2023, *arXiv e-prints*, p. arXiv:2308.01230

Maiolino R., et al., 2024, *Nature*, **627**, 59

Marques-Chaves R., et al., 2023, *arXiv e-prints*, p. arXiv:2307.04234

Martinez Z., et al., 2025, *arXiv e-prints*, p. arXiv:2510.21960

Matteucci F., 2012, Chemical Evolution of Galaxies, doi:10.1007/978-3-642-22491-1.

McClymont W., et al., 2025, *arXiv e-prints*, p. arXiv:2507.08787

Méndez-Delgado J. E., et al., 2023, *MNRAS*, **523**, 2952

Morel I., Schaefer D., Marques-Chaves R., Prantzos N., Charbonnel C., Brammer G., Xiao M., Dessauges-Zavadsky M., 2025, *arXiv e-prints*, p. arXiv:2511.20484

Nagele C., Umeda H., 2023, *ApJ*, **949**, L16

Naidu R. P., et al., 2025, *arXiv e-prints*, p. arXiv:2505.11263

Nandal D., Whalen D. J., Latif M. A., Heger A., 2025, *ApJ*, **994**, L11

Napolitano L., et al., 2025, *ApJ*, **989**, 75

Newville M., Stensitzki T., Allen D. B., Ingargiola A., 2014, LMFIT: Non-Linear Least-Square Minimization and Curve-Fitting for Python, doi:10.5281/zenodo.11813, <https://doi.org/10.5281/zenodo.11813>

Nicholls D. C., Sutherland R. S., Dopita M. A., Kewley L. J., Groves B. A., 2017, *MNRAS*, **466**, 4403

Nomoto K., Kobayashi C., Tominaga N., 2013, *ARA&A*, **51**, 457

Oesch P. A., et al., 2023, *MNRAS*, **525**, 2864

Pascale M., Dai L., McKee C. F., Tsang B. T.-H., 2023, *ApJ*, **957**, 77

Pasha I., Miller T. B., 2023, *The Journal of Open Source Software*, **8**, 5703

Peimbert M., Costero R., 1969, Boletín de los Observatorios Tonantzintla y Tacubaya, **5**, 3

Pérez-Montero E., Contini T., 2009, *MNRAS*, **398**, 949

Pilyugin L. S., Mattsson L., Vílchez J. M., Cedrés B., 2009, *MNRAS*, **398**, 485

Pilyugin L. S., Vílchez J. M., Mattsson L., Thuan T. X., 2012, *MNRAS*, **421**, 1624

Rieke M. J., et al., 2023, *ApJS*, **269**, 16

Rivera-Thorsen T. E., et al., 2025, *arXiv e-prints*, p. arXiv:2510.11702

Rizzuti F., Matteucci F., Molaro P., Cescutti G., Maiolino R., 2025, *A&A*, **697**, A96

Rogers N. S. J., Strom A. L., Rudie G. C., Trainor R. F., Raptis M., von Raesfeld C., 2023, *arXiv e-prints*, p. arXiv:2312.08427

Romano D., 2022, *A&ARv*, **30**, 7

Roy A., Dopita M. A., Krumholz M. R., Kewley L. J., Sutherland R. S., Heger A., 2021, *MNRAS*, **502**, 4359

Sander A. A. C., et al., 2025, *Nature Astronomy*,

Sanders R. L., et al., 2020, *MNRAS*, **491**, 1427

Sanders R. L., Shapley A. E., Topping M. W., Reddy N. A., Brammer G. B., 2023, *arXiv e-prints*, p. arXiv:2303.08149

Sanders R. L., et al., 2025, *arXiv e-prints*, p. arXiv:2508.10099

Schaerer D., Marques-Chaves R., Xiao M., Korber D., 2024, *A&A*, **687**, L11

Schaerer D., et al., 2026, *arXiv e-prints*, p. arXiv:2601.06968

Scholte D., et al., 2026, *arXiv e-prints*, p. arXiv:2601.02463

Scholtz J., et al., 2025a, *arXiv e-prints*, p. arXiv:2510.01034

Scholtz J., et al., 2025b, *A&A*, **697**, A175

Senchyna P., Plat A., Stark D. P., Rudie G. C., 2023, *arXiv e-prints*, p. arXiv:2303.04179

Shenar T., Gilkis A., Vink J. S., Sana H., Sander A. A. C., 2020, *A&A*, **634**, A79

Simmonds C., et al., 2024, *MNRAS*, **535**, 2998

Simmonds C., et al., 2025, *arXiv e-prints*, p. arXiv:2508.04410

Speagle J. S., Steinhardt C. L., Capak P. L., Silverman J. D., 2014, *ApJS*, **214**, 15

Steidel C. C., et al., 2014, *ApJ*, **795**, 165

Stiavelli M., et al., 2025, *ApJ*, **981**, 136

Strom A. L., Steidel C. C., Rudie G. C., Trainor R. F., Pettini M., 2018, *ApJ*, **868**, 117

Strom A. L., et al., 2023, *ApJ*, **958**, L11

Tacchella S., et al., 2022, *ApJ*, **927**, 170

Tapia T., Bekki K., Groves B., 2024, *MNRAS*, **534**, 2086

Topping M. W., et al., 2024, *MNRAS*, **529**, 3301

Topping M. W., et al., 2025, *ApJ*, **980**, 225

Übler H., et al., 2023, *A&A*, **677**, A145

Valentino F., et al., 2025, *A&A*, **699**, A358

Vila-Costas M. B., Edmunds M. G., 1993, *MNRAS*, **265**, 199

Vincenzo F., Kobayashi C., 2018, *MNRAS*, **478**, 155

Vink J. S., 2023, *A&A*, **679**, L9

Virtanen P., et al., 2020, *Nature Methods*, **17**, 261

Watanabe K., et al., 2024, *ApJ*, **962**, 50

Welch B., et al., 2025, *ApJ*, **980**, 33

Williams C. C., et al., 2023, *ApJS*, **268**, 64

Yates R. M., Schady P., Chen T.-W., Schweyer T., Wiseman P., 2020, *A&A*, **634**, A107

Zhang Y., Morishita T., Stiavelli M., 2025, *arXiv e-prints*, p. arXiv:2502.04817

Zhu P., Kewley L. J., Hsiao T. Y.-Y., Trussler J., 2025, *arXiv e-prints*, p. arXiv:2511.03681

van der Velden E., 2020, *The Journal of Open Source Software*, **5**, 2004

APPENDIX A: SPATIAL DECOMPOSITION OF GOODS-N-MEDIUMHST 31940

From imaging of gnmh_31940 (Figure 2, bottom panel), it is clear that the morphology comprises two separate components. The alignment of the slit allows for the spectra of these two clumps to be separated in the 2D spectrum, where we find that they are at the same redshift.

The top panels in Figure A1 show our extraction of the spectra of the two components of gnmh_31940 from the 2D spectrum. The extracted 1D spectra are shown in the subsequent panels, with the full-shutter extracted spectrum shown in black, ‘Component A’ (extracted from the lowermost two rows of spatial pixels in the object shutter) shown in green, and ‘Component B’ (extracted from the uppermost three rows of spatial pixels in the object shutter) shown in blue. We then fit the emission lines in the same way described in Section 2.2.

The 1D spectra shown have been renormalised to the H α flux and we find that the [O II]/H α flux ratios are very similar across the three 1D spectra. However, the [N II]/[O II] ratio is much higher in the spectrum extracted for Component B, corresponding to a nitrogen-to-oxygen abundance ratio of $\log(\text{N}/\text{O}) \approx -0.72$, around 0.2 dex higher than the value of $\log(\text{N}/\text{O}) = -0.9^{+0.62}_{-0.35}$ reported for the full-shutter extraction in Table 1. We find the [N II] line is undetected in the spectrum of Component A.

While a more detailed analysis is beyond the scope of this paper, this preliminary finding suggests that nitrogen abundances might vary significantly on small spatial scales, suggesting that the processes driving nitrogen-enhancement operate on small physical scales.

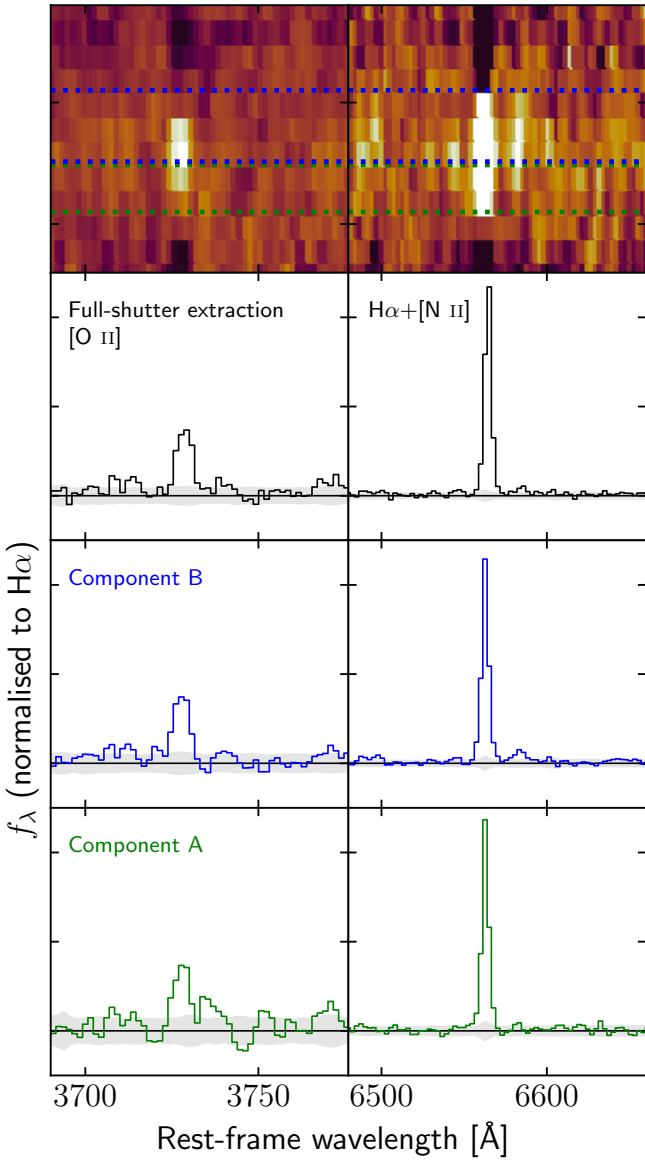


Figure A1. Re-extraction of the spectra for each component for the system observed as goods-n-mediumhst_39140. The imaging thumbnail of this system can be found in the bottom row of Figure 2. The top row shows the 2D spectra for gnmh_31940, zoomed in on the areas around $[\text{O II}] \lambda\lambda 3726, 3729$ and $\text{H}\alpha + [\text{N II}] \lambda 6583$, showing the extractions of component B as the area between the blue dotted lines and component A as the area between the green dotted lines. The full shutter extraction encompasses the union of these two areas. Lower panels show the 1D spectra for the full shutter extraction (black), component B (blue), and component A (green), with each spectrum normalised to the $\text{H}\alpha$ flux. We see that all three spectra have very similar $[\text{O II}]/\text{H}\alpha$ ratios, but component B has a particularly strong $[\text{N II}]$ feature, corresponding to a ~ 0.2 dex higher N/O abundance.

APPENDIX C: TABLE OF STRONG-LINE ABUNDANCE MEASUREMENTS

We present in Table C.1 our strong-line abundance measurements and associated galaxy properties measurements for galaxies with robust properties derived from SED and morphological fitting. In Table C.2 we report additional strong-line measurements for the galaxies without these photometrically-derived properties.

APPENDIX B: NITROGEN-ENHANCED GALAXIES

Figure B1 shows thumbnails and spectra for the other two nitrogen-enhanced galaxies from the T_e -based sample (with the other three being shown in Figure 2). Spectra and thumbnails of all nitrogen-enhanced galaxies from the strong-line sample are shown in Figures B2 – B6.

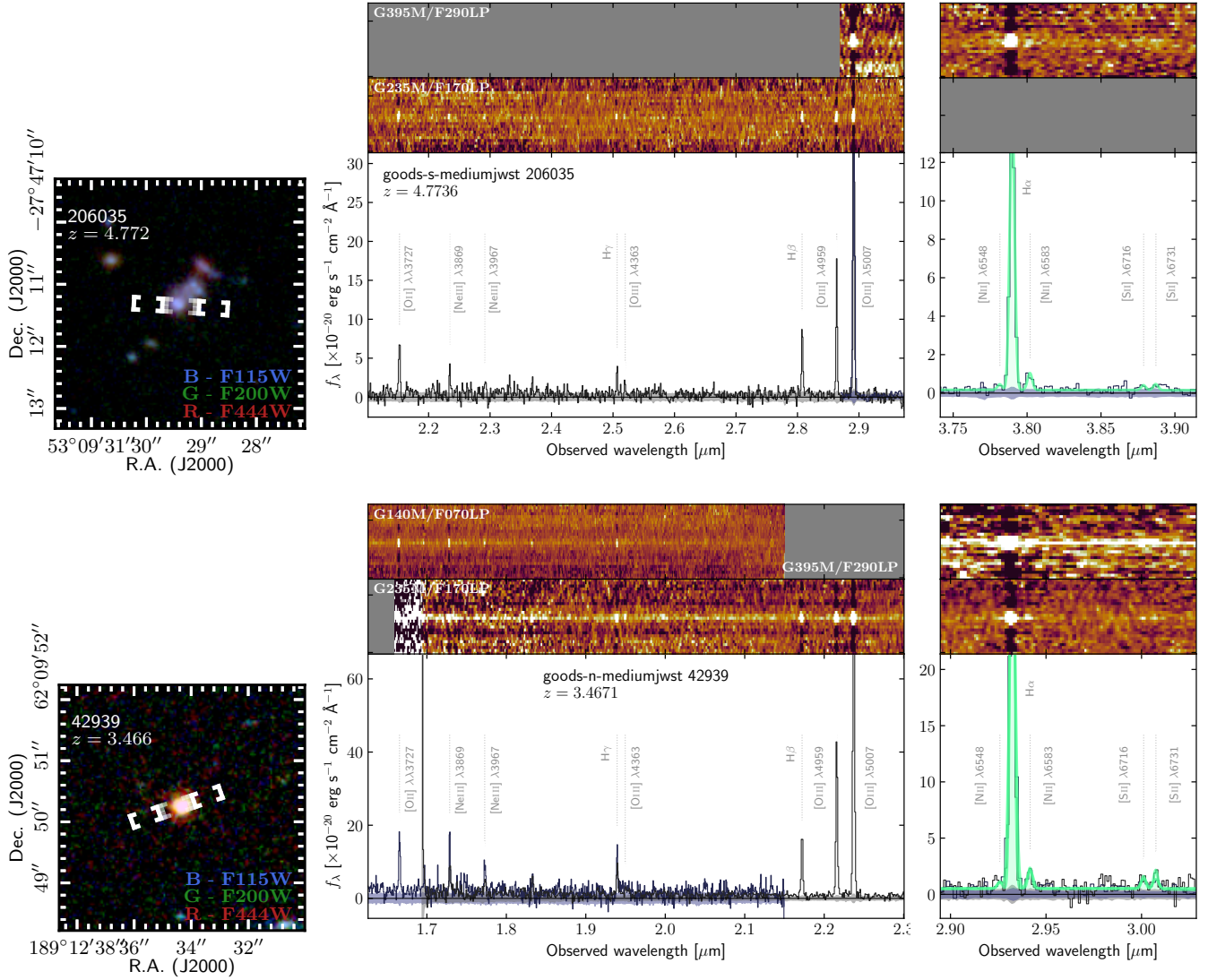


Figure B1. As for Figure 2, showing two additional nitrogen-enhanced galaxies from the T_e -based sample. The upper 2D panel of the second row (gnmj_42939) is shared between G140M/F070LP (left, covering $[\text{O III}] \lambda 5007$) and G395M/F290LP (right, covering $\text{H}\alpha$).

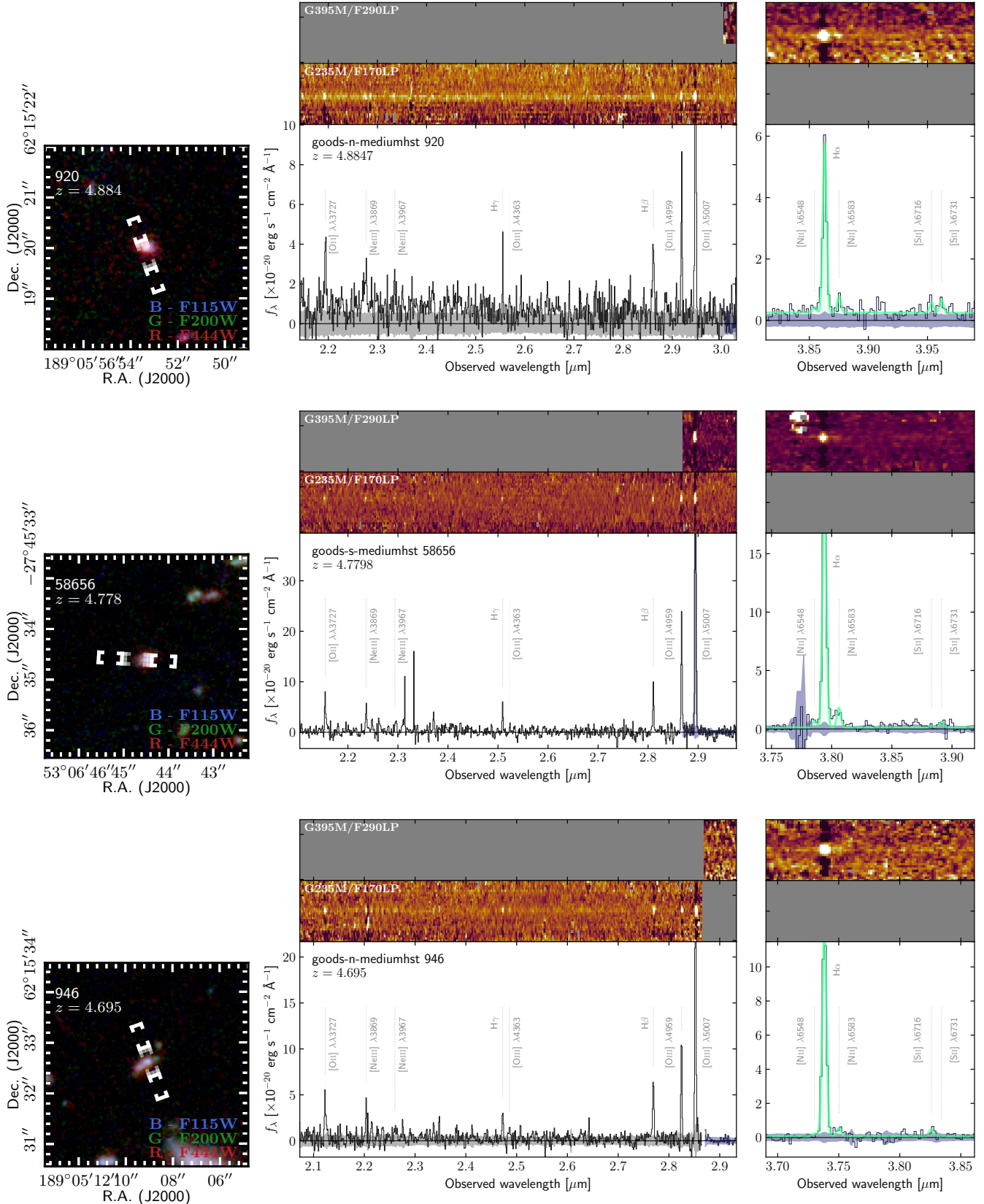


Figure B2. As for Figure B1, showing three nitrogen-enhanced galaxies from the strong-line sample.

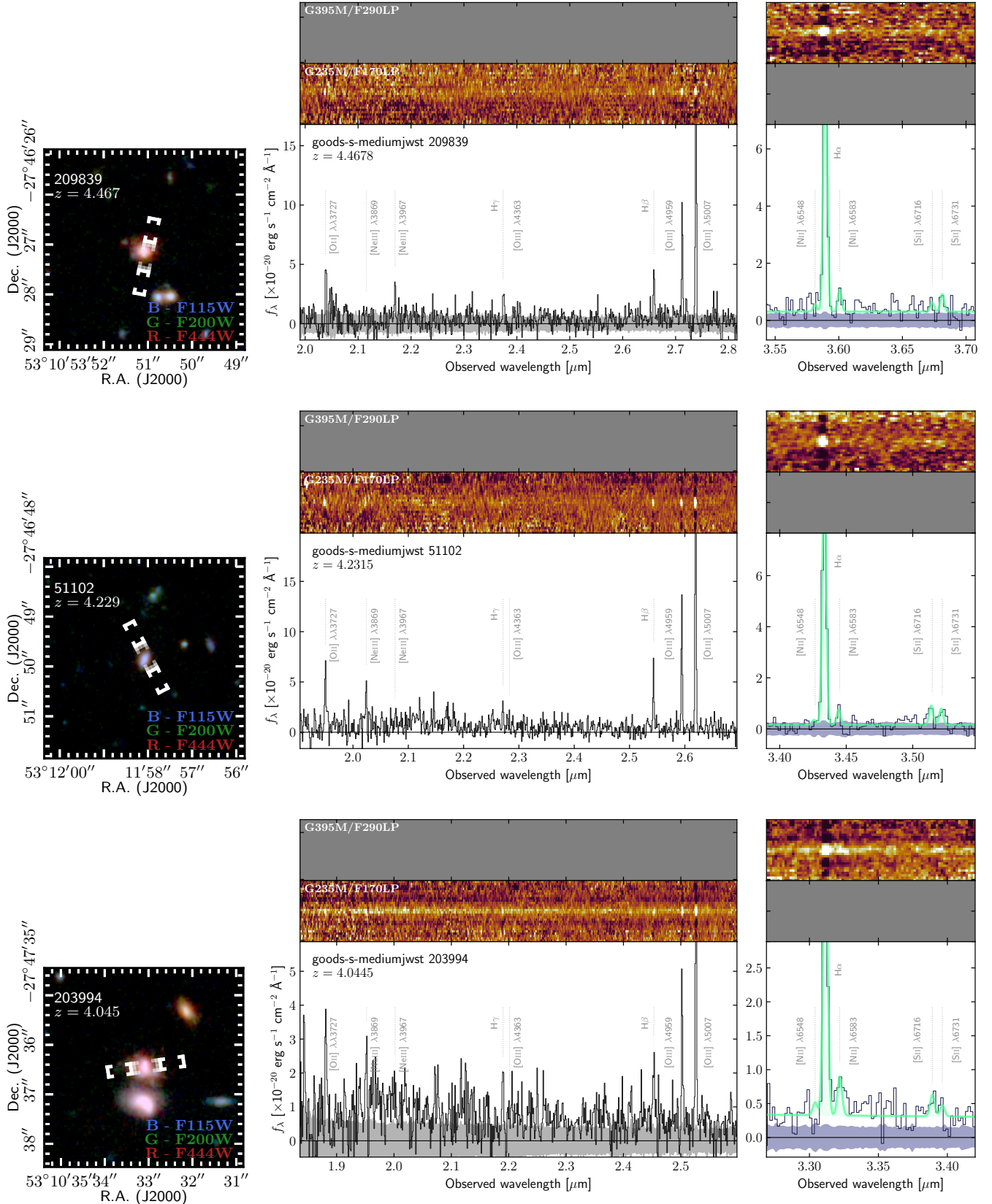


Figure B3. As for Figure B1, showing a further three nitrogen-enhanced galaxies from the strong-line sample.

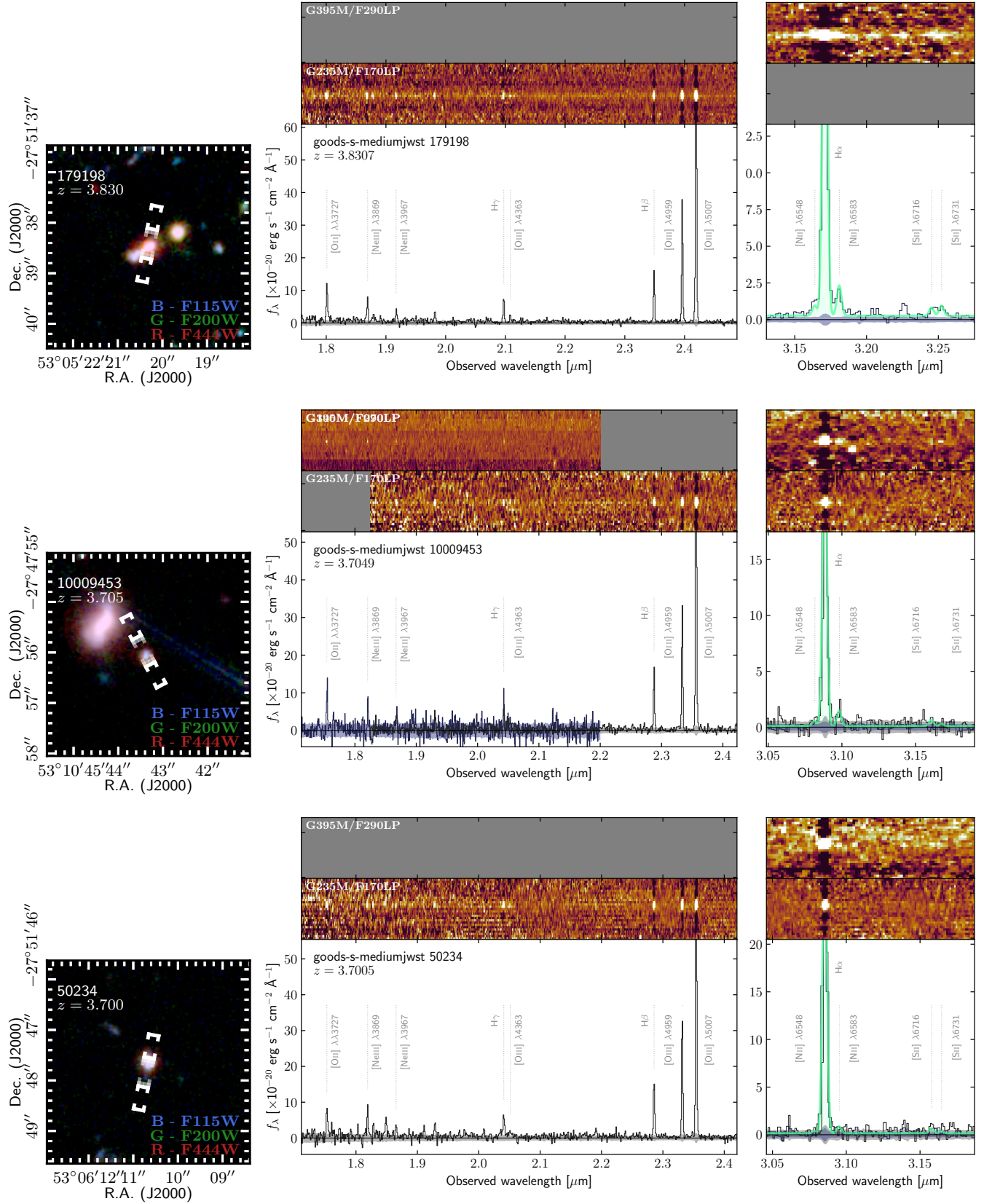


Figure B4. As for Figure B1, showing a further three nitrogen-enhanced galaxies from the strong-line sample.

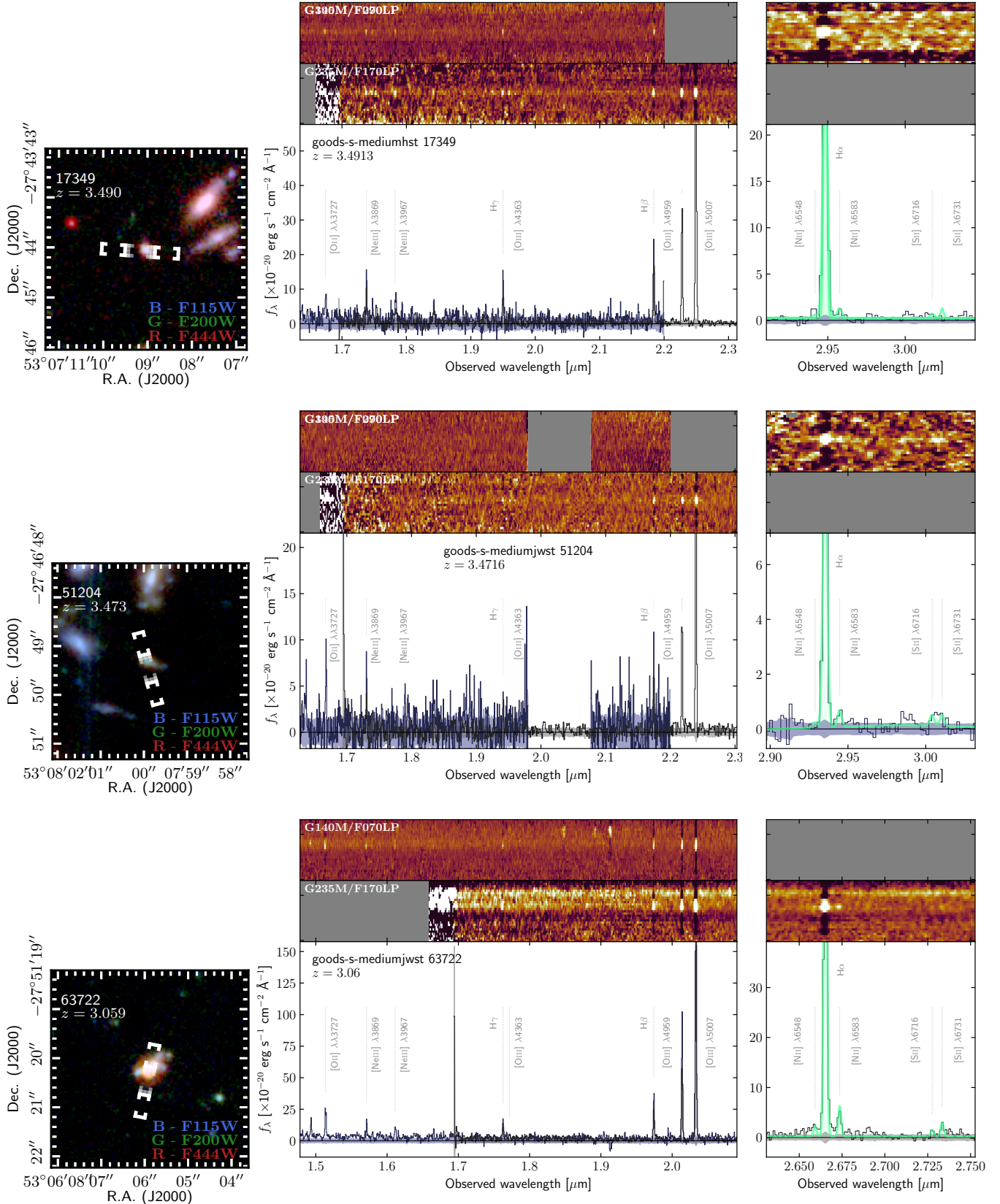


Figure B5. As for Figure B1, showing a further three nitrogen-enhanced galaxies from the strong-line sample.

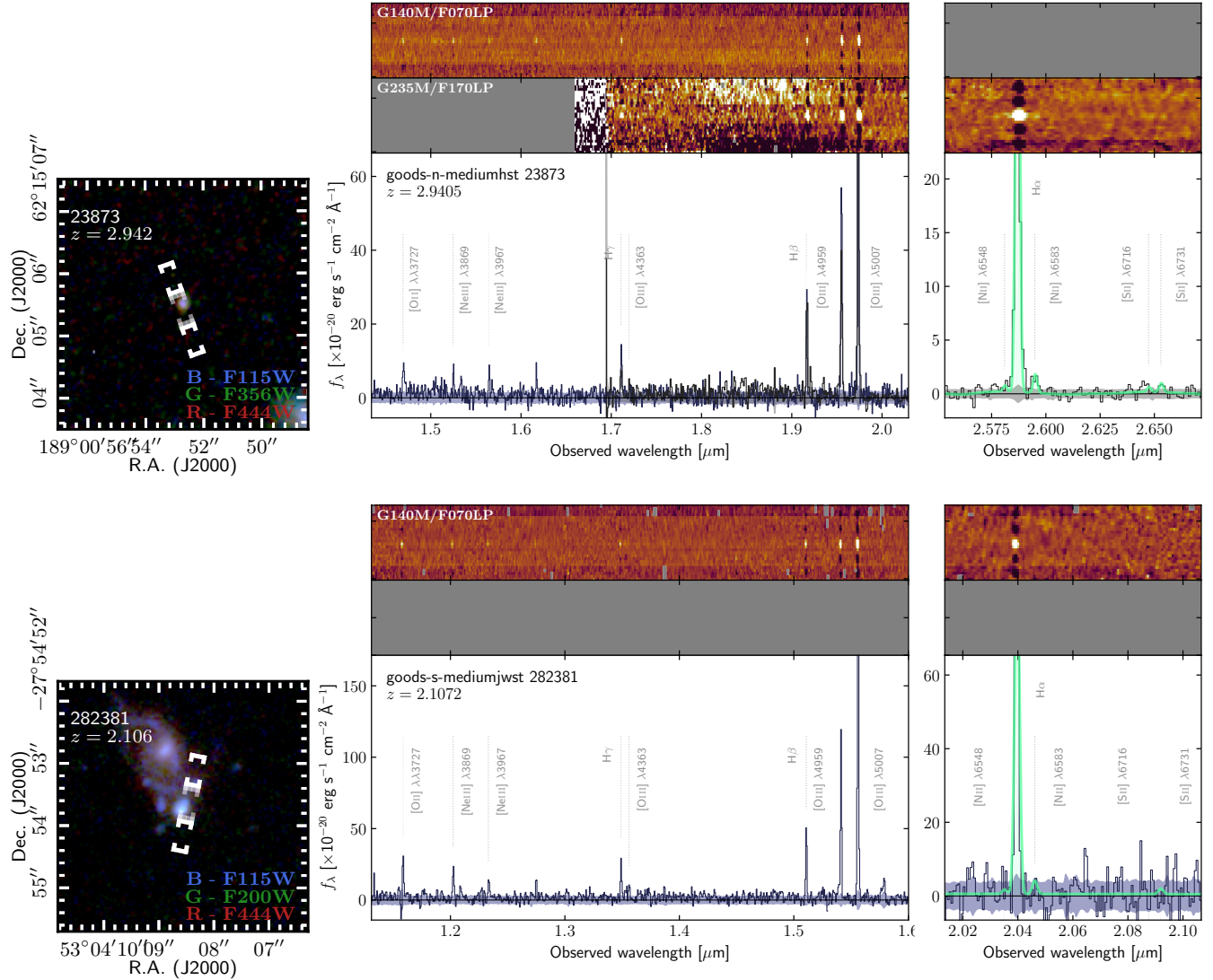


Figure B6. As for Figure B1, showing a further two nitrogen-enhanced galaxies from the strong-line sample.

Table C.1. Strong-line oxygen and nitrogen abundances for the 453 galaxies in our strong-line sample with galaxy properties derived from SED and morphological fitting. Details on the derivation of these quantities can be found in Sections 2 & 3.

Tier	ID	z_{spec}	12+log(O/H)	log(N/O)	log(M_*/M_{\odot})	SFR	Σ_{M_*}	Σ_{SFR}
goods-n-mediumhst	643	5.3458	8.02 $^{+0.1}_{-0.12}$	< -1.37	8.99 $^{+0.2}_{-0.52}$	1.11 $^{+0.07}_{-0.12}$	2.6 $^{+0.2}_{-0.52}$	0.72 $^{+0.07}_{-0.12}$
goods-n-mediumhst	721	5.1778	7.47 $^{+0.11}_{-0.09}$	< -0.49	7.96 $^{+0.25}_{-0.17}$	0.42 $^{+0.01}_{-0.03}$	3.6 $^{+0.25}_{-0.17}$	2.06 $^{+0.01}_{-0.03}$
goods-n-mediumhst	761	5.5449	7.59 $^{+0.16}_{-0.13}$	< -0.53	8.42 $^{+0.2}_{-0.35}$	0.38 $^{+0.09}_{-0.07}$	2.09 $^{+0.2}_{-0.35}$	0.05 $^{+0.09}_{-0.07}$
goods-n-mediumhst	772	3.847	7.96 $^{+0.12}_{-0.13}$	-1.24 $^{+0.09}_{-0.13}$	9.29 $^{+0.04}_{-0.06}$	0.69 $^{+0.05}_{-0.11}$	3.36 $^{+0.04}_{-0.06}$	0.75 $^{+0.05}_{-0.11}$
goods-n-mediumhst	804	3.6614	8.41 $^{+0.07}_{-0.09}$	-0.85 $^{+0.04}_{-0.04}$	9.92 $^{+0.1}_{-0.1}$	0.64 $^{+0.1}_{-0.43}$	3.47 $^{+0.1}_{-0.06}$	0.19 $^{+0.3}_{-0.43}$
goods-n-mediumhst	853	3.4723	8.3 $^{+0.08}_{-0.11}$	-0.89 $^{+0.04}_{-0.04}$	9.9 $^{+0.08}_{-0.08}$	0.93 $^{+0.27}_{-0.26}$	3.66 $^{+0.08}_{-0.08}$	0.69 $^{+0.27}_{-0.26}$
goods-n-mediumhst	896	6.7585	8.1 $^{+0.1}_{-0.12}$	-0.97 $^{+0.08}_{-0.1}$	9.82 $^{+0.13}_{-0.31}$	1.55 $^{+0.23}_{-0.26}$	4.28 $^{+0.13}_{-0.31}$	2.0 $^{+0.23}_{-0.26}$
goods-n-mediumhst	902	4.0612	8.08 $^{+0.13}_{-0.16}$	< -1.2	8.82 $^{+0.41}_{-0.2}$	0.85 $^{+0.06}_{-0.04}$	3.13 $^{+0.41}_{-0.2}$	1.17 $^{+0.06}_{-0.04}$
goods-n-mediumhst	917	4.3996	8.19 $^{+0.16}_{-0.13}$	-0.82 $^{+0.08}_{-0.1}$	9.38 $^{+0.11}_{-0.12}$	-0.14 $^{+0.46}_{-0.72}$	3.07 $^{+0.11}_{-0.12}$	-0.44 $^{+0.46}_{-0.72}$
goods-n-mediumhst	920	4.8849	7.75 $^{+0.28}_{-0.23}$	-0.96 $^{+0.12}_{-0.16}$	9.41 $^{+0.12}_{-0.11}$	0.88 $^{+0.07}_{-0.07}$	3.87 $^{+0.12}_{-0.11}$	1.34 $^{+0.07}_{-0.19}$
goods-n-mediumhst	926	6.7558	8.37 $^{+0.08}_{-0.09}$	-0.81 $^{+0.07}_{-0.08}$	9.59 $^{+0.23}_{-0.14}$	1.57 $^{+0.17}_{-0.25}$	4.01 $^{+0.2}_{-0.14}$	1.99 $^{+0.17}_{-0.25}$
goods-n-mediumhst	993	4.1706	7.77 $^{+0.13}_{-0.13}$	< -0.78	8.61 $^{+0.14}_{-0.27}$	0.42 $^{+0.09}_{-0.07}$	1.59 $^{+0.14}_{-0.27}$	-0.59 $^{+0.09}_{-0.07}$
goods-n-mediumhst	1044	4.0399	7.78 $^{+0.21}_{-0.17}$	< -0.74	8.79 $^{+0.27}_{-0.21}$	0.38 $^{+0.16}_{-0.23}$	2.64 $^{+0.27}_{-0.21}$	0.23 $^{+0.16}_{-0.23}$
goods-n-mediumhst	1048	3.8709	7.87 $^{+0.14}_{-0.14}$	< -1.21	9.05 $^{+0.16}_{-0.19}$	0.59 $^{+0.16}_{-0.12}$	3.25 $^{+0.16}_{-0.19}$	0.8 $^{+0.16}_{-0.12}$
goods-n-mediumhst	1069	3.3223	8.31 $^{+0.07}_{-0.09}$	-1.46 $^{+0.1}_{-0.14}$	9.78 $^{+0.08}_{-0.1}$	0.56 $^{+0.26}_{-0.22}$	2.8 $^{+0.08}_{-0.1}$	-0.42 $^{+0.26}_{-0.22}$
goods-n-mediumhst	1083	3.803	8.02 $^{+0.12}_{-0.13}$	< -1.0	9.22 $^{+0.1}_{-0.14}$	0.07 $^{+0.28}_{-0.38}$	3.94 $^{+0.1}_{-0.14}$	0.78 $^{+0.28}_{-0.38}$
goods-n-mediumhst	1109	3.9178	8.33 $^{+0.13}_{-0.13}$	-1.24 $^{+0.12}_{-0.17}$	9.43 $^{+0.13}_{-0.09}$	0.56 $^{+0.23}_{-0.19}$	3.05 $^{+0.13}_{-0.09}$	0.18 $^{+0.23}_{-0.19}$
goods-n-mediumhst	1121	3.3417	8.33 $^{+0.07}_{-0.08}$	-1.02 $^{+0.03}_{-0.03}$	9.8 $^{+0.13}_{-0.17}$	1.26 $^{+0.09}_{-0.17}$	3.58 $^{+0.13}_{-0.17}$	1.05 $^{+0.09}_{-0.19}$
goods-n-mediumhst	1130	3.967	7.64 $^{+0.18}_{-0.15}$	< -0.77	7.92 $^{+0.48}_{-0.21}$	0.32 $^{+0.11}_{-0.13}$	2.87 $^{+0.48}_{-0.21}$	1.27 $^{+0.11}_{-0.13}$
goods-n-mediumhst	1137	3.6612	8.14 $^{+0.09}_{-0.09}$	-1.27 $^{+0.06}_{-0.06}$	9.62 $^{+0.11}_{-0.24}$	1.02 $^{+0.18}_{-0.15}$	3.34 $^{+0.18}_{-0.24}$	0.74 $^{+0.18}_{-0.15}$
goods-n-mediumhst	1157	4.1627	8.09 $^{+0.11}_{-0.11}$	< -1.15	8.42 $^{+0.16}_{-0.47}$	0.24 $^{+0.2}_{-0.14}$	2.47 $^{+0.16}_{-0.47}$	0.29 $^{+0.2}_{-0.14}$
goods-n-mediumhst	1165	4.3817	7.99 $^{+0.14}_{-0.13}$	-1.27 $^{+0.07}_{-0.09}$	9.15 $^{+0.11}_{-0.17}$	0.69 $^{+0.16}_{-0.17}$	3.13 $^{+0.11}_{-0.17}$	0.67 $^{+0.16}_{-0.17}$
goods-n-mediumhst	1233	3.3324	8.4 $^{+0.06}_{-0.08}$	-0.99 $^{+0.06}_{-0.06}$	10.16 $^{+0.07}_{-0.07}$	1.18 $^{+0.17}_{-0.23}$	3.1 $^{+0.07}_{-0.07}$	0.11 $^{+0.17}_{-0.23}$
goods-n-mediumhst	1237	3.3301	8.39 $^{+0.07}_{-0.09}$	-1.05 $^{+0.05}_{-0.05}$	9.86 $^{+0.08}_{-0.15}$	1.18 $^{+0.24}_{-0.39}$	2.94 $^{+0.08}_{-0.15}$	0.26 $^{+0.24}_{-0.39}$
goods-n-mediumhst	1240	3.3346	8.14 $^{+0.1}_{-0.13}$	-1.18 $^{+0.1}_{-0.13}$	8.89 $^{+0.17}_{-0.32}$	0.81 $^{+0.11}_{-0.26}$	3.43 $^{+0.11}_{-0.32}$	1.35 $^{+0.11}_{-0.26}$
goods-n-mediumhst	1560	5.1968	8.09 $^{+0.18}_{-0.22}$	< -1.14	8.54 $^{+0.19}_{-0.34}$	0.34 $^{+0.12}_{-0.09}$	2.08 $^{+0.19}_{-0.34}$	-0.12 $^{+0.2}_{-0.09}$
goods-n-mediumhst	1580	5.2981	8.08 $^{+0.09}_{-0.1}$	< -1.38	9.23 $^{+0.12}_{-0.34}$	0.82 $^{+0.14}_{-0.08}$	3.79 $^{+0.12}_{-0.34}$	1.38 $^{+0.14}_{-0.08}$
goods-n-mediumhst	1674	4.0455	7.99 $^{+0.12}_{-0.14}$	< -1.02	8.92 $^{+0.14}_{-0.21}$	0.21 $^{+0.2}_{-0.15}$	1.71 $^{+0.14}_{-0.21}$	-1.0 $^{+0.2}_{-0.15}$
goods-n-mediumhst	1882	5.4434	8.06 $^{+0.11}_{-0.13}$	-1.08 $^{+0.07}_{-0.09}$	9.39 $^{+0.08}_{-0.41}$	0.83 $^{+0.27}_{-0.07}$	2.0 $^{+0.08}_{-0.41}$	-0.56 $^{+0.27}_{-0.07}$
goods-n-mediumhst	1924	4.4746	7.83 $^{+0.17}_{-0.16}$	< -0.77	8.5 $^{+0.19}_{-0.31}$	0.09 $^{+0.18}_{-0.17}$	2.03 $^{+0.19}_{-0.31}$	-0.38 $^{+0.18}_{-0.17}$
goods-n-mediumhst	1926	4.0413	8.42 $^{+0.06}_{-0.07}$	-1.34 $^{+0.09}_{-0.12}$	9.84 $^{+0.07}_{-0.1}$	0.67 $^{+0.17}_{-0.22}$	3.74 $^{+0.07}_{-0.22}$	0.56 $^{+0.27}_{-0.22}$
goods-n-mediumhst	1927	3.6593	8.27 $^{+0.08}_{-0.1}$	-0.86 $^{+0.04}_{-0.05}$	9.53 $^{+0.18}_{-0.15}$	1.2 $^{+0.13}_{-0.11}$	4.14 $^{+0.18}_{-0.15}$	1.81 $^{+0.13}_{-0.11}$
goods-n-mediumhst	1949	3.8561	8.37 $^{+0.08}_{-0.11}$	-1.06 $^{+0.07}_{-0.08}$	9.51 $^{+0.18}_{-0.2}$	0.83 $^{+0.28}_{-0.31}$	3.0 $^{+0.18}_{-0.2}$	0.31 $^{+0.28}_{-0.11}$
goods-n-mediumhst	1965	4.1914	7.78 $^{+0.18}_{-0.15}$	< -0.79	8.62 $^{+0.29}_{-0.35}$	0.24 $^{+0.18}_{-0.24}$	2.5 $^{+0.29}_{-0.35}$	0.12 $^{+0.18}_{-0.24}$
goods-n-mediumhst	1966	3.2139	8.35 $^{+0.08}_{-0.1}$	-1.12 $^{+0.08}_{-0.11}$	9.38 $^{+0.19}_{-0.18}$	1.07 $^{+0.13}_{-0.15}$	2.81 $^{+0.19}_{-0.18}$	0.5 $^{+0.13}_{-0.15}$
goods-n-mediumhst	1968	4.3246	8.09 $^{+0.09}_{-0.11}$	< -1.43	8.9 $^{+0.1}_{-0.06}$	0.64 $^{+0.11}_{-0.13}$	3.44 $^{+0.1}_{-0.06}$	1.18 $^{+0.11}_{-0.13}$
goods-n-mediumhst	2331	3.9662	8.53 $^{+0.05}_{-0.06}$	-0.87 $^{+0.04}_{-0.05}$	10.26 $^{+0.11}_{-0.2}$	1.73 $^{+0.3}_{-0.24}$	3.65 $^{+0.11}_{-0.2}$	1.12 $^{+0.3}_{-0.24}$
goods-n-mediumhst	2347	5.6349	8.09 $^{+0.09}_{-0.11}$	-1.26 $^{+0.09}_{-0.12}$	9.31 $^{+0.15}_{-0.17}$	0.96 $^{+0.11}_{-0.15}$	3.3 $^{+0.15}_{-0.17}$	0.94 $^{+0.11}_{-0.15}$
goods-n-mediumhst	2845	5.2732	8.22 $^{+0.08}_{-0.1}$	< -1.49	9.11 $^{+0.17}_{-0.25}$	0.68 $^{+0.15}_{-0.18}$	2.85 $^{+0.19}_{-0.25}$	0.42 $^{+0.18}_{-0.19}$
goods-n-mediumhst	2868	3.4026	8.46 $^{+0.07}_{-0.1}$	< -0.97	9.31 $^{+0.09}_{-0.08}$	0.57 $^{+0.18}_{-0.18}$	3.02 $^{+0.09}_{-0.08}$	0.27 $^{+0.18}_{-0.18}$
goods-n-mediumhst	2945	3.3353	8.37 $^{+0.06}_{-0.08}$	-0.97 $^{+0.02}_{-0.03}$	10.0 $^{+0.11}_{-0.1}$	1.54 $^{+0.11}_{-0.15}$	4.17 $^{+0.11}_{-0.1}$	1.71 $^{+0.11}_{-0.15}$
goods-n-mediumhst	3451	3.176	8.44 $^{+0.05}_{-0.06}$	-1.05 $^{+0.03}_{-0.03}$	10.13 $^{+0.09}_{-0.11}$	1.48 $^{+0.22}_{-0.17}$	3.11 $^{+0.09}_{-0.11}$	0.46 $^{+0.22}_{-0.17}$
goods-n-mediumhst	3527	3.4187	8.04 $^{+0.14}_{-0.17}$	< -0.99	9.02 $^{+0.07}_{-0.08}$	0.23 $^{+0.19}_{-0.19}$	2.46 $^{+0.07}_{-0.08}$	-0.33 $^{+0.19}_{-0.19}$
goods-n-mediumhst	3653	4.0828	7.99 $^{+0.17}_{-0.17}$	< -1.1	9.0 $^{+0.1}_{-0.17}$	0.41 $^{+0.14}_{-0.14}$	3.54 $^{+0.1}_{-0.17}$	0.95 $^{+0.14}_{-0.14}$
goods-n-mediumhst	3683	3.6621	7.87 $^{+0.13}_{-0.14}$	-1.11 $^{+0.12}_{-0.18}$	9.09 $^{+0.12}_{-0.17}$	0.5 $^{+0.13}_{-0.14}$	3.0 $^{+0.12}_{-0.15}$	0.41 $^{+0.13}_{-0.14}$
goods-n-mediumhst	18679	2.7449	7.68 $^{+0.2}_{-0.14}$	< -0.79	8.49 $^{+0.08}_{-0.17}$	-0.21 $^{+0.16}_{-0.07}$	2.41 $^{+0.08}_{-0.17}$	-0.3 $^{+0.16}_{-0.07}$
goods-n-mediumhst	20163	1.9826	8.14 $^{+0.11}_{-0.14}$	< -1.24	8.63 $^{+0.28}_{-0.12}$	0.14 $^{+0.07}_{-0.11}$	1.89 $^{+0.28}_{-0.12}$	-0.6 $^{+0.07}_{-0.11}$

Table C.1. (continued)

Tier	ID	z_{spec}	12+log(O/H)	log(N/O)	log(M_*/M_{\odot})	SFR	Σ_{M_*}	Σ_{SFR}
goods-n-mediumhst	20185	2.9302	8.42 $^{+0.06}_{-0.07}$	-1.22 $^{+0.05}_{-0.05}$	9.24 $^{+0.71}_{-0.02}$	1.69 $^{+0.02}_{-0.23}$	2.56 $^{+0.71}_{-0.02}$	1.01 $^{+0.02}_{-0.23}$
goods-n-mediumhst	21747	3.1623	8.19 $^{+0.09}_{-0.11}$	< -1.42	9.21 $^{+0.15}_{-0.14}$	0.6 $^{+0.13}_{-0.09}$	3.38 $^{+0.15}_{-0.14}$	0.78 $^{+0.13}_{-0.09}$
goods-n-mediumhst	21823	2.9889	7.84 $^{+0.15}_{-0.14}$	< -0.96	8.38 $^{+0.12}_{-0.09}$	0.13 $^{+0.05}_{-0.09}$	2.88 $^{+0.12}_{-0.09}$	0.63 $^{+0.05}_{-0.09}$
goods-n-mediumhst	21916	2.3032	8.17 $^{+0.14}_{-0.12}$	< -1.28	8.85 $^{+0.12}_{-0.09}$	0.12 $^{+0.28}_{-0.28}$	2.82 $^{+0.12}_{-0.16}$	0.09 $^{+0.28}_{-0.28}$
goods-n-mediumhst	22279	2.3265	8.4 $^{+0.06}_{-0.07}$	-1.06 $^{+0.03}_{-0.03}$	9.69 $^{+0.11}_{-0.11}$	1.05 $^{+0.16}_{-0.24}$	3.06 $^{+0.11}_{-0.12}$	0.42 $^{+0.16}_{-0.24}$
goods-n-mediumhst	22411	3.6804	8.1 $^{+0.15}_{-0.19}$	-0.76 $^{+0.1}_{-0.13}$	9.11 $^{+0.12}_{-0.12}$	0.63 $^{+0.16}_{-0.14}$	2.38 $^{+0.12}_{-0.26}$	-0.09 $^{+0.16}_{-0.14}$
goods-n-mediumhst	22481	3.3345	8.49 $^{+0.05}_{-0.06}$	-1.1 $^{+0.04}_{-0.04}$	10.12 $^{+0.06}_{-0.09}$	1.42 $^{+0.19}_{-0.22}$	3.16 $^{+0.06}_{-0.09}$	0.46 $^{+0.19}_{-0.22}$
goods-n-mediumhst	22737	3.0721	8.3 $^{+0.08}_{-0.09}$	< -1.47	9.5 $^{+0.12}_{-0.17}$	0.55 $^{+0.17}_{-0.17}$	2.8 $^{+0.12}_{-0.17}$	-0.15 $^{+0.17}_{-0.17}$
goods-n-mediumhst	22812	3.0727	7.86 $^{+0.18}_{-0.18}$	< -1.05	8.83 $^{+0.01}_{-0.01}$	0.43 $^{+0.11}_{-0.01}$	3.34 $^{+0.01}_{-0.1}$	0.94 $^{+0.11}_{-0.01}$
goods-n-mediumhst	22837	4.1515	8.3 $^{+0.1}_{-0.13}$	-0.74 $^{+0.06}_{-0.07}$	9.45 $^{+0.14}_{-0.14}$	1.0 $^{+0.25}_{-0.25}$	3.14 $^{+0.14}_{-0.3}$	0.69 $^{+0.25}_{-0.25}$
goods-n-mediumhst	23167	2.1935	8.33 $^{+0.07}_{-0.07}$	-1.5 $^{+0.09}_{-0.12}$	8.87 $^{+0.47}_{-0.47}$	0.52 $^{+0.06}_{-0.24}$	3.08 $^{+0.47}_{-0.09}$	0.74 $^{+0.24}_{-0.24}$
goods-n-mediumhst	23314	2.3271	8.22 $^{+0.11}_{-0.15}$	-1.28 $^{+0.11}_{-0.15}$	8.96 $^{+0.11}_{-0.35}$	0.34 $^{+0.11}_{-0.12}$	3.08 $^{+0.11}_{-0.35}$	0.46 $^{+0.11}_{-0.12}$
goods-n-mediumhst	23742	3.1263	8.21 $^{+0.11}_{-0.11}$	-0.98 $^{+0.03}_{-0.04}$	9.58 $^{+0.08}_{-0.13}$	1.06 $^{+0.07}_{-0.07}$	3.15 $^{+0.08}_{-0.13}$	0.63 $^{+0.07}_{-0.07}$
goods-n-mediumhst	24249	1.7011	8.03 $^{+0.13}_{-0.16}$	< -1.15	8.44 $^{+0.1}_{-0.21}$	0.03 $^{+0.16}_{-0.12}$	0.68 $^{+0.1}_{-0.21}$	-1.73 $^{+0.16}_{-0.12}$
goods-n-mediumhst	24257	2.9217	8.09 $^{+0.11}_{-0.13}$	< -0.97	8.04 $^{+0.17}_{-0.3}$	-0.16 $^{+0.09}_{-0.08}$	2.83 $^{+0.17}_{-0.3}$	0.63 $^{+0.09}_{-0.08}$
goods-n-mediumhst	24603	1.871	8.14 $^{+0.11}_{-0.14}$	< -1.14	8.96 $^{+0.1}_{-0.2}$	-0.01 $^{+0.15}_{-0.14}$	2.77 $^{+0.1}_{-0.2}$	-0.19 $^{+0.15}_{-0.14}$
goods-n-mediumhst	24728	1.9088	8.5 $^{+0.05}_{-0.06}$	-1.08 $^{+0.03}_{-0.03}$	9.81 $^{+0.21}_{-0.17}$	1.3 $^{+0.24}_{-0.17}$	3.08 $^{+0.21}_{-0.17}$	0.57 $^{+0.24}_{-0.17}$
goods-n-mediumhst	25393	2.9956	8.11 $^{+0.12}_{-0.12}$	< -1.13	8.75 $^{+0.19}_{-0.14}$	0.21 $^{+0.06}_{-0.08}$	2.22 $^{+0.19}_{-0.14}$	-0.32 $^{+0.06}_{-0.08}$
goods-n-mediumhst	26089	1.9941	8.38 $^{+0.06}_{-0.07}$	< -1.41	9.28 $^{+0.1}_{-0.22}$	-0.03 $^{+0.36}_{-0.52}$	2.05 $^{+0.1}_{-0.22}$	-1.26 $^{+0.36}_{-0.52}$
goods-n-mediumhst	26544	2.9722	8.6 $^{+0.04}_{-0.04}$	-1.01 $^{+0.05}_{-0.05}$	10.23 $^{+0.17}_{-0.08}$	1.71 $^{+0.31}_{-0.07}$	3.23 $^{+0.17}_{-0.08}$	0.7 $^{+0.31}_{-0.07}$
goods-n-mediumhst	26566	3.1281	8.31 $^{+0.07}_{-0.08}$	-1.45 $^{+0.08}_{-0.1}$	9.65 $^{+0.07}_{-0.1}$	0.88 $^{+0.18}_{-0.16}$	4.06 $^{+0.07}_{-0.1}$	1.29 $^{+0.18}_{-0.16}$
goods-n-mediumhst	27003	5.596	8.24 $^{+0.08}_{-0.1}$	-1.08 $^{+0.08}_{-0.09}$	9.36 $^{+0.14}_{-0.27}$	0.94 $^{+0.19}_{-0.21}$	3.02 $^{+0.14}_{-0.27}$	0.61 $^{+0.19}_{-0.21}$
goods-n-mediumhst	27145	3.1922	8.19 $^{+0.08}_{-0.09}$	-1.12 $^{+0.05}_{-0.05}$	9.42 $^{+0.15}_{-0.23}$	0.94 $^{+0.15}_{-0.13}$	3.95 $^{+0.15}_{-0.23}$	1.47 $^{+0.15}_{-0.13}$
goods-n-mediumhst	27286	3.1304	8.07 $^{+0.13}_{-0.13}$	-1.14 $^{+0.11}_{-0.15}$	9.52 $^{+0.13}_{-0.3}$	0.68 $^{+0.23}_{-0.23}$	3.32 $^{+0.13}_{-0.3}$	0.48 $^{+0.23}_{-0.23}$
goods-n-mediumhst	27676	2.9789	8.23 $^{+0.09}_{-0.1}$	-1.13 $^{+0.1}_{-0.14}$	9.21 $^{+0.2}_{-0.32}$	0.68 $^{+0.08}_{-0.12}$	2.79 $^{+0.2}_{-0.32}$	0.25 $^{+0.08}_{-0.12}$
goods-n-mediumhst	28044	2.9708	8.25 $^{+0.08}_{-0.1}$	-1.27 $^{+0.1}_{-0.14}$	9.41 $^{+0.14}_{-0.15}$	0.69 $^{+0.14}_{-0.22}$	2.29 $^{+0.14}_{-0.15}$	-0.43 $^{+0.14}_{-0.22}$
goods-n-mediumhst	28082	2.029	8.66 $^{+0.04}_{-0.05}$	-0.91 $^{+0.08}_{-0.1}$	10.15 $^{+0.14}_{-0.23}$	1.05 $^{+0.2}_{-0.41}$	2.83 $^{+0.14}_{-0.23}$	-0.27 $^{+0.2}_{-0.41}$
goods-n-mediumhst	28187	3.2069	8.45 $^{+0.06}_{-0.08}$	-1.01 $^{+0.06}_{-0.07}$	10.03 $^{+0.31}_{-0.24}$	1.38 $^{+0.22}_{-0.37}$	4.05 $^{+0.31}_{-0.24}$	1.4 $^{+0.22}_{-0.37}$
goods-n-mediumhst	28390	1.6766	8.59 $^{+0.04}_{-0.05}$	-1.0 $^{+0.06}_{-0.07}$	9.75 $^{+0.19}_{-0.37}$	1.03 $^{+0.11}_{-0.05}$	3.03 $^{+0.19}_{-0.37}$	0.31 $^{+0.11}_{-0.05}$
goods-n-mediumhst	28640	2.0925	8.35 $^{+0.11}_{-0.17}$	-0.93 $^{+0.09}_{-0.12}$	9.22 $^{+0.13}_{-0.14}$	0.12 $^{+0.31}_{-0.47}$	2.94 $^{+0.13}_{-0.14}$	-0.16 $^{+0.31}_{-0.47}$
goods-n-mediumhst	28752	2.094	8.29 $^{+0.07}_{-0.09}$	< -1.4	9.22 $^{+0.06}_{-0.27}$	0.42 $^{+0.25}_{-0.09}$	2.45 $^{+0.06}_{-0.27}$	-0.35 $^{+0.25}_{-0.09}$
goods-n-mediumhst	29023	2.0925	8.51 $^{+0.05}_{-0.05}$	-1.06 $^{+0.04}_{-0.04}$	10.29 $^{+0.1}_{-0.11}$	1.0 $^{+0.18}_{-0.25}$	3.4 $^{+0.1}_{-0.11}$	0.11 $^{+0.18}_{-0.25}$
goods-n-mediumhst	29034	2.0931	8.62 $^{+0.04}_{-0.04}$	-0.96 $^{+0.04}_{-0.04}$	9.74 $^{+0.17}_{-0.18}$	1.33 $^{+0.2}_{-0.19}$	2.68 $^{+0.17}_{-0.18}$	0.27 $^{+0.2}_{-0.19}$
goods-n-mediumhst	29554	3.205	7.87 $^{+0.16}_{-0.15}$	< -0.78	8.67 $^{+0.07}_{-0.29}$	0.24 $^{+0.25}_{-0.06}$	1.99 $^{+0.07}_{-0.29}$	-0.44 $^{+0.25}_{-0.06}$
goods-n-mediumhst	29582	1.6778	8.25 $^{+0.09}_{-0.13}$	< -1.28	8.66 $^{+0.51}_{-0.44}$	0.55 $^{+0.1}_{-0.06}$	2.3 $^{+0.51}_{-0.44}$	0.19 $^{+0.1}_{-0.06}$
goods-n-mediumhst	29715	1.8792	8.42 $^{+0.06}_{-0.06}$	-1.05 $^{+0.04}_{-0.05}$	9.8 $^{+0.06}_{-0.1}$	0.88 $^{+0.12}_{-0.21}$	4.16 $^{+0.06}_{-0.1}$	1.23 $^{+0.12}_{-0.21}$
goods-n-mediumhst	29938	2.4836	8.05 $^{+0.15}_{-0.18}$	-1.29 $^{+0.1}_{-0.13}$	8.82 $^{+0.01}_{-0.05}$	0.6 $^{+0.02}_{-0.02}$	2.16 $^{+0.01}_{-0.05}$	-0.06 $^{+0.02}_{-0.02}$
goods-n-mediumhst	30039	1.6319	8.31 $^{+0.07}_{-0.08}$	< -1.4	8.83 $^{+0.33}_{-0.19}$	0.72 $^{+0.05}_{-0.15}$	2.11 $^{+0.33}_{-0.19}$	-0.0 $^{+0.05}_{-0.15}$
goods-n-mediumhst	30263	2.0129	8.53 $^{+0.05}_{-0.05}$	-1.01 $^{+0.05}_{-0.06}$	10.06 $^{+0.1}_{-0.23}$	0.65 $^{+0.49}_{-0.72}$	3.59 $^{+0.1}_{-0.23}$	0.17 $^{+0.49}_{-0.72}$
goods-n-mediumhst	30631	1.5852	8.3 $^{+0.08}_{-0.11}$	< -1.48	8.87 $^{+0.09}_{-0.34}$	0.04 $^{+0.08}_{-0.13}$	3.08 $^{+0.09}_{-0.34}$	0.25 $^{+0.08}_{-0.13}$
goods-n-mediumhst	30748	1.7279	8.57 $^{+0.04}_{-0.05}$	< -1.25	9.32 $^{+0.14}_{-0.17}$	0.2 $^{+0.26}_{-0.23}$	2.66 $^{+0.14}_{-0.17}$	-0.46 $^{+0.26}_{-0.23}$
goods-n-mediumhst	30817	2.2447	8.37 $^{+0.07}_{-0.08}$	-0.96 $^{+0.02}_{-0.02}$	10.35 $^{+0.07}_{-0.09}$	2.27 $^{+0.01}_{-0.34}$	3.67 $^{+0.07}_{-0.09}$	1.59 $^{+0.01}_{-0.34}$
goods-n-mediumhst	30989	2.3777	8.35 $^{+0.07}_{-0.09}$	-1.27 $^{+0.04}_{-0.04}$	9.55 $^{+0.11}_{-0.12}$	0.23 $^{+0.31}_{-0.3}$	3.79 $^{+0.11}_{-0.12}$	0.47 $^{+0.31}_{-0.3}$
goods-n-mediumhst	31012	3.6617	8.33 $^{+0.09}_{-0.14}$	< -1.07	9.42 $^{+0.12}_{-0.12}$	0.64 $^{+0.2}_{-0.17}$	3.1 $^{+0.12}_{-0.18}$	0.32 $^{+0.2}_{-0.17}$
goods-n-mediumhst	31372	2.9417	8.18 $^{+0.09}_{-0.09}$	-1.34 $^{+0.07}_{-0.09}$	9.33 $^{+0.18}_{-0.18}$	0.7 $^{+0.09}_{-0.07}$	3.37 $^{+0.1}_{-0.08}$	0.74 $^{+0.09}_{-0.07}$
goods-n-mediumhst	32556	4.5337	8.01 $^{+0.14}_{-0.16}$	< -0.82	9.21 $^{+0.09}_{-0.24}$	0.7 $^{+0.15}_{-0.12}$	2.85 $^{+0.09}_{-0.24}$	0.34 $^{+0.15}_{-0.12}$
goods-n-mediumhst	38432	6.7169	8.06 $^{+0.11}_{-0.12}$	< -1.22	9.87 $^{+0.32}_{-0.65}$	1.05 $^{+0.44}_{-0.72}$	3.69 $^{+0.32}_{-0.65}$	0.87 $^{+0.44}_{-0.72}$

Table C.1. (continued)

Tier	ID	z_{spec}	$12+\log(\text{O/H})$	$\log(\text{N/O})$	$\log(M_*/M_\odot)$	SFR	Σ_{M_*}	Σ_{SFR}
goods-n-mediumhst	46778	3.9642	$8.12^{+0.09}_{-0.1}$	< -1.33	$8.95^{+0.2}_{-0.26}$	$0.26^{+0.23}_{-0.17}$	$2.47^{+0.2}_{-0.26}$	$-0.22^{+0.23}_{-0.17}$
goods-n-mediumhst	64685	2.2099	$8.38^{+0.06}_{-0.07}$	$-1.26^{+0.03}_{-0.03}$	$9.59^{+0.18}_{-0.24}$	$0.81^{+0.3}_{-0.25}$	$3.73^{+0.18}_{-0.24}$	$0.95^{+0.3}_{-0.25}$
goods-n-mediumhst	64975	2.2703	$7.76^{+0.22}_{-0.19}$	< -0.66	$9.46^{+0.37}_{-0.48}$	$-0.04^{+0.65}_{-0.15}$	$3.33^{+0.37}_{-0.48}$	$-0.17^{+0.65}_{-1.66}$
goods-n-mediumhst	65032	1.7932	$8.45^{+0.07}_{-0.08}$	< -1.16	$9.27^{+0.15}_{-0.15}$	$0.17^{+0.34}_{-0.36}$	$2.38^{+0.15}_{-0.17}$	$-0.72^{+0.34}_{-0.36}$
goods-n-mediumhst	65053	2.4407	$8.17^{+0.09}_{-0.11}$	< -1.46	$9.45^{+0.11}_{-0.19}$	$0.62^{+0.16}_{-0.13}$	$2.61^{+0.11}_{-0.19}$	$-0.21^{+0.16}_{-0.13}$
goods-n-mediumhst	65099	2.8102	$8.34^{+0.06}_{-0.07}$	$-1.35^{+0.05}_{-0.05}$	$9.9^{+0.19}_{-0.34}$	$1.21^{+0.29}_{-0.28}$	$2.94^{+0.19}_{-0.34}$	$0.25^{+0.29}_{-0.28}$
goods-n-mediumhst	65114	1.6753	$8.23^{+0.09}_{-0.11}$	< -1.15	$8.96^{+0.15}_{-0.16}$	$0.22^{+0.22}_{-0.29}$	$2.15^{+0.15}_{-0.16}$	$-0.59^{+0.22}_{-0.29}$
goods-n-mediumhst	65128	1.8112	$8.39^{+0.08}_{-0.09}$	< -1.12	$9.41^{+0.12}_{-0.13}$	$0.16^{+0.34}_{-0.74}$	$2.89^{+0.12}_{-0.13}$	$-0.37^{+0.34}_{-0.74}$
goods-n-mediumhst	69348	1.7908	$8.51^{+0.06}_{-0.08}$	< -0.96	$8.9^{+0.14}_{-0.22}$	$-0.34^{+0.35}_{-0.49}$	$2.55^{+0.14}_{-0.22}$	$-0.69^{+0.35}_{-0.49}$
goods-n-mediumjwst	95	3.909	$7.79^{+0.14}_{-0.14}$	< -0.85	$8.72^{+0.16}_{-0.21}$	$0.24^{+0.19}_{-0.16}$	$3.75^{+0.16}_{-0.21}$	$1.27^{+0.19}_{-0.16}$
goods-n-mediumjwst	110	4.064	$8.31^{+0.07}_{-0.08}$	$-1.12^{+0.02}_{-0.03}$	$9.55^{+0.3}_{-0.67}$	$1.49^{+0.11}_{-0.25}$	$3.19^{+0.3}_{-0.67}$	$1.13^{+0.11}_{-0.25}$
goods-n-mediumjwst	1673	2.3985	$7.99^{+0.13}_{-0.15}$	< -1.02	$8.78^{+0.1}_{-0.1}$	$-0.12^{+0.2}_{-0.1}$	$3.31^{+0.1}_{-0.1}$	$0.41^{+0.2}_{-0.1}$
goods-n-mediumjwst	3577	2.6335	$8.19^{+0.1}_{-0.12}$	< -1.47	$8.99^{+0.08}_{-0.14}$	$0.43^{+0.07}_{-0.1}$	$2.83^{+0.08}_{-0.14}$	$0.27^{+0.07}_{-0.1}$
goods-n-mediumjwst	4550	3.2439	$7.98^{+0.11}_{-0.13}$	$-1.33^{+0.1}_{-0.14}$	$9.14^{+0.05}_{-0.09}$	$0.57^{+0.12}_{-0.08}$	$3.69^{+0.05}_{-0.09}$	$1.12^{+0.12}_{-0.08}$
goods-n-mediumjwst	7732	3.1895	$7.42^{+0.18}_{-0.15}$	< -0.55	$9.08^{+0.1}_{-0.15}$	$-0.17^{+0.3}_{-0.45}$	$3.38^{+0.1}_{-0.15}$	$0.13^{+0.3}_{-0.45}$
goods-n-mediumjwst	8299	3.424	$8.19^{+0.08}_{-0.1}$	< -1.36	$9.01^{+0.12}_{-0.16}$	$0.13^{+0.24}_{-0.23}$	$3.48^{+0.12}_{-0.16}$	$0.6^{+0.24}_{-0.23}$
goods-n-mediumjwst	8403	2.4165	$7.67^{+0.19}_{-0.15}$	< -0.57	$8.38^{+0.1}_{-0.4}$	$-0.05^{+0.08}_{-0.09}$	$2.18^{+0.1}_{-0.4}$	$-0.24^{+0.08}_{-0.09}$
goods-n-mediumjwst	8534	2.4186	$7.46^{+0.16}_{-0.13}$	< -0.79	$8.0^{+0.14}_{-0.14}$	$-0.19^{+0.09}_{-0.09}$	$1.76^{+0.14}_{-0.14}$	$-0.44^{+0.09}_{-0.09}$
goods-n-mediumjwst	8823	2.7301	$8.16^{+0.11}_{-0.14}$	$-1.31^{+0.06}_{-0.07}$	$8.97^{+0.07}_{-0.07}$	$0.51^{+0.08}_{-0.11}$	$3.02^{+0.07}_{-0.16}$	$0.57^{+0.08}_{-0.11}$
goods-n-mediumjwst	10886	2.9612	$7.54^{+0.15}_{-0.12}$	< -0.85	$8.2^{+0.11}_{-0.24}$	$0.13^{+0.18}_{-0.08}$	$2.82^{+0.11}_{-0.24}$	$0.74^{+0.18}_{-0.08}$
goods-n-mediumjwst	11108	1.9506	$7.93^{+0.16}_{-0.16}$	< -0.68	$8.13^{+0.12}_{-0.22}$	$-0.41^{+0.14}_{-0.14}$	$2.22^{+0.12}_{-0.22}$	$-0.32^{+0.14}_{-0.14}$
goods-n-mediumjwst	12067	4.0579	$8.25^{+0.09}_{-0.12}$	< -1.17	$9.05^{+0.12}_{-0.12}$	$0.41^{+0.23}_{-0.15}$	$2.56^{+0.12}_{-0.3}$	$-0.08^{+0.23}_{-0.15}$
goods-n-mediumjwst	13410	5.0172	$8.17^{+0.09}_{-0.11}$	< -1.2	$9.28^{+0.12}_{-0.12}$	$0.41^{+0.21}_{-0.26}$	$2.09^{+0.12}_{-0.22}$	$-0.78^{+0.21}_{-0.26}$
goods-n-mediumjwst	14475	3.3203	$7.68^{+0.13}_{-0.13}$	< -0.76	$7.69^{+0.47}_{-0.17}$	$0.3^{+0.07}_{-0.14}$	$1.82^{+0.47}_{-0.17}$	$0.44^{+0.07}_{-0.14}$
goods-n-mediumjwst	15529	3.8708	$8.14^{+0.1}_{-0.12}$	$-1.47^{+0.08}_{-0.09}$	$9.55^{+0.06}_{-0.07}$	$0.89^{+0.09}_{-0.07}$	$3.38^{+0.06}_{-0.07}$	$0.71^{+0.09}_{-0.07}$
goods-n-mediumjwst	17004	3.205	$8.04^{+0.11}_{-0.13}$	< -1.04	$8.46^{+0.1}_{-0.17}$	$-0.2^{+0.11}_{-0.16}$	$2.07^{+0.1}_{-0.17}$	$-0.59^{+0.11}_{-0.16}$
goods-n-mediumjwst	17722	4.9344	$7.87^{+0.19}_{-0.18}$	< -1.17	$8.81^{+0.19}_{-0.19}$	$0.44^{+0.06}_{-0.14}$	$2.73^{+0.17}_{-0.19}$	$0.36^{+0.06}_{-0.14}$
goods-n-mediumjwst	18536	6.8086	$7.89^{+0.12}_{-0.12}$	< -0.98	$8.68^{+0.21}_{-0.3}$	$0.82^{+0.1}_{-0.09}$	$2.74^{+0.21}_{-0.3}$	$0.88^{+0.1}_{-0.09}$
goods-n-mediumjwst	24835	2.9329	$8.48^{+0.06}_{-0.07}$	$-0.91^{+0.05}_{-0.06}$	$10.11^{+0.08}_{-0.13}$	$0.97^{+0.3}_{-0.41}$	$3.13^{+0.08}_{-0.13}$	$-0.01^{+0.3}_{-0.41}$
goods-n-mediumjwst	25351	3.1287	$8.39^{+0.06}_{-0.07}$	$-0.84^{+0.02}_{-0.03}$	$10.15^{+0.18}_{-0.42}$	$1.65^{+0.31}_{-0.31}$	$3.02^{+0.18}_{-0.42}$	$0.52^{+0.31}_{-0.16}$
goods-n-mediumjwst	25603	2.9893	$8.38^{+0.07}_{-0.08}$	$-1.01^{+0.03}_{-0.04}$	$9.6^{+0.47}_{-0.04}$	$1.56^{+0.08}_{-0.18}$	$3.42^{+0.47}_{-0.04}$	$1.38^{+0.08}_{-0.18}$
goods-n-mediumjwst	25844	2.2733	$8.43^{+0.06}_{-0.08}$	$-1.38^{+0.08}_{-0.1}$	$9.52^{+0.25}_{-0.14}$	$0.64^{+0.22}_{-0.19}$	$2.36^{+0.25}_{-0.14}$	$-0.52^{+0.22}_{-0.16}$
goods-n-mediumjwst	27139	3.5167	$7.93^{+0.22}_{-0.22}$	< -1.07	$8.7^{+0.2}_{-0.21}$	$0.61^{+0.42}_{-0.16}$	$0.64^{+0.2}_{-0.21}$	$-1.46^{+0.42}_{-0.19}$
goods-n-mediumjwst	27248	3.6667	$7.92^{+0.15}_{-0.16}$	< -1.12	$8.38^{+0.21}_{-0.29}$	$0.17^{+0.13}_{-0.16}$	$1.32^{+0.21}_{-0.29}$	$-0.88^{+0.13}_{-0.16}$
goods-n-mediumjwst	27519	2.9507	$8.12^{+0.11}_{-0.13}$	< -1.44	$9.3^{+0.12}_{-0.17}$	$0.56^{+0.15}_{-0.16}$	$2.45^{+0.12}_{-0.17}$	$-0.3^{+0.15}_{-0.16}$
goods-n-mediumjwst	27761	2.9545	$7.97^{+0.12}_{-0.13}$	< -0.94	$8.76^{+0.08}_{-0.07}$	$-0.19^{+0.16}_{-0.14}$	$2.89^{+0.08}_{-0.07}$	$-0.06^{+0.16}_{-0.14}$
goods-n-mediumjwst	28174	4.4016	$8.22^{+0.08}_{-0.1}$	$-1.24^{+0.05}_{-0.05}$	$9.41^{+0.2}_{-0.67}$	$1.1^{+0.2}_{-0.17}$	$2.78^{+0.2}_{-0.67}$	$0.47^{+0.2}_{-0.17}$
goods-n-mediumjwst	28746	4.4139	$8.33^{+0.08}_{-0.1}$	$-0.9^{+0.04}_{-0.05}$	$10.36^{+0.11}_{-0.12}$	$1.4^{+0.18}_{-0.36}$	$2.94^{+0.11}_{-0.12}$	$-0.03^{+0.18}_{-0.36}$
goods-n-mediumjwst	29648	2.9591	$8.47^{+0.05}_{-0.06}$	$-0.92^{+0.02}_{-0.02}$	$10.16^{+0.13}_{-0.13}$	$1.45^{+0.13}_{-0.26}$	$2.35^{+0.13}_{-0.13}$	$-0.35^{+0.13}_{-0.26}$
goods-n-mediumjwst	33332	1.6444	$8.26^{+0.08}_{-0.1}$	$-1.34^{+0.09}_{-0.12}$	$8.32^{+0.17}_{-0.53}$	$0.22^{+0.15}_{-0.09}$	$1.49^{+0.17}_{-0.53}$	$-0.6^{+0.15}_{-0.09}$
goods-n-mediumjwst	42740	2.028	$8.49^{+0.06}_{-0.08}$	< -1.05	$9.26^{+0.21}_{-0.27}$	$0.41^{+0.26}_{-0.34}$	$2.84^{+0.21}_{-0.27}$	$-0.01^{+0.26}_{-0.34}$
goods-n-mediumjwst	44099	5.8586	$8.32^{+0.07}_{-0.09}$	$-1.13^{+0.07}_{-0.08}$	$9.49^{+0.16}_{-0.21}$	$1.07^{+0.26}_{-0.16}$	$3.23^{+0.16}_{-0.21}$	$0.81^{+0.26}_{-0.16}$
goods-n-mediumjwst	44124	6.6862	$8.11^{+0.1}_{-0.11}$	< -1.02	$8.19^{+0.31}_{-0.28}$	$0.64^{+0.07}_{-0.12}$	$3.0^{+0.31}_{-0.28}$	$1.44^{+0.07}_{-0.12}$
goods-n-mediumjwst	46239	3.7273	$7.94^{+0.16}_{-0.17}$	< -0.77	$8.82^{+0.13}_{-0.12}$	$0.04^{+0.27}_{-0.47}$	$3.05^{+0.13}_{-0.2}$	$0.26^{+0.27}_{-0.47}$
goods-n-mediumjwst	52923	4.0192	$7.77^{+0.13}_{-0.13}$	< -0.69	$8.62^{+0.14}_{-0.21}$	$0.18^{+0.12}_{-0.15}$	$3.12^{+0.14}_{-0.21}$	$0.69^{+0.12}_{-0.15}$
goods-n-mediumjwst	53927	5.872	$8.14^{+0.09}_{-0.11}$	< -1.21	$9.01^{+0.11}_{-0.19}$	$0.61^{+0.14}_{-0.13}$	$3.79^{+0.11}_{-0.19}$	$1.39^{+0.14}_{-0.13}$
goods-n-mediumjwst	55967	2.0853	$8.29^{+0.07}_{-0.08}$	$-1.47^{+0.05}_{-0.05}$	$9.3^{+0.17}_{-0.47}$	$0.58^{+0.33}_{-0.18}$	$3.22^{+0.17}_{-0.47}$	$0.49^{+0.33}_{-0.18}$

Table C.1. (continued)

Tier	ID	z_{spec}	12+log(O/H)	log(N/O)	log(M_*/M_{\odot})	SFR	Σ_{M_*}	Σ_{SFR}
goods-n-mediumjwst	56785	3.4367	$8.07^{+0.09}_{-0.11}$	< -1.31	$8.94^{+0.14}_{-0.27}$	$0.28^{+0.11}_{-0.18}$	$2.34^{+0.14}_{-0.27}$	$-0.33^{+0.11}_{-0.18}$
goods-n-mediumjwst	58441	5.9687	$7.74^{+0.15}_{-0.13}$	< -0.7	$7.89^{+0.23}_{-0.44}$	$0.39^{+0.04}_{-0.06}$	$1.9^{+0.23}_{-0.44}$	$0.39^{+0.04}_{-0.06}$
goods-n-mediumjwst	59156	5.2205	$8.26^{+0.13}_{-0.13}$	< -0.9	$9.35^{+0.13}_{-0.19}$	$0.68^{+0.28}_{-0.2}$	$2.49^{+0.13}_{-0.19}$	$-0.18^{+0.28}_{-0.02}$
goods-n-mediumjwst	59412	5.1838	$8.11^{+0.1}_{-0.1}$	$-1.29^{+0.07}_{-0.08}$	$9.27^{+0.15}_{-0.15}$	$0.85^{+0.17}_{-0.2}$	$3.26^{+0.15}_{-0.15}$	$0.84^{+0.17}_{-0.17}$
goods-n-mediumjwst	61712	5.1839	$8.11^{+0.11}_{-0.12}$	< -1.04	$9.03^{+0.16}_{-0.21}$	$0.6^{+0.17}_{-0.1}$	$2.8^{+0.16}_{-0.21}$	$0.36^{+0.17}_{-0.17}$
goods-n-mediumjwst	62309	5.1711	$7.77^{+0.14}_{-0.13}$	< -0.93	$8.23^{+0.24}_{-0.23}$	$0.43^{+0.1}_{-0.06}$	$2.14^{+0.24}_{-0.23}$	$0.34^{+0.1}_{-0.06}$
goods-n-mediumjwst	62955	5.1831	$7.62^{+0.12}_{-0.11}$	< -0.73	$8.32^{+0.13}_{-0.2}$	$0.68^{+0.02}_{-0.08}$	$2.53^{+0.13}_{-0.2}$	$0.89^{+0.02}_{-0.08}$
goods-n-mediumjwst	65891	2.9219	$7.97^{+0.19}_{-0.2}$	< -1.35	$8.38^{+0.13}_{-0.25}$	$0.23^{+0.05}_{-0.08}$	$3.7^{+0.13}_{-0.25}$	$1.54^{+0.05}_{-0.08}$
goods-n-mediumjwst	69736	1.6114	$8.26^{+0.07}_{-0.08}$	$-1.67^{+0.1}_{-0.14}$	$9.09^{+0.09}_{-0.42}$	$0.34^{+0.22}_{-0.12}$	$2.75^{+0.09}_{-0.42}$	$-0.01^{+0.22}_{-0.12}$
goods-n-mediumjwst	71723	2.461	$8.33^{+0.07}_{-0.08}$	$-1.2^{+0.04}_{-0.04}$	$9.3^{+0.21}_{-0.13}$	$1.47^{+0.24}_{-0.1}$	$2.02^{+0.21}_{-0.13}$	$0.18^{+0.24}_{-0.01}$
goods-n-mediumjwst	71890	3.4138	$8.33^{+0.07}_{-0.08}$	$-0.95^{+0.03}_{-0.03}$	$9.68^{+0.12}_{-0.06}$	$1.18^{+0.08}_{-0.19}$	$4.31^{+0.12}_{-0.06}$	$1.81^{+0.08}_{-0.19}$
goods-n-mediumjwst	71914	2.4583	$8.52^{+0.05}_{-0.05}$	$-0.81^{+0.02}_{-0.03}$	$9.75^{+0.29}_{-0.13}$	$1.26^{+0.37}_{-0.28}$	$3.5^{+0.29}_{-0.13}$	$1.0^{+0.37}_{-0.28}$
goods-n-mediumjwst	72208	3.9298	$7.88^{+0.13}_{-0.14}$	< -0.99	$8.72^{+0.13}_{-0.34}$	$0.45^{+0.06}_{-0.14}$	$2.58^{+0.13}_{-0.34}$	$0.31^{+0.06}_{-0.14}$
goods-n-mediumjwst	72321	2.7587	$8.26^{+0.09}_{-0.11}$	$-1.42^{+0.07}_{-0.09}$	$9.86^{+0.09}_{-0.14}$	$0.34^{+0.39}_{-0.08}$	$2.77^{+0.09}_{-0.14}$	$-0.75^{+0.39}_{-0.58}$
goods-n-mediumjwst	72558	3.3796	$8.13^{+0.11}_{-0.13}$	< -1.43	$9.7^{+0.14}_{-0.09}$	$1.06^{+0.19}_{-0.22}$	$2.59^{+0.14}_{-0.09}$	$-0.05^{+0.19}_{-0.22}$
goods-n-mediumjwst	76015	3.6669	$8.3^{+0.1}_{-0.13}$	$-1.18^{+0.09}_{-0.12}$	$9.29^{+0.13}_{-0.15}$	$0.8^{+0.19}_{-0.15}$	$2.71^{+0.13}_{-0.15}$	$0.22^{+0.19}_{-0.15}$
goods-n-mediumjwst	76348	1.787	$8.3^{+0.07}_{-0.08}$	< -1.46	$9.13^{+0.3}_{-0.35}$	$0.67^{+0.13}_{-0.39}$	$3.16^{+0.3}_{-0.35}$	$0.7^{+0.13}_{-0.39}$
goods-n-mediumjwst	76927	4.4133	$8.19^{+0.11}_{-0.12}$	< -1.26	$9.57^{+0.14}_{-0.25}$	$0.72^{+0.22}_{-0.28}$	$2.86^{+0.14}_{-0.25}$	$0.01^{+0.22}_{-0.28}$
goods-n-mediumjwst	76983	2.851	$8.21^{+0.13}_{-0.2}$	$-0.78^{+0.04}_{-0.05}$	$9.32^{+0.1}_{-0.09}$	$0.49^{+0.23}_{-0.18}$	$3.56^{+0.1}_{-0.09}$	$0.74^{+0.23}_{-0.18}$
goods-n-mediumjwst	77071	2.9748	$8.42^{+0.06}_{-0.07}$	$-1.02^{+0.05}_{-0.02}$	$10.32^{+0.09}_{-0.19}$	$1.72^{+0.21}_{-0.11}$	$3.96^{+0.09}_{-0.19}$	$1.35^{+0.21}_{-0.11}$
goods-n-mediumjwst	78032	2.4421	$8.11^{+0.09}_{-0.11}$	< -1.58	$9.1^{+0.11}_{-0.15}$	$0.05^{+0.15}_{-0.27}$	$3.08^{+0.11}_{-0.15}$	$0.04^{+0.15}_{-0.27}$
goods-n-mediumjwst	78501	1.795	$8.46^{+0.06}_{-0.07}$	< -1.43	$8.81^{+0.58}_{-0.06}$	$0.61^{+0.27}_{-0.07}$	$1.72^{+0.58}_{-0.06}$	$-0.48^{+0.27}_{-0.07}$
goods-n-mediumjwst	78773	5.1872	$8.17^{+0.09}_{-0.11}$	$-1.03^{+0.06}_{-0.07}$	$9.91^{+0.13}_{-0.24}$	$1.78^{+0.1}_{-0.11}$	$2.78^{+0.13}_{-0.24}$	$0.65^{+0.1}_{-0.11}$
goods-n-mediumjwst	78888	3.6757	$8.24^{+0.07}_{-0.08}$	$-1.47^{+0.07}_{-0.09}$	$9.66^{+0.08}_{-0.17}$	$0.83^{+0.21}_{-0.24}$	$2.97^{+0.08}_{-0.17}$	$0.15^{+0.21}_{-0.24}$
goods-n-mediumjwst	78891	6.5484	$8.07^{+0.1}_{-0.12}$	$-1.12^{+0.07}_{-0.09}$	$9.05^{+0.13}_{-0.15}$	$1.43^{+0.23}_{-0.14}$	$3.27^{+0.13}_{-0.15}$	$1.65^{+0.23}_{-0.14}$
goods-n-mediumjwst	78931	2.8034	$7.96^{+0.13}_{-0.13}$	< -1.15	$8.46^{+0.09}_{-0.19}$	$0.02^{+0.07}_{-0.07}$	$2.76^{+0.09}_{-0.19}$	$0.31^{+0.07}_{-0.07}$
goods-n-mediumjwst	79203	2.2701	$8.52^{+0.05}_{-0.05}$	$-1.02^{+0.03}_{-0.04}$	$9.8^{+0.3}_{-0.28}$	$1.11^{+0.24}_{-0.13}$	$2.7^{+0.3}_{-0.28}$	$0.01^{+0.24}_{-0.13}$
goods-n-mediumjwst	79294	2.0649	$8.28^{+0.08}_{-0.09}$	< -1.41	$8.34^{+0.04}_{-0.04}$	$0.21^{+0.07}_{-0.04}$	$1.57^{+0.04}_{-0.04}$	$-0.56^{+0.07}_{-0.04}$
goods-n-mediumjwst	79309	1.7957	$8.34^{+0.07}_{-0.08}$	$-1.1^{+0.03}_{-0.03}$	$9.67^{+0.11}_{-0.21}$	$0.91^{+0.16}_{-0.21}$	$2.67^{+0.11}_{-0.21}$	$-0.09^{+0.16}_{-0.21}$
goods-n-mediumjwst	79393	2.9657	$8.04^{+0.11}_{-0.12}$	$-1.38^{+0.08}_{-0.1}$	$8.84^{+0.07}_{-0.31}$	$0.42^{+0.13}_{-0.1}$	$3.2^{+0.07}_{-0.31}$	$0.78^{+0.13}_{-0.1}$
goods-n-mediumjwst	79534	3.2262	$7.94^{+0.14}_{-0.16}$	< -0.79	$8.67^{+0.16}_{-0.34}$	$0.24^{+0.09}_{-0.11}$	$2.5^{+0.16}_{-0.34}$	$0.07^{+0.09}_{-0.11}$
goods-n-mediumjwst	80185	5.4875	$7.77^{+0.13}_{-0.12}$	< -0.69	$8.63^{+0.12}_{-0.4}$	$0.44^{+0.16}_{-0.05}$	$1.96^{+0.12}_{-0.4}$	$-0.23^{+0.16}_{-0.05}$
goods-n-mediumjwst	80742	2.4201	$8.27^{+0.08}_{-0.09}$	$-1.18^{+0.03}_{-0.04}$	$9.34^{+0.13}_{-0.13}$	$0.51^{+0.22}_{-0.12}$	$2.86^{+0.13}_{-0.11}$	$0.04^{+0.22}_{-0.13}$
goods-n-mediumjwst	81046	2.4429	$8.03^{+0.12}_{-0.14}$	$-1.3^{+0.1}_{-0.04}$	$8.88^{+0.12}_{-0.13}$	$0.13^{+0.13}_{-0.09}$	$0.97^{+0.12}_{-0.13}$	$-1.79^{+0.12}_{-0.12}$
goods-n-mediumjwst	81621	2.0513	$8.38^{+0.06}_{-0.07}$	$-1.12^{+0.03}_{-0.04}$	$9.72^{+0.24}_{-0.09}$	$0.98^{+0.16}_{-0.08}$	$3.65^{+0.24}_{-0.09}$	$0.91^{+0.16}_{-0.08}$
goods-n-mediumjwst	82948	3.9056	$8.42^{+0.05}_{-0.06}$	$-1.09^{+0.02}_{-0.02}$	$10.18^{+0.17}_{-0.07}$	$1.68^{+0.08}_{-0.35}$	$3.63^{+0.17}_{-0.07}$	$1.13^{+0.08}_{-0.35}$
goods-n-mediumjwst	10003642	3.2349	$8.37^{+0.06}_{-0.08}$	$-1.06^{+0.03}_{-0.03}$	$10.06^{+0.24}_{-0.16}$	$1.91^{+0.19}_{-0.3}$	$2.93^{+0.24}_{-0.16}$	$0.77^{+0.19}_{-0.3}$
goods-n-mediumjwst	10026755	2.8104	$7.84^{+0.17}_{-0.17}$	< -1.1	$8.4^{+0.16}_{-0.2}$	$0.35^{+0.12}_{-0.14}$	$2.15^{+0.16}_{-0.2}$	$0.11^{+0.12}_{-0.14}$
goods-n-mediumjwst	10038778	4.1259	$8.19^{+0.12}_{-0.17}$	< -1.05	$8.25^{+0.21}_{-0.33}$	$0.03^{+0.15}_{-0.1}$	$3.09^{+0.33}_{-0.33}$	$0.88^{+0.15}_{-0.13}$
goods-s-deephst	3184	3.4674	$8.16^{+0.17}_{-0.14}$	< -1.2	$9.17^{+0.08}_{-0.21}$	$0.49^{+0.13}_{-0.06}$	$2.2^{+0.08}_{-0.21}$	$-0.48^{+0.13}_{-0.06}$
goods-s-deephst	3753	1.7676	$8.36^{+0.06}_{-0.08}$	$-1.28^{+0.02}_{-0.02}$	$9.57^{+0.09}_{-0.1}$	$0.75^{+0.32}_{-0.16}$	$3.64^{+0.09}_{-0.14}$	$0.82^{+0.32}_{-0.16}$
goods-s-deephst	3892	2.8072	$8.25^{+0.07}_{-0.09}$	$-1.35^{+0.03}_{-0.03}$	$9.36^{+0.04}_{-0.04}$	$1.33^{+0.02}_{-0.08}$	$2.97^{+0.04}_{-0.04}$	$0.94^{+0.02}_{-0.08}$
goods-s-deephst	4404	5.7632	$7.58^{+0.13}_{-0.13}$	< -0.71	$8.14^{+0.12}_{-0.4}$	$0.5^{+0.16}_{-0.09}$	$3.2^{+0.12}_{-0.4}$	$1.56^{+0.16}_{-0.09}$
goods-s-deephst	6002	5.9365	$7.7^{+0.14}_{-0.14}$	< -0.59	$7.81^{+0.17}_{-0.19}$	$0.06^{+0.1}_{-0.04}$	$2.5^{+0.17}_{-0.19}$	$0.74^{+0.1}_{-0.04}$
goods-s-deephst	6246	5.5614	$8.27^{+0.09}_{-0.11}$	< -0.93	$8.34^{+0.2}_{-0.26}$	$0.1^{+0.15}_{-0.15}$	$3.13^{+0.2}_{-0.26}$	$0.89^{+0.15}_{-0.2}$
goods-s-deephst	7762	4.1481	$8.21^{+0.09}_{-0.11}$	< -1.55	$8.9^{+0.19}_{-0.15}$	$0.51^{+0.27}_{-0.15}$	$2.95^{+0.19}_{-0.15}$	$0.56^{+0.27}_{-0.15}$
goods-s-deephst	7938	4.806	$7.8^{+0.13}_{-0.13}$	< -1.03	$8.04^{+0.52}_{-0.13}$	$0.5^{+0.08}_{-0.06}$	$2.38^{+0.52}_{-0.13}$	$0.85^{+0.08}_{-0.06}$

Table C.1. (continued)

Tier	ID	z_{spec}	12+log(O/H)	log(N/O)	log(M_*/M_{\odot})	SFR	Σ_{M_*}	Σ_{SFR}
goods-s-deephst	16745	5.5663	8.18 $^{+0.08}_{-0.09}$	< -1.64	8.62 $^{+0.18}_{-0.49}$	0.61 $^{+0.07}_{-0.16}$	1.47 $^{+0.18}_{-0.49}$	-0.54 $^{+0.07}_{-0.16}$
goods-s-deephst	18090	4.7748	7.95 $^{+0.12}_{-0.13}$	< -1.14	8.74 $^{+0.09}_{-0.1}$	0.58 $^{+0.1}_{-0.2}$	2.33 $^{+0.09}_{-0.17}$	0.17 $^{+0.1}_{-0.2}$
goods-s-deephst	18970	3.7239	8.2 $^{+0.1}_{-0.13}$	-1.25 $^{+0.08}_{-0.1}$	9.48 $^{+0.14}_{-0.1}$	0.58 $^{+0.26}_{-0.44}$	3.23 $^{+0.14}_{-0.17}$	0.33 $^{+0.26}_{-0.44}$
goods-s-deephst	19519	3.6044	8.14 $^{+0.11}_{-0.13}$	< -1.3	8.66 $^{+0.1}_{-0.1}$	0.09 $^{+0.15}_{-0.17}$	3.4 $^{+0.1}_{-0.1}$	0.83 $^{+0.15}_{-0.17}$
goods-s-deephst	19607	1.8474	8.34 $^{+0.12}_{-0.2}$	< -1.14	8.52 $^{+0.17}_{-0.22}$	0.24 $^{+0.01}_{-0.04}$	1.64 $^{+0.17}_{-0.22}$	-0.64 $^{+0.01}_{-0.04}$
goods-s-deephst	21150	3.0878	8.1 $^{+0.1}_{-0.12}$	-1.24 $^{+0.08}_{-0.1}$	9.08 $^{+0.08}_{-0.17}$	0.77 $^{+0.05}_{-0.04}$	2.21 $^{+0.08}_{-0.17}$	-0.1 $^{+0.05}_{-0.04}$
goods-s-deephst	21598	1.7151	7.32 $^{+0.16}_{-0.11}$	< -0.69	7.3 $^{+0.31}_{-0.88}$	-0.64 $^{+0.07}_{-0.25}$	1.6 $^{+0.31}_{-0.88}$	-0.34 $^{+0.07}_{-0.25}$
goods-s-deephst	22078	1.6105	8.24 $^{+0.08}_{-0.09}$	-1.53 $^{+0.1}_{-0.14}$	8.61 $^{+0.09}_{-0.12}$	0.07 $^{+0.13}_{-0.07}$	3.24 $^{+0.09}_{-0.12}$	0.7 $^{+0.13}_{-0.07}$
goods-s-deephst	10009506	3.5991	7.93 $^{+0.13}_{-0.14}$	< -1.31	8.73 $^{+0.16}_{-0.35}$	0.16 $^{+0.21}_{-0.36}$	3.61 $^{+0.16}_{-0.35}$	1.04 $^{+0.21}_{-0.36}$
goods-s-deephst	10011378	2.5771	8.39 $^{+0.07}_{-0.08}$	-1.18 $^{+0.07}_{-0.09}$	9.12 $^{+0.09}_{-0.14}$	0.02 $^{+0.23}_{-0.35}$	2.04 $^{+0.09}_{-0.14}$	-1.06 $^{+0.23}_{-0.35}$
goods-s-deephst	10011849	2.6937	8.17 $^{+0.1}_{-0.11}$	-1.32 $^{+0.07}_{-0.09}$	8.83 $^{+0.12}_{-0.5}$	0.43 $^{+0.15}_{-0.17}$	3.65 $^{+0.12}_{-0.5}$	1.25 $^{+0.15}_{-0.17}$
goods-s-deephst	10013609	6.9284	7.5 $^{+0.15}_{-0.13}$	< -0.24	8.11 $^{+0.35}_{-0.2}$	0.73 $^{+0.1}_{-0.12}$	2.1 $^{+0.35}_{-0.2}$	0.72 $^{+0.1}_{-0.12}$
goods-s-deephst	10013620	5.9169	8.04 $^{+0.13}_{-0.16}$	-0.89 $^{+0.12}_{-0.17}$	8.72 $^{+0.27}_{-0.26}$	0.66 $^{+0.05}_{-0.16}$	1.92 $^{+0.27}_{-0.26}$	-0.15 $^{+0.05}_{-0.16}$
goods-s-deepjwst	13271	5.5144	7.82 $^{+0.17}_{-0.17}$	< -0.83	8.65 $^{+0.16}_{-0.3}$	0.3 $^{+0.15}_{-0.12}$	2.85 $^{+0.16}_{-0.3}$	0.5 $^{+0.15}_{-0.12}$
goods-s-deepjwst	44938	5.1159	7.91 $^{+0.13}_{-0.14}$	< -1.1	8.58 $^{+0.16}_{-0.23}$	0.26 $^{+0.06}_{-0.12}$	1.09 $^{+0.16}_{-0.23}$	-1.23 $^{+0.06}_{-0.12}$
goods-s-deepjwst	52538	2.8075	8.42 $^{+0.06}_{-0.07}$	-1.46 $^{+0.08}_{-0.1}$	9.45 $^{+0.14}_{-0.18}$	0.48 $^{+0.22}_{-0.19}$	3.35 $^{+0.14}_{-0.18}$	0.38 $^{+0.22}_{-0.19}$
goods-s-deepjwst	60318988	6.0475	7.65 $^{+0.15}_{-0.13}$	< -0.6	8.17 $^{+0.23}_{-0.23}$	0.6 $^{+0.07}_{-0.07}$	2.64 $^{+0.23}_{-0.23}$	1.07 $^{+0.07}_{-0.07}$
goods-s-mediumhst	6384	2.6714	8.23 $^{+0.08}_{-0.09}$	-1.48 $^{+0.07}_{-0.09}$	9.32 $^{+0.08}_{-0.12}$	0.8 $^{+0.2}_{-0.16}$	3.34 $^{+0.08}_{-0.12}$	0.82 $^{+0.2}_{-0.16}$
goods-s-mediumhst	6821	1.6107	8.32 $^{+0.06}_{-0.06}$	-1.58 $^{+0.07}_{-0.08}$	9.66 $^{+0.09}_{-0.21}$	1.0 $^{+0.22}_{-0.12}$	2.9 $^{+0.09}_{-0.21}$	0.24 $^{+0.22}_{-0.12}$
goods-s-mediumhst	7091	2.8057	8.18 $^{+0.09}_{-0.11}$	< -1.3	9.07 $^{+0.07}_{-0.09}$	0.72 $^{+0.06}_{-0.08}$	3.26 $^{+0.07}_{-0.09}$	0.91 $^{+0.06}_{-0.08}$
goods-s-mediumhst	7511	2.0795	8.19 $^{+0.09}_{-0.11}$	< -1.2	8.65 $^{+0.16}_{-0.15}$	0.12 $^{+0.12}_{-0.18}$	2.37 $^{+0.3}_{-0.15}$	-0.16 $^{+0.12}_{-0.18}$
goods-s-mediumhst	8654	2.3428	8.42 $^{+0.11}_{-0.09}$	-1.08 $^{+0.07}_{-0.09}$	9.49 $^{+0.08}_{-0.07}$	0.24 $^{+0.14}_{-0.14}$	3.23 $^{+0.08}_{-0.07}$	-0.02 $^{+0.14}_{-0.29}$
goods-s-mediumhst	9598	3.3244	8.22 $^{+0.08}_{-0.1}$	-1.24 $^{+0.05}_{-0.06}$	8.72 $^{+0.7}_{-0.27}$	1.19 $^{+0.26}_{-0.02}$	2.19 $^{+0.27}_{-0.27}$	0.65 $^{+0.26}_{-0.02}$
goods-s-mediumhst	9881	3.3236	8.13 $^{+0.09}_{-0.11}$	< -1.49	9.05 $^{+0.06}_{-0.4}$	1.27 $^{+0.16}_{-0.01}$	2.45 $^{+0.06}_{-0.4}$	0.67 $^{+0.16}_{-0.01}$
goods-s-mediumhst	12122	2.5436	8.05 $^{+0.11}_{-0.13}$	< -1.28	8.14 $^{+0.1}_{-0.08}$	-0.07 $^{+0.06}_{-0.08}$	2.96 $^{+0.1}_{-0.08}$	0.76 $^{+0.06}_{-0.08}$
goods-s-mediumhst	12225	2.6908	8.18 $^{+0.1}_{-0.12}$	-1.05 $^{+0.05}_{-0.06}$	9.25 $^{+0.11}_{-0.15}$	0.82 $^{+0.11}_{-0.15}$	3.11 $^{+0.11}_{-0.15}$	0.67 $^{+0.11}_{-0.15}$
goods-s-mediumhst	12314	2.6265	7.95 $^{+0.12}_{-0.14}$	< -1.15	8.98 $^{+0.04}_{-0.06}$	0.11 $^{+0.13}_{-0.07}$	4.06 $^{+0.04}_{-0.06}$	1.19 $^{+0.13}_{-0.07}$
goods-s-mediumhst	12324	2.8103	8.13 $^{+0.11}_{-0.14}$	< -1.15	9.01 $^{+0.14}_{-0.11}$	0.37 $^{+0.14}_{-0.13}$	2.63 $^{+0.14}_{-0.21}$	-0.01 $^{+0.14}_{-0.13}$
goods-s-mediumhst	12382	2.2345	8.16 $^{+0.09}_{-0.11}$	< -1.39	8.97 $^{+0.11}_{-0.41}$	0.55 $^{+0.09}_{-0.13}$	2.5 $^{+0.27}_{-0.41}$	0.08 $^{+0.09}_{-0.13}$
goods-s-mediumhst	12663	2.4525	8.09 $^{+0.12}_{-0.14}$	-0.97 $^{+0.09}_{-0.11}$	9.16 $^{+0.1}_{-0.26}$	0.25 $^{+0.18}_{-0.18}$	2.6 $^{+0.1}_{-0.26}$	-0.31 $^{+0.18}_{-0.18}$
goods-s-mediumhst	12698	1.7609	8.32 $^{+0.07}_{-0.08}$	-1.26 $^{+0.05}_{-0.05}$	9.08 $^{+0.3}_{-0.16}$	0.81 $^{+0.12}_{-0.09}$	2.57 $^{+0.3}_{-0.16}$	0.3 $^{+0.12}_{-0.09}$
goods-s-mediumhst	12954	1.7567	8.6 $^{+0.04}_{-0.04}$	-0.76 $^{+0.04}_{-0.04}$	9.6 $^{+0.31}_{-0.21}$	1.55 $^{+0.09}_{-0.11}$	2.66 $^{+0.31}_{-0.21}$	0.61 $^{+0.09}_{-0.11}$
goods-s-mediumhst	13144	1.9959	8.14 $^{+0.15}_{-0.18}$	< -1.04	8.28 $^{+0.11}_{-0.11}$	-0.01 $^{+0.06}_{-0.06}$	1.46 $^{+0.11}_{-0.16}$	-0.83 $^{+0.06}_{-0.19}$
goods-s-mediumhst	14011	3.6031	7.73 $^{+0.14}_{-0.15}$	< -0.89	8.49 $^{+0.18}_{-0.17}$	0.41 $^{+0.04}_{-0.12}$	3.99 $^{+0.18}_{-0.17}$	1.9 $^{+0.07}_{-0.12}$
goods-s-mediumhst	14279	2.5435	8.61 $^{+0.04}_{-0.04}$	-0.78 $^{+0.02}_{-0.02}$	10.6 $^{+0.0}_{-0.51}$	2.66 $^{+0.0}_{-0.0}$	4.01 $^{+0.0}_{-0.51}$	2.07 $^{+0.0}_{-0.0}$
goods-s-mediumhst	15343	3.5791	8.06 $^{+0.13}_{-0.16}$	< -1.18	8.77 $^{+0.22}_{-0.42}$	0.56 $^{+0.13}_{-0.14}$	2.74 $^{+0.22}_{-0.42}$	0.54 $^{+0.13}_{-0.14}$
goods-s-mediumhst	15377	3.5456	8.56 $^{+0.04}_{-0.05}$	< -1.53	9.34 $^{+0.23}_{-0.29}$	1.14 $^{+0.23}_{-0.29}$	2.55 $^{+0.23}_{-0.29}$	0.35 $^{+0.23}_{-0.29}$
goods-s-mediumhst	36806	3.0176	8.34 $^{+0.07}_{-0.09}$	-1.5 $^{+0.06}_{-0.07}$	9.74 $^{+0.11}_{-0.1}$	0.66 $^{+0.23}_{-0.32}$	3.13 $^{+0.11}_{-0.1}$	0.05 $^{+0.23}_{-0.32}$
goods-s-mediumhst	38099	2.4997	8.35 $^{+0.06}_{-0.08}$	-1.35 $^{+0.05}_{-0.06}$	9.51 $^{+0.14}_{-0.16}$	0.6 $^{+0.28}_{-0.27}$	3.35 $^{+0.14}_{-0.16}$	0.44 $^{+0.28}_{-0.27}$
goods-s-mediumhst	39679	2.3037	8.31 $^{+0.07}_{-0.08}$	< -1.56	9.13 $^{+0.11}_{-0.17}$	0.17 $^{+0.18}_{-0.21}$	2.92 $^{+0.16}_{-0.17}$	-0.04 $^{+0.18}_{-0.21}$
goods-s-mediumhst	40450	2.4835	7.8 $^{+0.13}_{-0.12}$	< -0.9	8.28 $^{+0.08}_{-0.06}$	-0.05 $^{+0.08}_{-0.06}$	2.1 $^{+0.08}_{-0.1}$	-0.22 $^{+0.08}_{-0.06}$
goods-s-mediumhst	40847	1.5839	8.2 $^{+0.07}_{-0.09}$	< -1.65	9.22 $^{+0.11}_{-0.1}$	0.17 $^{+0.24}_{-0.18}$	3.23 $^{+0.11}_{-0.1}$	0.18 $^{+0.24}_{-0.18}$
goods-s-mediumhst	41241	2.6176	8.42 $^{+0.06}_{-0.07}$	-0.91 $^{+0.02}_{-0.02}$	9.86 $^{+0.11}_{-0.15}$	1.41 $^{+0.13}_{-0.26}$	3.45 $^{+0.11}_{-0.15}$	1.0 $^{+0.13}_{-0.26}$
goods-s-mediumhst	42987	2.6888	8.27 $^{+0.08}_{-0.09}$	-1.27 $^{+0.11}_{-0.15}$	8.72 $^{+0.6}_{-0.6}$	0.88 $^{+0.17}_{-0.04}$	1.75 $^{+0.6}_{-0.14}$	-0.08 $^{+0.17}_{-0.04}$
goods-s-mediumhst	45474	2.8515	8.13 $^{+0.12}_{-0.15}$	< -1.16	8.16 $^{+0.13}_{-0.09}$	-0.07 $^{+0.07}_{-0.1}$	1.79 $^{+0.13}_{-0.09}$	-0.44 $^{+0.07}_{-0.1}$
goods-s-mediumjwst	2150	2.5766	8.21 $^{+0.09}_{-0.12}$	-1.05 $^{+0.04}_{-0.04}$	9.23 $^{+0.09}_{-0.24}$	0.45 $^{+0.16}_{-0.12}$	3.34 $^{+0.09}_{-0.24}$	0.56 $^{+0.16}_{-0.12}$
goods-s-mediumjwst	3869	6.5676	8.19 $^{+0.12}_{-0.11}$	< -1.08	9.34 $^{+0.14}_{-0.21}$	0.65 $^{+0.32}_{-0.27}$	3.32 $^{+0.14}_{-0.21}$	0.63 $^{+0.32}_{-0.27}$

Table C.1. (continued)

Tier	ID	z_{spec}	12+log(O/H)	log(N/O)	log(M_*/M_{\odot})	SFR	Σ_{M_*}	Σ_{SFR}
goods-s-mediumjwst	4491	3.6538	8.19 $^{+0.09}_{-0.11}$	-1.22 $^{+0.04}_{-0.05}$	9.52 $^{+0.16}_{-0.24}$	1.06 $^{+0.27}_{-0.22}$	3.61 $^{+0.16}_{-0.24}$	1.15 $^{+0.27}_{-0.22}$
goods-s-mediumjwst	7212	3.6118	7.7 $^{+0.17}_{-0.14}$	< -0.64	8.31 $^{+0.06}_{-0.31}$	0.65 $^{+0.05}_{-0.44}$	2.17 $^{+0.06}_{-0.31}$	0.51 $^{+0.05}_{-0.44}$
goods-s-mediumjwst	8656	2.9727	8.27 $^{+0.18}_{-0.24}$	< -0.9	8.77 $^{+0.12}_{-0.12}$	-0.57 $^{+0.52}_{-0.83}$	2.01 $^{+0.12}_{-0.26}$	-1.33 $^{+0.52}_{-0.83}$
goods-s-mediumjwst	8825	2.8564	8.17 $^{+0.1}_{-0.11}$	< -1.33	8.71 $^{+0.11}_{-0.11}$	0.12 $^{+0.1}_{-0.08}$	2.56 $^{+0.11}_{-0.15}$	-0.03 $^{+0.1}_{-0.11}$
goods-s-mediumjwst	9045	2.1917	8.32 $^{+0.11}_{-0.13}$	< -0.88	8.81 $^{+0.25}_{-0.09}$	0.14 $^{+0.16}_{-0.11}$	2.07 $^{+0.25}_{-0.09}$	-0.6 $^{+0.16}_{-0.11}$
goods-s-mediumjwst	11813	1.739	8.02 $^{+0.11}_{-0.12}$	-1.13 $^{+0.11}_{-0.15}$	8.79 $^{+0.1}_{-0.14}$	-0.32 $^{+0.14}_{-0.12}$	2.89 $^{+0.1}_{-0.14}$	-0.22 $^{+0.14}_{-0.12}$
goods-s-mediumjwst	12709	2.6746	7.06 $^{+0.07}_{-0.06}$	< -0.49	8.21 $^{+0.2}_{-0.44}$	0.31 $^{+0.06}_{-0.06}$	3.85 $^{+0.2}_{-0.44}$	1.94 $^{+0.06}_{-0.06}$
goods-s-mediumjwst	13938	3.7034	8.2 $^{+0.09}_{-0.11}$	-1.34 $^{+0.12}_{-0.17}$	9.18 $^{+0.13}_{-0.13}$	0.45 $^{+0.29}_{-0.27}$	2.49 $^{+0.13}_{-0.17}$	-0.24 $^{+0.29}_{-0.27}$
goods-s-mediumjwst	28043	5.5539	8.09 $^{+0.14}_{-0.17}$	< -0.99	8.82 $^{+0.19}_{-0.17}$	0.58 $^{+0.13}_{-0.06}$	2.92 $^{+0.19}_{-0.17}$	0.68 $^{+0.13}_{-0.06}$
goods-s-mediumjwst	29686	3.1717	8.25 $^{+0.08}_{-0.09}$	< -1.51	8.97 $^{+0.22}_{-0.14}$	0.32 $^{+0.1}_{-0.13}$	3.57 $^{+0.22}_{-0.14}$	0.91 $^{+0.1}_{-0.13}$
goods-s-mediumjwst	33499	3.6982	8.22 $^{+0.13}_{-0.18}$	< -1.06	8.98 $^{+0.39}_{-0.29}$	0.75 $^{+0.11}_{-0.11}$	2.73 $^{+0.39}_{-0.29}$	0.51 $^{+0.11}_{-0.11}$
goods-s-mediumjwst	34104	5.6064	8.19 $^{+0.1}_{-0.13}$	-0.92 $^{+0.05}_{-0.05}$	9.08 $^{+0.25}_{-0.37}$	1.29 $^{+0.16}_{-0.08}$	3.88 $^{+0.25}_{-0.37}$	2.09 $^{+0.16}_{-0.08}$
goods-s-mediumjwst	35152	2.0211	8.25 $^{+0.1}_{-0.12}$	< -1.5	8.67 $^{+0.19}_{-0.19}$	0.33 $^{+0.17}_{-0.16}$	1.79 $^{+0.3}_{-0.19}$	-0.54 $^{+0.17}_{-0.16}$
goods-s-mediumjwst	35274	3.6002	8.12 $^{+0.12}_{-0.15}$	< -1.08	8.8 $^{+0.14}_{-0.18}$	0.05 $^{+0.2}_{-0.19}$	3.25 $^{+0.14}_{-0.18}$	0.49 $^{+0.2}_{-0.19}$
goods-s-mediumjwst	35472	4.6609	8.3 $^{+0.11}_{-0.12}$	-1.24 $^{+0.04}_{-0.04}$	9.98 $^{+0.12}_{-0.06}$	1.79 $^{+0.36}_{-0.43}$	3.34 $^{+0.12}_{-0.6}$	1.15 $^{+0.36}_{-0.43}$
goods-s-mediumjwst	36323	2.6714	8.52 $^{+0.05}_{-0.06}$	-0.89 $^{+0.05}_{-0.06}$	9.49 $^{+0.09}_{-0.59}$	0.64 $^{+0.32}_{-0.61}$	2.63 $^{+0.09}_{-0.59}$	-0.23 $^{+0.32}_{-0.61}$
goods-s-mediumjwst	36452	2.2805	8.21 $^{+0.08}_{-0.1}$	< -1.33	9.06 $^{+0.11}_{-0.08}$	-0.44 $^{+0.26}_{-0.51}$	2.89 $^{+0.11}_{-0.08}$	-0.61 $^{+0.26}_{-0.51}$
goods-s-mediumjwst	36679	2.6169	8.61 $^{+0.04}_{-0.05}$	-1.04 $^{+0.04}_{-0.05}$	9.62 $^{+0.83}_{-0.32}$	2.07 $^{+0.07}_{-0.32}$	2.65 $^{+0.83}_{-0.06}$	1.1 $^{+0.07}_{-0.32}$
goods-s-mediumjwst	37488	2.4339	8.23 $^{+0.07}_{-0.08}$	-1.53 $^{+0.07}_{-0.09}$	9.7 $^{+0.07}_{-0.06}$	1.05 $^{+0.27}_{-0.32}$	3.05 $^{+0.07}_{-0.3}$	0.4 $^{+0.27}_{-0.13}$
goods-s-mediumjwst	39215	1.9384	8.06 $^{+0.14}_{-0.17}$	< -0.73	8.36 $^{+0.24}_{-0.52}$	0.03 $^{+0.06}_{-0.22}$	2.16 $^{+0.24}_{-0.52}$	-0.17 $^{+0.06}_{-0.22}$
goods-s-mediumjwst	39302	2.6178	8.22 $^{+0.08}_{-0.1}$	-1.5 $^{+0.07}_{-0.09}$	8.69 $^{+0.09}_{-0.13}$	0.38 $^{+0.06}_{-0.05}$	1.98 $^{+0.09}_{-0.13}$	-0.32 $^{+0.06}_{-0.05}$
goods-s-mediumjwst	39411	4.0362	8.26 $^{+0.15}_{-0.23}$	< -1.01	9.14 $^{+0.11}_{-0.15}$	0.31 $^{+0.23}_{-0.17}$	2.86 $^{+0.11}_{-0.15}$	0.03 $^{+0.23}_{-0.17}$
goods-s-mediumjwst	39898	3.1692	8.43 $^{+0.05}_{-0.07}$	-1.16 $^{+0.04}_{-0.04}$	10.2 $^{+0.1}_{-0.14}$	1.21 $^{+0.36}_{-0.14}$	2.88 $^{+0.1}_{-0.14}$	-0.11 $^{+0.36}_{-0.18}$
goods-s-mediumjwst	40045	5.1274	8.01 $^{+0.15}_{-0.15}$	< -0.83	8.7 $^{+0.13}_{-0.37}$	0.32 $^{+0.18}_{-0.18}$	3.66 $^{+0.13}_{-0.37}$	1.28 $^{+0.14}_{-0.18}$
goods-s-mediumjwst	40069	4.0364	8.42 $^{+0.06}_{-0.07}$	-1.19 $^{+0.04}_{-0.04}$	9.61 $^{+0.16}_{-0.08}$	0.9 $^{+0.27}_{-0.19}$	3.14 $^{+0.16}_{-0.08}$	0.43 $^{+0.27}_{-0.19}$
goods-s-mediumjwst	41052	1.9647	8.3 $^{+0.09}_{-0.12}$	-1.36 $^{+0.11}_{-0.16}$	9.13 $^{+0.12}_{-0.05}$	0.2 $^{+0.18}_{-0.28}$	2.59 $^{+0.12}_{-0.05}$	-0.35 $^{+0.18}_{-0.28}$
goods-s-mediumjwst	41360	3.4704	8.18 $^{+0.09}_{-0.11}$	-1.41 $^{+0.03}_{-0.14}$	9.21 $^{+0.25}_{-0.25}$	0.8 $^{+0.15}_{-0.23}$	3.81 $^{+0.25}_{-0.25}$	1.4 $^{+0.15}_{-0.23}$
goods-s-mediumjwst	41457	3.327	8.06 $^{+0.1}_{-0.1}$	< -1.27	8.77 $^{+0.14}_{-0.14}$	0.3 $^{+0.15}_{-0.12}$	2.87 $^{+0.14}_{-0.14}$	0.41 $^{+0.15}_{-0.12}$
goods-s-mediumjwst	41503	2.8037	8.15 $^{+0.08}_{-0.1}$	-1.18 $^{+0.05}_{-0.05}$	9.51 $^{+0.06}_{-0.11}$	0.26 $^{+0.12}_{-0.1}$	3.48 $^{+0.06}_{-0.11}$	0.24 $^{+0.12}_{-0.1}$
goods-s-mediumjwst	41862	1.8369	8.45 $^{+0.07}_{-0.09}$	< -1.11	8.69 $^{+0.24}_{-0.22}$	0.03 $^{+0.23}_{-0.22}$	2.69 $^{+0.24}_{-0.22}$	0.03 $^{+0.23}_{-0.22}$
goods-s-mediumjwst	42789	2.8071	8.23 $^{+0.09}_{-0.11}$	-1.24 $^{+0.03}_{-0.03}$	9.53 $^{+0.06}_{-0.39}$	1.16 $^{+0.19}_{-0.1}$	3.06 $^{+0.06}_{-0.39}$	0.68 $^{+0.19}_{-0.1}$
goods-s-mediumjwst	43415	2.8903	8.1 $^{+0.12}_{-0.15}$	< -1.41	8.73 $^{+0.33}_{-0.39}$	0.61 $^{+0.08}_{-0.05}$	2.44 $^{+0.33}_{-0.14}$	0.32 $^{+0.08}_{-0.05}$
goods-s-mediumjwst	43457	1.7687	8.11 $^{+0.13}_{-0.18}$	< -1.05	8.66 $^{+0.15}_{-0.1}$	0.02 $^{+0.15}_{-0.07}$	3.04 $^{+0.15}_{-0.1}$	0.4 $^{+0.15}_{-0.07}$
goods-s-mediumjwst	45796	3.7743	8.37 $^{+0.08}_{-0.1}$	-1.03 $^{+0.09}_{-0.11}$	9.83 $^{+0.09}_{-0.07}$	0.75 $^{+0.32}_{-0.28}$	3.47 $^{+0.09}_{-0.07}$	0.38 $^{+0.32}_{-0.28}$
goods-s-mediumjwst	46274	2.6764	7.67 $^{+0.13}_{-0.12}$	< -0.8	8.65 $^{+0.03}_{-0.04}$	0.04 $^{+0.05}_{-0.02}$	3.65 $^{+0.03}_{-0.04}$	1.04 $^{+0.05}_{-0.02}$
goods-s-mediumjwst	47436	2.8605	7.89 $^{+0.12}_{-0.13}$	< -1.24	8.43 $^{+0.61}_{-0.12}$	0.86 $^{+0.06}_{-0.32}$	2.21 $^{+0.61}_{-0.12}$	0.64 $^{+0.06}_{-0.04}$
goods-s-mediumjwst	47870	1.9069	8.53 $^{+0.04}_{-0.05}$	-1.06 $^{+0.02}_{-0.02}$	10.06 $^{+0.08}_{-0.08}$	1.39 $^{+0.32}_{-0.26}$	3.17 $^{+0.08}_{-0.08}$	0.5 $^{+0.32}_{-0.26}$
goods-s-mediumjwst	48489	3.6445	8.18 $^{+0.1}_{-0.12}$	-1.3 $^{+0.11}_{-0.15}$	9.24 $^{+0.15}_{-0.31}$	0.91 $^{+0.15}_{-0.13}$	2.69 $^{+0.15}_{-0.31}$	0.37 $^{+0.15}_{-0.13}$
goods-s-mediumjwst	48769	1.8547	8.06 $^{+0.13}_{-0.13}$	< -1.36	8.95 $^{+0.17}_{-0.14}$	0.17 $^{+0.28}_{-0.21}$	3.17 $^{+0.17}_{-0.14}$	0.39 $^{+0.28}_{-0.21}$
goods-s-mediumjwst	48839	1.6123	8.41 $^{+0.06}_{-0.07}$	-1.48 $^{+0.1}_{-0.13}$	7.99 $^{+0.0}_{-0.0}$	0.36 $^{+0.01}_{-0.01}$	1.72 $^{+0.0}_{-0.0}$	0.08 $^{+0.01}_{-0.01}$
goods-s-mediumjwst	48912	2.4537	8.34 $^{+0.06}_{-0.07}$	-1.51 $^{+0.03}_{-0.03}$	9.68 $^{+0.24}_{-0.06}$	0.9 $^{+0.31}_{-0.11}$	3.35 $^{+0.24}_{-0.06}$	0.57 $^{+0.31}_{-0.11}$
goods-s-mediumjwst	48915	5.5224	8.14 $^{+0.09}_{-0.1}$	< -1.19	9.07 $^{+0.14}_{-0.16}$	0.49 $^{+0.14}_{-0.1}$	3.11 $^{+0.14}_{-0.16}$	0.53 $^{+0.14}_{-0.1}$
goods-s-mediumjwst	49246	3.6053	8.38 $^{+0.1}_{-0.18}$	< -0.87	9.08 $^{+0.08}_{-0.05}$	0.56 $^{+0.12}_{-0.08}$	3.09 $^{+0.08}_{-0.08}$	0.57 $^{+0.12}_{-0.08}$
goods-s-mediumjwst	49303	2.8806	8.27 $^{+0.08}_{-0.09}$	< -1.65	9.14 $^{+0.14}_{-0.14}$	0.28 $^{+0.21}_{-0.1}$	2.85 $^{+0.14}_{-0.19}$	-0.0 $^{+0.21}_{-0.41}$
goods-s-mediumjwst	49310	3.0192	8.18 $^{+0.09}_{-0.09}$	< -1.56	8.87 $^{+0.27}_{-0.19}$	0.32 $^{+0.11}_{-0.11}$	3.19 $^{+0.27}_{-0.08}$	0.64 $^{+0.11}_{-0.11}$
goods-s-mediumjwst	49738	2.3937	8.46 $^{+0.06}_{-0.06}$	-1.14 $^{+0.04}_{-0.04}$	9.53 $^{+0.18}_{-0.25}$	1.09 $^{+0.18}_{-0.18}$	2.49 $^{+0.18}_{-0.25}$	0.05 $^{+0.18}_{-0.13}$
goods-s-mediumjwst	50234	3.7004	7.63 $^{+0.14}_{-0.13}$	-1.09 $^{+0.11}_{-0.16}$	8.82 $^{+0.19}_{-0.19}$	0.67 $^{+0.15}_{-0.07}$	3.17 $^{+0.07}_{-0.19}$	1.03 $^{+0.15}_{-0.07}$

Table C.1. (continued)

Tier	ID	z_{spec}	12+log(O/H)	log(N/O)	log(M_*/M_{\odot})	SFR	Σ_{M_*}	Σ_{SFR}
goods-s-mediumjwst	50248	3.3217	$8.15^{+0.13}_{-0.17}$	< -0.94	$8.76^{+0.52}_{-0.11}$	$0.74^{+0.04}_{-0.11}$	$3.27^{+0.52}_{-0.11}$	$1.25^{+0.04}_{-0.11}$
goods-s-mediumjwst	51102	4.2304	$7.82^{+0.15}_{-0.14}$	$-0.91^{+0.12}_{-0.18}$	$8.66^{+0.23}_{-0.09}$	$0.34^{+0.11}_{-0.29}$	$2.78^{+0.23}_{-0.09}$	$0.47^{+0.11}_{-0.29}$
goods-s-mediumjwst	51300	2.5436	$8.37^{+0.07}_{-0.09}$	$-1.45^{+0.08}_{-0.09}$	$9.47^{+0.17}_{-0.14}$	$1.04^{+0.16}_{-0.19}$	$2.11^{+0.17}_{-0.17}$	$-0.32^{+0.16}_{-0.1}$
goods-s-mediumjwst	51318	3.4676	$8.3^{+0.09}_{-0.11}$	< -1.36	$9.24^{+0.34}_{-0.34}$	$0.85^{+0.1}_{-0.1}$	$2.05^{+0.34}_{-0.35}$	$-0.34^{+0.1}_{-0.1}$
goods-s-mediumjwst	51812	1.9025	$8.27^{+0.07}_{-0.08}$	$-1.72^{+0.07}_{-0.08}$	$9.43^{+0.08}_{-0.22}$	$0.76^{+0.23}_{-0.11}$	$2.75^{+0.08}_{-0.22}$	$0.08^{+0.23}_{-0.11}$
goods-s-mediumjwst	52500	3.6482	$7.78^{+0.15}_{-0.14}$	< -0.72	$5.97^{+0.11}_{-0.07}$	$-2.0^{+0.0}_{-0.0}$	$0.26^{+0.11}_{-0.07}$	$-1.71^{+0.0}_{-0.0}$
goods-s-mediumjwst	53237	2.9701	$8.36^{+0.07}_{-0.08}$	$-1.06^{+0.03}_{-0.03}$	$9.22^{+0.0}_{-0.0}$	$2.23^{+0.0}_{-0.0}$	$2.8^{+0.0}_{-0.0}$	$1.8^{+0.0}_{-0.0}$
goods-s-mediumjwst	53915	3.3273	$8.34^{+0.07}_{-0.09}$	$-1.43^{+0.09}_{-0.12}$	$9.37^{+0.22}_{-0.12}$	$0.95^{+0.07}_{-0.08}$	$3.04^{+0.22}_{-0.12}$	$0.62^{+0.07}_{-0.08}$
goods-s-mediumjwst	53979	4.0299	$7.89^{+0.13}_{-0.14}$	< -0.92	$8.72^{+0.1}_{-0.58}$	$0.47^{+0.1}_{-0.2}$	$3.5^{+0.1}_{-0.58}$	$1.25^{+0.1}_{-0.2}$
goods-s-mediumjwst	54418	2.9433	$7.85^{+0.16}_{-0.16}$	< -0.94	$8.65^{+0.11}_{-0.11}$	$-0.32^{+0.11}_{-0.09}$	$3.06^{+0.11}_{-0.11}$	$0.09^{+0.11}_{-0.09}$
goods-s-mediumjwst	54970	3.703	$8.25^{+0.13}_{-0.19}$	< -0.94	$8.89^{+0.15}_{-0.22}$	$0.53^{+0.13}_{-0.12}$	$2.8^{+0.15}_{-0.22}$	$0.44^{+0.13}_{-0.12}$
goods-s-mediumjwst	58815	4.9247	$8.06^{+0.13}_{-0.14}$	$-1.04^{+0.12}_{-0.17}$	$9.35^{+0.23}_{-0.14}$	$1.03^{+0.11}_{-0.18}$	$3.57^{+0.23}_{-0.18}$	$1.25^{+0.11}_{-0.18}$
goods-s-mediumjwst	60280	2.314	$8.39^{+0.06}_{-0.07}$	$-1.2^{+0.05}_{-0.06}$	$9.55^{+0.44}_{-0.03}$	$1.4^{+0.22}_{-0.22}$	$2.67^{+0.44}_{-0.03}$	$0.51^{+0.22}_{-0.22}$
goods-s-mediumjwst	61321	4.8419	$8.08^{+0.09}_{-0.1}$	$-1.08^{+0.05}_{-0.06}$	$8.7^{+0.08}_{-0.21}$	$0.87^{+0.07}_{-0.03}$	$3.64^{+0.08}_{-0.21}$	$1.81^{+0.07}_{-0.03}$
goods-s-mediumjwst	61360	2.6175	$7.89^{+0.13}_{-0.14}$	$-1.13^{+0.11}_{-0.14}$	$8.36^{+0.08}_{-0.06}$	$0.05^{+0.03}_{-0.06}$	$3.06^{+0.08}_{-0.06}$	$0.76^{+0.03}_{-0.06}$
goods-s-mediumjwst	62328	2.5734	$8.22^{+0.08}_{-0.1}$	$-1.17^{+0.03}_{-0.03}$	$9.9^{+0.02}_{-0.05}$	$1.14^{+0.01}_{-0.05}$	$2.99^{+0.02}_{-0.05}$	$0.23^{+0.01}_{-0.05}$
goods-s-mediumjwst	63722	3.0601	$7.96^{+0.12}_{-0.13}$	$-0.89^{+0.06}_{-0.07}$	$9.14^{+0.06}_{-0.04}$	$0.55^{+0.07}_{-0.05}$	$2.38^{+0.06}_{-0.04}$	$-0.21^{+0.07}_{-0.05}$
goods-s-mediumjwst	63829	2.6475	$8.42^{+0.05}_{-0.06}$	$-1.5^{+0.05}_{-0.05}$	$9.8^{+0.1}_{-0.1}$	$0.62^{+0.32}_{-0.33}$	$2.99^{+0.1}_{-0.1}$	$-0.19^{+0.32}_{-0.33}$
goods-s-mediumjwst	67776	2.8063	$8.16^{+0.09}_{-0.1}$	< -1.4	$9.18^{+0.12}_{-0.05}$	$0.87^{+0.08}_{-0.13}$	$3.04^{+0.12}_{-0.05}$	$0.74^{+0.08}_{-0.13}$
goods-s-mediumjwst	69251	2.6998	$8.35^{+0.07}_{-0.07}$	$-1.26^{+0.05}_{-0.06}$	$9.35^{+0.16}_{-0.17}$	$0.53^{+0.18}_{-0.23}$	$3.59^{+0.16}_{-0.17}$	$0.78^{+0.18}_{-0.23}$
goods-s-mediumjwst	73678	3.1636	$7.96^{+0.12}_{-0.14}$	< -1.14	$8.79^{+0.07}_{-0.11}$	$0.2^{+0.24}_{-0.1}$	$3.29^{+0.07}_{-0.11}$	$0.7^{+0.24}_{-0.1}$
goods-s-mediumjwst	76988	2.4094	$8.25^{+0.08}_{-0.1}$	$-1.67^{+0.1}_{-0.13}$	$8.96^{+0.22}_{-0.22}$	$0.48^{+0.17}_{-0.11}$	$3.25^{+0.22}_{-0.22}$	$0.77^{+0.17}_{-0.11}$
goods-s-mediumjwst	79065	3.5833	$7.62^{+0.17}_{-0.14}$	< -0.7	$7.97^{+0.12}_{-0.16}$	$-0.02^{+0.05}_{-0.11}$	$1.85^{+0.12}_{-0.16}$	$-0.14^{+0.05}_{-0.11}$
goods-s-mediumjwst	83231	3.1671	$7.49^{+0.15}_{-0.13}$	< -0.49	$7.83^{+0.19}_{-0.09}$	$-0.31^{+0.05}_{-0.08}$	$3.06^{+0.19}_{-0.09}$	$0.92^{+0.05}_{-0.08}$
goods-s-mediumjwst	83666	2.5459	$8.39^{+0.06}_{-0.07}$	$-1.08^{+0.03}_{-0.03}$	$10.02^{+0.07}_{-0.01}$	$0.36^{+0.38}_{-0.6}$	$3.0^{+0.07}_{-0.1}$	$-0.66^{+0.38}_{-0.6}$
goods-s-mediumjwst	85314	3.5851	$8.32^{+0.08}_{-0.09}$	< -1.25	$9.14^{+0.09}_{-0.15}$	$0.13^{+0.22}_{-0.2}$	$3.6^{+0.09}_{-0.15}$	$0.59^{+0.02}_{-0.2}$
goods-s-mediumjwst	86199	2.6983	$8.37^{+0.09}_{-0.12}$	< -1.14	$9.2^{+0.06}_{-0.08}$	$0.09^{+0.02}_{-0.08}$	$3.5^{+0.06}_{-0.08}$	$0.4^{+0.2}_{-0.2}$
goods-s-mediumjwst	86727	3.5934	$8.03^{+0.16}_{-0.18}$	< -0.78	$8.85^{+0.1}_{-0.15}$	$-0.14^{+0.26}_{-0.21}$	$3.12^{+0.1}_{-0.15}$	$0.14^{+0.26}_{-0.21}$
goods-s-mediumjwst	88540	2.6209	$8.29^{+0.07}_{-0.07}$	$-1.35^{+0.04}_{-0.05}$	$9.84^{+0.43}_{-0.07}$	$-0.13^{+0.43}_{-0.61}$	$3.61^{+0.07}_{-0.07}$	$-0.36^{+0.43}_{-0.61}$
goods-s-mediumjwst	89372	2.6747	$8.29^{+0.09}_{-0.11}$	$-1.26^{+0.09}_{-0.11}$	$8.9^{+0.19}_{-0.13}$	$0.57^{+0.21}_{-0.16}$	$2.29^{+0.19}_{-0.13}$	$-0.05^{+0.21}_{-0.16}$
goods-s-mediumjwst	91285	5.7328	$7.71^{+0.14}_{-0.13}$	< -0.5	$8.16^{+0.29}_{-0.39}$	$0.61^{+0.04}_{-0.03}$	$1.97^{+0.29}_{-0.39}$	$0.41^{+0.04}_{-0.03}$
goods-s-mediumjwst	91345	1.6126	$8.22^{+0.08}_{-0.09}$	$-1.4^{+0.09}_{-0.11}$	$8.77^{+0.18}_{-0.13}$	$0.12^{+0.12}_{-0.18}$	$2.98^{+0.18}_{-0.18}$	$0.32^{+0.12}_{-0.18}$
goods-s-mediumjwst	91992	1.8984	$8.42^{+0.06}_{-0.07}$	$-1.48^{+0.06}_{-0.07}$	$9.46^{+0.13}_{-0.19}$	$0.13^{+0.32}_{-0.32}$	$2.34^{+0.12}_{-0.19}$	$-0.99^{+0.32}_{-0.32}$
goods-s-mediumjwst	94511	3.5558	$7.92^{+0.12}_{-0.13}$	< -1.06	$8.72^{+0.12}_{-0.32}$	$0.29^{+0.05}_{-0.19}$	$3.37^{+0.12}_{-0.32}$	$0.94^{+0.05}_{-0.36}$
goods-s-mediumjwst	95278	4.4783	$8.01^{+0.11}_{-0.13}$	< -1.27	$8.88^{+0.1}_{-0.26}$	$1.01^{+0.16}_{-0.2}$	$2.32^{+0.1}_{-0.26}$	$0.45^{+0.16}_{-0.2}$
goods-s-mediumjwst	105581	3.9996	$8.22^{+0.11}_{-0.14}$	$-1.17^{+0.06}_{-0.07}$	$9.03^{+0.39}_{-0.39}$	$1.02^{+0.12}_{-0.37}$	$3.09^{+0.39}_{-0.39}$	$1.08^{+0.12}_{-0.37}$
goods-s-mediumjwst	114786	2.9927	$7.78^{+0.18}_{-0.15}$	< -0.9	$8.33^{+0.19}_{-0.13}$	$0.19^{+0.14}_{-0.13}$	$2.36^{+0.19}_{-0.31}$	$0.21^{+0.14}_{-0.13}$
goods-s-mediumjwst	119227	2.8683	$8.05^{+0.13}_{-0.14}$	< -0.91	$8.31^{+0.31}_{-0.54}$	$-0.07^{+0.06}_{-0.43}$	$2.4^{+0.12}_{-0.54}$	$0.03^{+0.06}_{-0.17}$
goods-s-mediumjwst	124032	2.6412	$8.21^{+0.1}_{-0.12}$	< -1.29	$8.88^{+0.11}_{-0.16}$	$0.18^{+0.17}_{-0.19}$	$2.29^{+0.11}_{-0.18}$	$-0.4^{+0.17}_{-0.19}$
goods-s-mediumjwst	125579	4.8745	$7.99^{+0.12}_{-0.13}$	$-1.21^{+0.12}_{-0.16}$	$8.94^{+0.15}_{-0.15}$	$0.49^{+0.15}_{-0.12}$	$2.38^{+0.15}_{-0.15}$	$-0.07^{+0.15}_{-0.12}$
goods-s-mediumjwst	126215	3.6065	$8.27^{+0.07}_{-0.08}$	< -1.56	$9.52^{+0.1}_{-0.08}$	$-0.08^{+0.36}_{-0.43}$	$4.08^{+0.1}_{-0.08}$	$0.48^{+0.36}_{-0.43}$
goods-s-mediumjwst	126865	2.8496	$8.0^{+0.13}_{-0.16}$	< -1.33	$8.86^{+0.21}_{-0.26}$	$0.6^{+0.05}_{-0.08}$	$2.58^{+0.21}_{-0.26}$	$0.32^{+0.05}_{-0.08}$
goods-s-mediumjwst	128723	2.3303	$8.04^{+0.17}_{-0.2}$	< -1.18	$8.04^{+0.32}_{-0.2}$	$0.08^{+0.05}_{-0.08}$	$2.55^{+0.32}_{-0.2}$	$0.58^{+0.05}_{-0.08}$
goods-s-mediumjwst	129636	3.5494	$8.03^{+0.15}_{-0.16}$	< -0.99	$8.23^{+0.14}_{-0.14}$	$0.37^{+0.05}_{-0.05}$	$3.07^{+0.14}_{-0.14}$	$1.21^{+0.05}_{-0.08}$
goods-s-mediumjwst	132638	3.3233	$8.13^{+0.09}_{-0.12}$	< -1.63	$9.05^{+0.06}_{-0.06}$	$1.27^{+0.16}_{-0.16}$	$2.45^{+0.06}_{-0.16}$	$0.67^{+0.16}_{-0.16}$
goods-s-mediumjwst	145445	1.9217	$8.52^{+0.05}_{-0.05}$	$-1.0^{+0.03}_{-0.03}$	$9.68^{+0.18}_{-0.14}$	$0.92^{+0.22}_{-0.21}$	$4.71^{+0.18}_{-0.14}$	$1.94^{+0.22}_{-0.23}$
goods-s-mediumjwst	147779	6.6253	$7.84^{+0.16}_{-0.16}$	< -0.52	$8.41^{+0.11}_{-0.26}$	$0.46^{+0.09}_{-0.06}$	$2.91^{+0.11}_{-0.26}$	$0.96^{+0.09}_{-0.06}$

Table C.1. (continued)

Tier	ID	z_{spec}	12+log(O/H)	log(N/O)	log(M_*/M_{\odot})	SFR	Σ_{M_*}	Σ_{SFR}
goods-s-mediumjwst	147993	3.3201	$8.51^{+0.06}_{-0.06}$	$-1.37^{+0.11}_{-0.14}$	$9.78^{+0.13}_{-0.19}$	$1.07^{+0.4}_{-0.32}$	$2.7^{+0.13}_{-0.19}$	$-0.02^{+0.4}_{-0.32}$
goods-s-mediumjwst	155596	2.4858	$8.39^{+0.07}_{-0.09}$	$-1.27^{+0.06}_{-0.07}$	$9.44^{+0.12}_{-0.17}$	$0.34^{+0.44}_{-0.68}$	$3.03^{+0.12}_{-0.17}$	$-0.06^{+0.44}_{-0.68}$
goods-s-mediumjwst	157811	1.612	$8.15^{+0.11}_{-0.14}$	$-0.97^{+0.07}_{-0.09}$	$9.0^{+0.15}_{-0.15}$	$-0.06^{+0.25}_{-0.27}$	$3.34^{+0.15}_{-0.15}$	$0.28^{+0.25}_{-0.27}$
goods-s-mediumjwst	158011	1.6197	$7.68^{+0.14}_{-0.13}$	< -0.87	$8.28^{+0.09}_{-0.19}$	$0.19^{+0.09}_{-0.11}$	$2.96^{+0.09}_{-0.19}$	$0.87^{+0.09}_{-0.11}$
goods-s-mediumjwst	158633	2.5675	$8.42^{+0.06}_{-0.07}$	$-1.1^{+0.03}_{-0.03}$	$9.82^{+0.18}_{-0.14}$	$0.93^{+0.27}_{-0.38}$	$3.17^{+0.18}_{-0.14}$	$0.28^{+0.27}_{-0.38}$
goods-s-mediumjwst	159386	2.5723	$8.21^{+0.12}_{-0.12}$	$-1.26^{+0.09}_{-0.12}$	$9.6^{+0.13}_{-0.13}$	$0.77^{+0.16}_{-0.21}$	$2.86^{+0.13}_{-0.13}$	$0.03^{+0.16}_{-0.21}$
goods-s-mediumjwst	159401	2.5659	$8.19^{+0.1}_{-0.12}$	< -1.47	$9.09^{+0.08}_{-0.08}$	$0.26^{+0.09}_{-0.14}$	$3.43^{+0.08}_{-0.08}$	$0.6^{+0.09}_{-0.14}$
goods-s-mediumjwst	159802	3.6117	$8.25^{+0.07}_{-0.09}$	< -1.48	$9.48^{+0.06}_{-0.12}$	$0.49^{+0.19}_{-0.2}$	$2.97^{+0.06}_{-0.12}$	$-0.02^{+0.19}_{-0.2}$
goods-s-mediumjwst	159811	1.8751	$8.45^{+0.05}_{-0.06}$	$-1.06^{+0.02}_{-0.02}$	$10.06^{+0.06}_{-0.15}$	$1.42^{+0.14}_{-0.55}$	$3.23^{+0.06}_{-0.15}$	$0.59^{+0.14}_{-0.55}$
goods-s-mediumjwst	162894	2.0149	$8.38^{+0.06}_{-0.07}$	$-1.25^{+0.05}_{-0.06}$	$9.43^{+0.17}_{-0.12}$	$0.27^{+0.25}_{-0.87}$	$3.47^{+0.17}_{-0.12}$	$0.31^{+0.25}_{-0.87}$
goods-s-mediumjwst	165209	3.4206	$8.49^{+0.05}_{-0.07}$	< -1.39	$9.88^{+0.13}_{-0.48}$	$1.24^{+0.26}_{-0.35}$	$2.33^{+0.13}_{-0.48}$	$-0.31^{+0.26}_{-0.35}$
goods-s-mediumjwst	165355	2.5697	$8.39^{+0.06}_{-0.07}$	$-1.03^{+0.02}_{-0.02}$	$9.84^{+0.12}_{-0.1}$	$1.12^{+0.28}_{-0.13}$	$4.04^{+0.12}_{-0.1}$	$1.32^{+0.28}_{-0.13}$
goods-s-mediumjwst	166295	1.9302	$8.35^{+0.06}_{-0.08}$	$-1.29^{+0.05}_{-0.05}$	$9.47^{+0.09}_{-0.13}$	$0.39^{+0.37}_{-0.3}$	$2.83^{+0.09}_{-0.13}$	$-0.25^{+0.37}_{-0.3}$
goods-s-mediumjwst	167512	2.3261	$8.4^{+0.07}_{-0.09}$	$-1.29^{+0.05}_{-0.06}$	$9.56^{+0.15}_{-0.25}$	$0.89^{+0.14}_{-0.21}$	$1.67^{+0.15}_{-0.25}$	$-1.0^{+0.14}_{-0.21}$
goods-s-mediumjwst	167639	5.552	$7.69^{+0.14}_{-0.12}$	< -0.57	$8.17^{+0.24}_{-0.27}$	$0.59^{+0.06}_{-0.08}$	$2.58^{+0.24}_{-0.27}$	$1.0^{+0.06}_{-0.08}$
goods-s-mediumjwst	167669	3.7003	$8.32^{+0.09}_{-0.12}$	< -1.2	$9.34^{+0.14}_{-0.17}$	$0.78^{+0.12}_{-0.18}$	$3.09^{+0.14}_{-0.17}$	$0.53^{+0.12}_{-0.18}$
goods-s-mediumjwst	167774	2.8587	$8.42^{+0.06}_{-0.08}$	$-1.18^{+0.03}_{-0.04}$	$9.76^{+0.21}_{-0.28}$	$1.51^{+0.24}_{-0.09}$	$4.29^{+0.21}_{-0.28}$	$2.05^{+0.24}_{-0.09}$
goods-s-mediumjwst	169690	2.5655	$8.36^{+0.07}_{-0.09}$	$-0.93^{+0.05}_{-0.05}$	$9.87^{+0.1}_{-0.1}$	$0.46^{+0.26}_{-0.33}$	$3.37^{+0.1}_{-0.1}$	$-0.03^{+0.26}_{-0.33}$
goods-s-mediumjwst	172074	4.4305	$7.95^{+0.13}_{-0.15}$	< -1.07	$8.59^{+0.25}_{-0.35}$	$0.4^{+0.15}_{-0.1}$	$2.18^{+0.25}_{-0.35}$	$-0.01^{+0.15}_{-0.1}$
goods-s-mediumjwst	173246	3.7	$8.25^{+0.08}_{-0.09}$	< -1.52	$9.5^{+0.06}_{-0.1}$	$0.86^{+0.13}_{-0.13}$	$2.64^{+0.06}_{-0.1}$	$0.01^{+0.13}_{-0.13}$
goods-s-mediumjwst	173895	2.3226	$8.34^{+0.1}_{-0.13}$	< -0.96	$7.28^{+0.16}_{-0.29}$	$-1.1^{+0.21}_{-0.3}$	$0.76^{+0.16}_{-0.29}$	$-1.62^{+0.21}_{-0.3}$
goods-s-mediumjwst	175034	3.4697	$8.3^{+0.09}_{-0.11}$	< -1.22	$8.91^{+0.11}_{-0.06}$	$0.5^{+0.11}_{-0.15}$	$2.22^{+0.11}_{-0.06}$	$-0.19^{+0.11}_{-0.15}$
goods-s-mediumjwst	175166	2.0792	$8.41^{+0.06}_{-0.06}$	$-1.51^{+0.07}_{-0.09}$	$9.12^{+0.16}_{-0.13}$	$0.19^{+0.26}_{-0.2}$	$2.56^{+0.16}_{-0.13}$	$-0.37^{+0.26}_{-0.2}$
goods-s-mediumjwst	176562	2.0771	$8.57^{+0.25}_{-0.24}$	$-1.18^{+0.03}_{-0.03}$	$9.87^{+0.25}_{-0.21}$	$1.8^{+0.15}_{-0.18}$	$3.06^{+0.25}_{-0.21}$	$0.99^{+0.15}_{-0.18}$
goods-s-mediumjwst	177520	3.4703	$8.18^{+0.1}_{-0.11}$	< -1.33	$9.04^{+0.26}_{-0.26}$	$0.42^{+0.21}_{-0.19}$	$2.98^{+0.16}_{-0.28}$	$0.36^{+0.19}_{-0.19}$
goods-s-mediumjwst	179198	3.8306	$7.91^{+0.12}_{-0.13}$	$-0.92^{+0.05}_{-0.06}$	$8.3^{+0.48}_{-0.0}$	$0.82^{+0.01}_{-0.18}$	$0.89^{+0.48}_{-0.0}$	$-0.59^{+0.01}_{-0.18}$
goods-s-mediumjwst	180657	3.5826	$8.15^{+0.09}_{-0.11}$	$-1.35^{+0.07}_{-0.08}$	$9.47^{+0.28}_{-0.22}$	$1.13^{+0.12}_{-0.12}$	$2.99^{+0.28}_{-0.22}$	$0.65^{+0.12}_{-0.12}$
goods-s-mediumjwst	180813	2.0716	$8.39^{+0.06}_{-0.08}$	$-1.25^{+0.06}_{-0.07}$	$9.74^{+0.08}_{-0.06}$	$0.34^{+0.16}_{-0.23}$	$3.27^{+0.08}_{-0.06}$	$-0.13^{+0.16}_{-0.23}$
goods-s-mediumjwst	181082	2.8039	$8.4^{+0.06}_{-0.07}$	$-1.01^{+0.02}_{-0.02}$	$9.98^{+0.28}_{-0.17}$	$1.59^{+0.23}_{-0.17}$	$3.38^{+0.28}_{-0.17}$	$0.99^{+0.23}_{-0.17}$
goods-s-mediumjwst	181867	3.7015	$7.8^{+0.13}_{-0.13}$	< -1.12	$8.63^{+0.07}_{-0.21}$	$0.53^{+0.05}_{-0.11}$	$2.69^{+0.07}_{-0.21}$	$0.59^{+0.05}_{-0.11}$
goods-s-mediumjwst	182666	2.0328	$8.32^{+0.09}_{-0.11}$	$-1.03^{+0.09}_{-0.11}$	$8.69^{+0.21}_{-0.17}$	$-0.12^{+0.14}_{-0.14}$	$2.87^{+0.11}_{-0.1}$	$0.06^{+0.14}_{-0.1}$
goods-s-mediumjwst	184060	4.7372	$7.85^{+0.14}_{-0.14}$	< -0.93	$8.61^{+0.33}_{-0.07}$	$0.48^{+0.07}_{-0.06}$	$3.09^{+0.22}_{-0.07}$	$0.96^{+0.07}_{-0.06}$
goods-s-mediumjwst	184490	3.8301	$8.05^{+0.11}_{-0.13}$	$-1.33^{+0.09}_{-0.11}$	$8.72^{+0.32}_{-0.18}$	$0.8^{+0.08}_{-0.12}$	$2.44^{+0.32}_{-0.18}$	$0.52^{+0.08}_{-0.12}$
goods-s-mediumjwst	184541	2.2938	$8.38^{+0.06}_{-0.08}$	$-1.48^{+0.11}_{-0.16}$	$9.42^{+0.15}_{-0.13}$	$0.76^{+0.13}_{-0.27}$	$2.93^{+0.15}_{-0.13}$	$0.27^{+0.13}_{-0.27}$
goods-s-mediumjwst	184677	3.1994	$8.28^{+0.07}_{-0.1}$	< -1.13	$9.1^{+0.1}_{-0.2}$	$0.36^{+0.21}_{-0.19}$	$3.8^{+0.1}_{-0.2}$	$1.06^{+0.21}_{-0.19}$
goods-s-mediumjwst	185049	2.6537	$7.42^{+0.13}_{-0.11}$	< -0.88	$8.52^{+0.13}_{-0.86}$	$0.36^{+0.24}_{-0.12}$	$2.57^{+0.13}_{-0.86}$	$0.42^{+0.24}_{-0.12}$
goods-s-mediumjwst	185550	2.0767	$8.24^{+0.09}_{-0.11}$	$-1.31^{+0.1}_{-0.13}$	$9.16^{+0.07}_{-0.09}$	$0.13^{+0.12}_{-0.15}$	$2.53^{+0.07}_{-0.09}$	$-0.49^{+0.12}_{-0.15}$
goods-s-mediumjwst	186024	1.6121	$8.05^{+0.1}_{-0.13}$	< -1.52	$8.58^{+0.17}_{-0.13}$	$0.21^{+0.17}_{-0.07}$	$2.82^{+0.17}_{-0.23}$	$0.45^{+0.1}_{-0.07}$
goods-s-mediumjwst	187034	3.6534	$8.3^{+0.07}_{-0.09}$	$-1.45^{+0.1}_{-0.13}$	$9.52^{+0.11}_{-0.1}$	$1.12^{+0.12}_{-0.12}$	$3.64^{+0.11}_{-0.1}$	$1.24^{+0.12}_{-0.17}$
goods-s-mediumjwst	187036	1.9881	$8.44^{+0.06}_{-0.07}$	$-1.07^{+0.03}_{-0.03}$	$9.88^{+0.16}_{-0.17}$	$0.99^{+0.17}_{-0.21}$	$3.07^{+0.16}_{-0.17}$	$0.18^{+0.17}_{-0.21}$
goods-s-mediumjwst	188465	1.6086	$8.35^{+0.09}_{-0.13}$	< -1.05	$8.96^{+0.06}_{-0.11}$	$-0.22^{+0.18}_{-0.15}$	$3.2^{+0.06}_{-0.11}$	$0.01^{+0.18}_{-0.15}$
goods-s-mediumjwst	188720	2.3236	$8.4^{+0.06}_{-0.07}$	$-1.29^{+0.03}_{-0.03}$	$9.78^{+0.26}_{-0.31}$	$0.83^{+0.28}_{-0.2}$	$3.12^{+0.26}_{-0.31}$	$0.17^{+0.28}_{-0.2}$
goods-s-mediumjwst	188785	3.0566	$8.29^{+0.08}_{-0.08}$	$-1.1^{+0.04}_{-0.04}$	$9.66^{+0.12}_{-0.16}$	$1.07^{+0.2}_{-0.17}$	$2.74^{+0.12}_{-0.16}$	$0.15^{+0.1}_{-0.17}$
goods-s-mediumjwst	189417	3.7002	$8.1^{+0.11}_{-0.11}$	$-1.18^{+0.07}_{-0.07}$	$8.9^{+0.25}_{-0.25}$	$1.19^{+0.04}_{-0.07}$	$2.63^{+0.25}_{-0.25}$	$0.91^{+0.04}_{-0.11}$
goods-s-mediumjwst	189760	3.602	$8.23^{+0.08}_{-0.11}$	$-1.19^{+0.07}_{-0.09}$	$9.27^{+0.22}_{-0.22}$	$1.04^{+0.09}_{-0.11}$	$3.01^{+0.22}_{-0.08}$	$0.78^{+0.09}_{-0.09}$
goods-s-mediumjwst	190389	2.0356	$8.35^{+0.08}_{-0.1}$	$-0.94^{+0.03}_{-0.05}$	$9.71^{+0.08}_{-0.12}$	$0.44^{+0.98}_{-0.2}$	$3.51^{+0.08}_{-0.12}$	$0.24^{+0.88}_{-0.2}$
goods-s-mediumjwst	190921	2.9737	$8.17^{+0.08}_{-0.1}$	< -1.41	$9.0^{+0.07}_{-0.19}$	$0.38^{+0.11}_{-0.22}$	$3.56^{+0.07}_{-0.19}$	$0.94^{+0.11}_{-0.22}$

Table C.1. (continued)

Tier	ID	z_{spec}	12+log(O/H)	log(N/O)	log(M_*/M_{\odot})	SFR	Σ_{M_*}	Σ_{SFR}
goods-s-mediumjwst	191117	3.6522	8.36 $^{+0.07}_{-0.08}$	-1.25 $^{+0.06}_{-0.07}$	9.66 $^{+0.1}_{-0.22}$	0.95 $^{+0.22}_{-0.27}$	3.18 $^{+0.1}_{-0.22}$	0.46 $^{+0.22}_{-0.27}$
goods-s-mediumjwst	191250	5.3875	8.43 $^{+0.06}_{-0.06}$	-1.18 $^{+0.02}_{-0.02}$	10.3 $^{+0.09}_{-0.13}$	1.83 $^{+0.1}_{-0.2}$	3.44 $^{+0.09}_{-0.13}$	0.97 $^{+0.1}_{-0.2}$
goods-s-mediumjwst	192113	1.7799	8.35 $^{+0.07}_{-0.07}$	-1.33 $^{+0.05}_{-0.06}$	9.63 $^{+0.15}_{-0.28}$	0.94 $^{+0.21}_{-0.2}$	2.24 $^{+0.15}_{-0.15}$	-0.45 $^{+0.21}_{-0.2}$
goods-s-mediumjwst	192368	1.7649	8.02 $^{+0.11}_{-0.13}$	< -1.07	8.45 $^{+0.16}_{-0.2}$	-0.02 $^{+0.08}_{-0.09}$	1.94 $^{+0.16}_{-0.16}$	-0.53 $^{+0.08}_{-0.2}$
goods-s-mediumjwst	193784	2.7048	8.18 $^{+0.13}_{-0.16}$	< -1.0	8.66 $^{+0.07}_{-0.15}$	-0.66 $^{+0.39}_{-0.56}$	2.73 $^{+0.07}_{-0.15}$	-0.59 $^{+0.39}_{-0.56}$
goods-s-mediumjwst	194091	4.8359	8.14 $^{+0.18}_{-0.22}$	< -1.12	8.86 $^{+0.31}_{-0.18}$	0.55 $^{+0.08}_{-0.21}$	3.24 $^{+0.31}_{-0.18}$	0.93 $^{+0.08}_{-0.21}$
goods-s-mediumjwst	194580	1.9043	8.37 $^{+0.06}_{-0.08}$	-1.34 $^{+0.06}_{-0.07}$	9.48 $^{+0.14}_{-0.17}$	0.31 $^{+0.34}_{-0.28}$	3.23 $^{+0.14}_{-0.17}$	0.06 $^{+0.34}_{-0.28}$
goods-s-mediumjwst	195588	2.0361	8.42 $^{+0.06}_{-0.07}$	-1.22 $^{+0.03}_{-0.03}$	9.86 $^{+0.31}_{-0.3}$	1.49 $^{+0.19}_{-0.26}$	4.3 $^{+0.31}_{-0.3}$	1.93 $^{+0.19}_{-0.26}$
goods-s-mediumjwst	196423	4.5057	8.31 $^{+0.08}_{-0.11}$	-1.55 $^{+0.12}_{-0.17}$	9.2 $^{+0.11}_{-0.15}$	0.37 $^{+0.23}_{-0.26}$	2.59 $^{+0.11}_{-0.15}$	-0.25 $^{+0.23}_{-0.26}$
goods-s-mediumjwst	196916	3.6955	8.2 $^{+0.11}_{-0.13}$	< -1.29	8.97 $^{+0.14}_{-0.25}$	0.82 $^{+0.17}_{-0.12}$	3.38 $^{+0.14}_{-0.25}$	1.23 $^{+0.17}_{-0.12}$
goods-s-mediumjwst	200503	2.0729	8.1 $^{+0.11}_{-0.13}$	< -1.05	8.49 $^{+0.05}_{-0.09}$	0.08 $^{+0.02}_{-0.03}$	3.53 $^{+0.05}_{-0.09}$	1.11 $^{+0.02}_{-0.03}$
goods-s-mediumjwst	201295	1.9878	8.27 $^{+0.08}_{-0.09}$	-1.21 $^{+0.09}_{-0.11}$	9.42 $^{+0.07}_{-0.1}$	-0.66 $^{+0.42}_{-0.64}$	2.94 $^{+0.07}_{-0.1}$	-1.13 $^{+0.42}_{-0.64}$
goods-s-mediumjwst	202258	2.3462	8.54 $^{+0.05}_{-0.06}$	-0.79 $^{+0.04}_{-0.05}$	10.43 $^{+0.09}_{-0.11}$	1.42 $^{+0.34}_{-0.29}$	3.26 $^{+0.09}_{-0.11}$	0.26 $^{+0.34}_{-0.29}$
goods-s-mediumjwst	202630	2.6261	8.4 $^{+0.05}_{-0.06}$	-1.07 $^{+0.02}_{-0.02}$	9.9 $^{+0.1}_{-0.09}$	1.28 $^{+0.26}_{-0.1}$	3.79 $^{+0.1}_{-0.09}$	1.16 $^{+0.26}_{-0.1}$
goods-s-mediumjwst	203438	1.9058	8.52 $^{+0.04}_{-0.05}$	-0.93 $^{+0.02}_{-0.02}$	9.89 $^{+0.09}_{-0.1}$	1.58 $^{+0.09}_{-0.03}$	3.44 $^{+0.09}_{-0.1}$	1.13 $^{+0.09}_{-0.03}$
goods-s-mediumjwst	203768	2.994	8.44 $^{+0.06}_{-0.06}$	-1.27 $^{+0.04}_{-0.04}$	9.97 $^{+0.17}_{-0.21}$	0.88 $^{+0.28}_{-0.42}$	3.16 $^{+0.17}_{-0.21}$	0.07 $^{+0.28}_{-0.42}$
goods-s-mediumjwst	203924	2.8051	8.27 $^{+0.09}_{-0.11}$	< -1.49	9.13 $^{+0.12}_{-0.21}$	0.25 $^{+0.15}_{-0.2}$	2.01 $^{+0.12}_{-0.21}$	-0.87 $^{+0.15}_{-0.2}$
goods-s-mediumjwst	203973	2.345	8.3 $^{+0.07}_{-0.08}$	-1.38 $^{+0.03}_{-0.03}$	9.41 $^{+0.15}_{-0.25}$	0.97 $^{+0.21}_{-0.13}$	3.03 $^{+0.15}_{-0.25}$	0.6 $^{+0.21}_{-0.13}$
goods-s-mediumjwst	203994	4.0445	7.93 $^{+0.22}_{-0.23}$	-0.72 $^{+0.12}_{-0.12}$	9.05 $^{+0.44}_{-0.34}$	0.67 $^{+0.18}_{-0.37}$	2.91 $^{+0.44}_{-0.24}$	0.53 $^{+0.18}_{-0.18}$
goods-s-mediumjwst	204095	3.549	8.2 $^{+0.08}_{-0.08}$	-1.36 $^{+0.08}_{-0.08}$	9.33 $^{+0.16}_{-0.22}$	0.88 $^{+0.11}_{-0.14}$	3.09 $^{+0.16}_{-0.22}$	0.64 $^{+0.11}_{-0.14}$
goods-s-mediumjwst	204193	2.8424	8.25 $^{+0.08}_{-0.09}$	-1.5 $^{+0.1}_{-0.13}$	9.46 $^{+0.14}_{-0.3}$	0.91 $^{+0.11}_{-0.18}$	2.48 $^{+0.14}_{-0.3}$	-0.07 $^{+0.11}_{-0.18}$
goods-s-mediumjwst	204833	4.7865	8.11 $^{+0.1}_{-0.12}$	-1.19 $^{+0.07}_{-0.09}$	8.65 $^{+0.07}_{-0.05}$	0.94 $^{+0.03}_{-0.05}$	3.22 $^{+0.07}_{-0.05}$	1.5 $^{+0.03}_{-0.05}$
goods-s-mediumjwst	205802	4.3576	8.15 $^{+0.12}_{-0.16}$	< -0.97	9.5 $^{+0.12}_{-0.18}$	0.3 $^{+0.16}_{-0.33}$	2.62 $^{+0.12}_{-0.18}$	-0.59 $^{+0.16}_{-0.33}$
goods-s-mediumjwst	207382	6.7743	7.9 $^{+0.12}_{-0.13}$	< -0.68	8.45 $^{+0.11}_{-0.21}$	1.14 $^{+0.07}_{-0.06}$	2.12 $^{+0.11}_{-0.21}$	0.82 $^{+0.07}_{-0.06}$
goods-s-mediumjwst	207963	2.8463	8.24 $^{+0.08}_{-0.1}$	-1.27 $^{+0.1}_{-0.14}$	9.24 $^{+0.17}_{-0.16}$	0.44 $^{+0.18}_{-0.2}$	2.45 $^{+0.17}_{-0.16}$	-0.35 $^{+0.18}_{-0.2}$
goods-s-mediumjwst	208300	4.4114	8.21 $^{+0.1}_{-0.14}$	< -1.23	9.81 $^{+0.16}_{-0.24}$	0.46 $^{+0.61}_{-0.92}$	2.8 $^{+0.1}_{-0.24}$	-0.55 $^{+0.61}_{-0.92}$
goods-s-mediumjwst	209136	1.7552	8.35 $^{+0.07}_{-0.09}$	< -1.44	9.28 $^{+0.11}_{-0.22}$	0.31 $^{+0.19}_{-0.28}$	2.24 $^{+0.11}_{-0.22}$	-0.73 $^{+0.19}_{-0.28}$
goods-s-mediumjwst	209839	4.4681	7.85 $^{+0.2}_{-0.17}$	-0.81 $^{+0.12}_{-0.17}$	8.68 $^{+0.09}_{-0.05}$	0.8 $^{+0.04}_{-0.06}$	3.79 $^{+0.09}_{-0.05}$	1.92 $^{+0.04}_{-0.06}$
goods-s-mediumjwst	210231	2.6914	8.15 $^{+0.09}_{-0.11}$	-1.14 $^{+0.07}_{-0.09}$	9.28 $^{+0.07}_{-0.17}$	0.37 $^{+0.2}_{-0.13}$	2.54 $^{+0.07}_{-0.17}$	-0.37 $^{+0.2}_{-0.13}$
goods-s-mediumjwst	210262	2.8201	8.26 $^{+0.08}_{-0.09}$	-1.21 $^{+0.05}_{-0.06}$	9.64 $^{+0.09}_{-0.14}$	0.23 $^{+0.4}_{-0.49}$	3.38 $^{+0.09}_{-0.14}$	-0.03 $^{+0.4}_{-0.49}$
goods-s-mediumjwst	210343	2.8105	8.19 $^{+0.08}_{-0.09}$	-1.5 $^{+0.08}_{-0.08}$	8.89 $^{+0.04}_{-0.38}$	0.52 $^{+0.29}_{-0.11}$	2.66 $^{+0.04}_{-0.38}$	0.29 $^{+0.29}_{-0.39}$
goods-s-mediumjwst	210656	1.5706	8.49 $^{+0.05}_{-0.06}$	-1.06 $^{+0.05}_{-0.05}$	10.08 $^{+0.06}_{-0.08}$	0.9 $^{+0.11}_{-0.16}$	3.74 $^{+0.06}_{-0.08}$	0.56 $^{+0.11}_{-0.16}$
goods-s-mediumjwst	210751	3.4226	8.32 $^{+0.08}_{-0.09}$	-1.24 $^{+0.07}_{-0.09}$	9.8 $^{+0.06}_{-0.1}$	0.64 $^{+0.15}_{-0.17}$	3.41 $^{+0.06}_{-0.1}$	0.25 $^{+0.16}_{-0.17}$
goods-s-mediumjwst	213043	3.0328	8.18 $^{+0.09}_{-0.11}$	-1.22 $^{+0.05}_{-0.06}$	8.4 $^{+0.39}_{-0.11}$	0.93 $^{+0.02}_{-0.02}$	2.12 $^{+0.39}_{-0.11}$	0.65 $^{+0.02}_{-0.16}$
goods-s-mediumjwst	214331	2.4516	8.15 $^{+0.1}_{-0.12}$	< -1.46	9.16 $^{+0.1}_{-0.26}$	0.25 $^{+0.18}_{-0.18}$	2.6 $^{+0.1}_{-0.26}$	-0.31 $^{+0.18}_{-0.18}$
goods-s-mediumjwst	214697	1.8651	8.13 $^{+0.11}_{-0.13}$	< -1.15	8.48 $^{+0.32}_{-0.11}$	0.41 $^{+0.14}_{-0.26}$	2.23 $^{+0.32}_{-0.11}$	0.16 $^{+0.14}_{-0.26}$
goods-s-mediumjwst	214859	1.6133	8.37 $^{+0.06}_{-0.07}$	-1.72 $^{+0.08}_{-0.1}$	9.69 $^{+0.14}_{-0.1}$	1.11 $^{+0.17}_{-0.14}$	2.08 $^{+0.14}_{-0.1}$	-0.51 $^{+0.17}_{-0.14}$
goods-s-mediumjwst	214872	1.5512	8.5 $^{+0.05}_{-0.06}$	-1.38 $^{+0.12}_{-0.17}$	9.47 $^{+0.16}_{-0.23}$	0.51 $^{+0.24}_{-0.26}$	1.93 $^{+0.16}_{-0.23}$	-1.03 $^{+0.24}_{-0.26}$
goods-s-mediumjwst	215721	1.6139	8.36 $^{+0.06}_{-0.07}$	-1.57 $^{+0.08}_{-0.11}$	9.48 $^{+0.08}_{-0.13}$	0.29 $^{+0.26}_{-0.29}$	4.11 $^{+0.08}_{-0.29}$	0.92 $^{+0.26}_{-0.29}$
goods-s-mediumjwst	216808	3.6038	8.37 $^{+0.06}_{-0.07}$	-1.08 $^{+0.02}_{-0.02}$	9.76 $^{+0.18}_{-0.09}$	1.57 $^{+0.16}_{-0.07}$	3.74 $^{+0.14}_{-0.09}$	1.55 $^{+0.16}_{-0.07}$
goods-s-mediumjwst	217250	1.7619	8.24 $^{+0.09}_{-0.11}$	< -1.03	9.0 $^{+0.13}_{-0.14}$	0.18 $^{+0.26}_{-0.21}$	2.35 $^{+0.13}_{-0.14}$	-0.46 $^{+0.26}_{-0.21}$
goods-s-mediumjwst	218477	1.5983	8.2 $^{+0.1}_{-0.13}$	< -1.07	8.74 $^{+0.19}_{-0.26}$	0.02 $^{+0.22}_{-0.22}$	2.51 $^{+0.19}_{-0.26}$	-0.21 $^{+0.22}_{-0.22}$
goods-s-mediumjwst	225123	1.5766	8.25 $^{+0.11}_{-0.15}$	< -1.09	8.19 $^{+0.18}_{-0.19}$	-0.05 $^{+0.14}_{-0.1}$	1.98 $^{+0.18}_{-0.19}$	-0.26 $^{+0.14}_{-0.1}$
goods-s-mediumjwst	225678	1.7126	8.19 $^{+0.11}_{-0.13}$	< -1.03	8.48 $^{+0.09}_{-0.09}$	-0.49 $^{+0.22}_{-0.22}$	2.26 $^{+0.09}_{-0.09}$	-0.71 $^{+0.22}_{-0.11}$
goods-s-mediumjwst	227211	3.6742	8.23 $^{+0.08}_{-0.13}$	-1.37 $^{+0.1}_{-0.13}$	9.32 $^{+0.11}_{-0.11}$	1.16 $^{+0.13}_{-0.11}$	2.9 $^{+0.11}_{-0.12}$	0.74 $^{+0.13}_{-0.12}$
goods-s-mediumjwst	227330	2.0838	8.27 $^{+0.08}_{-0.09}$	-1.1 $^{+0.03}_{-0.03}$	9.6 $^{+0.09}_{-0.1}$	0.32 $^{+0.21}_{-0.21}$	3.51 $^{+0.09}_{-0.1}$	0.23 $^{+0.12}_{-0.21}$
goods-s-mediumjwst	279582	3.0018	8.02 $^{+0.1}_{-0.12}$	< -1.37	8.15 $^{+0.27}_{-0.24}$	0.22 $^{+0.06}_{-0.05}$	1.73 $^{+0.27}_{-0.24}$	-0.2 $^{+0.06}_{-0.05}$
goods-s-mediumjwst	282381	2.1072	7.74 $^{+0.14}_{-0.13}$	-0.95 $^{+0.11}_{-0.16}$	8.7 $^{+0.15}_{-0.25}$	0.46 $^{+0.09}_{-0.09}$	2.54 $^{+0.15}_{-0.25}$	0.3 $^{+0.09}_{-0.09}$
goods-s-mediumjwst	283734	4.1393	8.24 $^{+0.1}_{-0.12}$	< -1.21	8.39 $^{+0.41}_{-0.34}$	0.33 $^{+0.13}_{-0.03}$	1.86 $^{+0.41}_{-0.34}$	-0.2 $^{+0.13}_{-0.03}$

Table C.1. (continued)

Tier	ID	z_{spec}	12+log(O/H)	log(N/O)	log(M_*/M_{\odot})	SFR	Σ_{M_*}	Σ_{SFR}
goods-s-mediumjwst	10006044	1.9243	$8.39^{+0.08}_{-0.12}$	< -1.04	$8.94^{+0.1}_{-0.21}$	$-0.28^{+0.24}_{-0.47}$	$2.69^{+0.1}_{-0.21}$	$-0.53^{+0.24}_{-0.47}$
goods-s-mediumjwst	10006739	2.5868	$8.45^{+0.07}_{-0.08}$	$-1.14^{+0.06}_{-0.07}$	$9.65^{+0.16}_{-0.22}$	$1.05^{+0.11}_{-0.19}$	$2.67^{+0.16}_{-0.22}$	$0.08^{+0.11}_{-0.19}$
goods-s-mediumjwst	10007235	2.3951	$7.9^{+0.13}_{-0.14}$	< -1.27	$8.78^{+0.04}_{-0.14}$	$0.21^{+0.06}_{-0.13}$	$2.66^{+0.04}_{-0.14}$	$0.09^{+0.06}_{-0.13}$
goods-s-mediumjwst	10008989	2.394	$8.1^{+0.12}_{-0.15}$	< -1.14	$9.18^{+0.12}_{-0.17}$	$0.43^{+0.21}_{-0.19}$	$2.11^{+0.12}_{-0.17}$	$-0.64^{+0.21}_{-0.13}$
goods-s-mediumjwst	10009336	3.4689	$7.97^{+0.16}_{-0.17}$	< -0.88	$8.74^{+0.07}_{-0.14}$	$0.67^{+0.08}_{-0.44}$	$2.69^{+0.07}_{-0.14}$	$0.62^{+0.08}_{-0.44}$
goods-s-mediumjwst	10009453	3.705	$7.73^{+0.14}_{-0.14}$	$-0.8^{+0.08}_{-0.09}$	$8.3^{+0.04}_{-0.03}$	$0.69^{+0.05}_{-0.02}$	$2.96^{+0.04}_{-0.03}$	$1.35^{+0.05}_{-0.02}$
goods-s-mediumjwst	10009642	4.8382	$8.17^{+0.11}_{-0.11}$	$-1.0^{+0.06}_{-0.06}$	$9.4^{+0.13}_{-0.18}$	$1.07^{+0.14}_{-0.13}$	$2.94^{+0.13}_{-0.18}$	$0.61^{+0.14}_{-0.13}$
goods-s-mediumjwst	10011015	2.8491	$8.29^{+0.1}_{-0.14}$	$-1.22^{+0.11}_{-0.16}$	$8.93^{+0.16}_{-0.17}$	$0.56^{+0.08}_{-0.08}$	$1.8^{+0.26}_{-0.17}$	$-0.56^{+0.08}_{-0.08}$
goods-s-mediumjwst	10011809	2.8346	$8.03^{+0.11}_{-0.12}$	< -1.29	$9.11^{+0.13}_{-0.16}$	$0.34^{+0.14}_{-0.14}$	$2.76^{+0.13}_{-0.16}$	$-0.02^{+0.14}_{-0.14}$
goods-s-mediumjwst	10012996	1.9444	$8.31^{+0.19}_{-0.24}$	< -0.95	$9.12^{+0.15}_{-0.47}$	$0.14^{+0.2}_{-0.7}$	$1.8^{+0.15}_{-0.47}$	$-1.18^{+0.2}_{-0.7}$
goods-s-mediumjwst	10013169	5.0362	$8.01^{+0.12}_{-0.15}$	$-0.89^{+0.03}_{-0.03}$	$9.65^{+0.08}_{-0.21}$	$1.18^{+0.12}_{-0.08}$	$3.24^{+0.08}_{-0.21}$	$0.77^{+0.12}_{-0.08}$
goods-s-mediumjwst	10013316	3.7041	$8.17^{+0.12}_{-0.15}$	< -1.1	$9.48^{+0.14}_{-0.18}$	$0.48^{+0.25}_{-0.33}$	$3.2^{+0.14}_{-0.18}$	$0.2^{+0.25}_{-0.33}$
goods-s-mediumjwst	10013534	5.3772	$7.71^{+0.19}_{-0.16}$	< -0.69	$9.13^{+0.09}_{-0.18}$	$-0.52^{+0.55}_{-1.0}$	$3.38^{+0.09}_{-0.18}$	$-0.27^{+0.55}_{-1.0}$
goods-s-mediumjwst	10013560	3.9382	$8.07^{+0.13}_{-0.15}$	< -1.03	$8.99^{+0.06}_{-0.1}$	$-0.27^{+0.2}_{-0.18}$	$2.66^{+0.06}_{-0.1}$	$-0.6^{+0.2}_{-0.18}$
goods-s-mediumjwst	10021735	2.5384	$8.12^{+0.1}_{-0.11}$	< -1.31	$8.61^{+0.05}_{-0.06}$	$0.83^{+0.09}_{-0.09}$	$0.6^{+0.05}_{-0.06}$	$-1.18^{+0.09}_{-0.09}$
goods-s-mediumjwst	10024789	2.524	$8.22^{+0.09}_{-0.12}$	$-1.14^{+0.08}_{-0.1}$	$9.44^{+0.08}_{-0.11}$	$-0.09^{+0.3}_{-0.52}$	$3.05^{+0.08}_{-0.11}$	$-0.47^{+0.3}_{-0.52}$
goods-s-mediumjwst	10027810	3.4786	$8.48^{+0.05}_{-0.07}$	$-1.32^{+0.07}_{-0.08}$	$7.73^{+0.05}_{-0.07}$	$-1.4^{+0.18}_{-0.12}$	$0.15^{+0.05}_{-0.07}$	$-2.97^{+0.18}_{-0.12}$
goods-s-mediumjwst	10030190	2.0194	$7.72^{+0.16}_{-0.14}$	< -0.85	$7.96^{+0.08}_{-0.12}$	$-0.35^{+0.12}_{-0.12}$	$2.43^{+0.08}_{-0.12}$	$0.13^{+0.12}_{-0.12}$
goods-s-mediumjwst	20201124	5.8213	$8.3^{+0.08}_{-0.09}$	$-1.15^{+0.07}_{-0.08}$	$9.54^{+0.12}_{-0.05}$	$1.45^{+0.05}_{-0.12}$	$3.52^{+0.12}_{-0.05}$	$1.44^{+0.05}_{-0.12}$
goods-s-mediumjwst	40000170	5.7771	$7.73^{+0.12}_{-0.12}$	< -0.8	$8.32^{+0.0}_{-0.07}$	$0.43^{+0.06}_{-0.01}$	$3.09^{+0.0}_{-0.07}$	$1.2^{+0.06}_{-0.01}$
goods-s-mediumjwst	60141305	1.7556	$8.1^{+0.14}_{-0.16}$	< -0.9	$8.47^{+0.22}_{-0.1}$	$-0.37^{+0.15}_{-0.2}$	$1.88^{+0.22}_{-0.1}$	$-0.95^{+0.15}_{-0.2}$
goods-s-mediumjwst	60146727	2.9249	$8.26^{+0.11}_{-0.16}$	< -1.05	$9.19^{+0.05}_{-0.1}$	$0.09^{+0.23}_{-0.15}$	$3.18^{+0.05}_{-0.1}$	$0.08^{+0.23}_{-0.15}$
goods-s-mediumjwst	60148140	3.9156	$8.24^{+0.08}_{-0.1}$	$-1.1^{+0.02}_{-0.02}$	$9.45^{+0.32}_{-0.3}$	$1.22^{+0.08}_{-0.26}$	$4.11^{+0.32}_{-0.3}$	$1.87^{+0.08}_{-0.26}$
goods-s-mediumjwst	60151588	2.3363	$8.1^{+0.11}_{-0.14}$	< -1.38	$8.8^{+0.09}_{-0.12}$	$0.38^{+0.1}_{-0.11}$	$2.85^{+0.09}_{-0.12}$	$0.43^{+0.1}_{-0.11}$
goods-s-mediumjwst	60309096	1.8989	$7.86^{+0.17}_{-0.17}$	< -0.86	$8.33^{+0.04}_{-0.93}$	$-0.09^{+0.12}_{-0.1}$	$1.94^{+0.93}_{-0.93}$	$-0.47^{+0.12}_{-0.1}$
goods-s-mediumjwst	60310158	2.1547	$8.54^{+0.05}_{-0.06}$	$-1.0^{+0.03}_{-0.03}$	$9.62^{+0.09}_{-0.09}$	$2.16^{+0.13}_{-0.33}$	$2.37^{+0.09}_{-0.09}$	$0.91^{+0.13}_{-0.32}$
goods-s-mediumjwst	60311826	2.7839	$8.11^{+0.11}_{-0.14}$	< -1.06	$9.01^{+0.16}_{-0.21}$	$0.45^{+0.22}_{-0.29}$	$2.35^{+0.16}_{-0.21}$	$-0.21^{+0.22}_{-0.29}$
goods-s-mediumjwst	60312119	1.7178	$8.26^{+0.08}_{-0.1}$	< -1.34	$8.8^{+0.1}_{-0.11}$	$0.16^{+0.14}_{-0.11}$	$2.65^{+0.1}_{-0.11}$	$0.0^{+0.14}_{-0.11}$

Table C.2. Strong-line oxygen and nitrogen abundances for the 95 galaxies in our strong-line sample without galaxy properties derived from SED and morphological fitting.

Tier	ID	z_{spec}	12+log(O/H)	log(N/O)
goods-n-mediumhst	910	4.4144	$8.39^{+0.08}_{-0.1}$	< -1.31
goods-n-mediumhst	946	4.6948	$7.64^{+0.16}_{-0.14}$	$-0.99^{+0.12}_{-0.17}$
goods-n-mediumhst	956	5.4225	$7.82^{+0.13}_{-0.13}$	< -1.15
goods-n-mediumhst	964	5.5992	$8.1^{+0.13}_{-0.13}$	< -1.01
goods-n-mediumhst	971	4.4221	$8.25^{+0.1}_{-0.13}$	$-1.29^{+0.11}_{-0.16}$
goods-n-mediumhst	1940	3.6602	$8.19^{+0.08}_{-0.1}$	$-1.29^{+0.05}_{-0.06}$
goods-n-mediumhst	2890	3.3335	$8.03^{+0.12}_{-0.13}$	< -0.89
goods-n-mediumhst	22517	2.5343	$8.01^{+0.11}_{-0.12}$	< -1.16
goods-n-mediumhst	23682	3.1255	$8.35^{+0.06}_{-0.08}$	$-1.33^{+0.04}_{-0.05}$
goods-n-mediumhst	23873	2.9412	$7.68^{+0.18}_{-0.15}$	$-0.93^{+0.1}_{-0.13}$
goods-n-mediumhst	23874	2.2721	$8.2^{+0.12}_{-0.12}$	$-1.32^{+0.08}_{-0.1}$
goods-n-mediumhst	24006	5.4467	$8.32^{+0.08}_{-0.11}$	$-1.01^{+0.05}_{-0.06}$
goods-n-mediumhst	24722	1.6308	$8.23^{+0.09}_{-0.12}$	$-1.36^{+0.1}_{-0.14}$
goods-n-mediumhst	25528	2.0388	$8.57^{+0.05}_{-0.05}$	$-0.95^{+0.06}_{-0.07}$
goods-n-mediumhst	26113	3.2263	$8.25^{+0.08}_{-0.09}$	$-1.27^{+0.04}_{-0.05}$
goods-n-mediumhst	27665	2.9272	$8.23^{+0.11}_{-0.14}$	< -1.17
goods-n-mediumhst	28271	2.093	$8.26^{+0.08}_{-0.09}$	$-1.23^{+0.03}_{-0.03}$
goods-n-mediumhst	29815	2.048	$8.13^{+0.09}_{-0.09}$	< -1.44
goods-n-mediumhst	31166	2.0481	$8.44^{+0.07}_{-0.08}$	$-1.23^{+0.08}_{-0.1}$
goods-n-mediumhst	31483	2.3067	$8.36^{+0.07}_{-0.09}$	$-1.04^{+0.07}_{-0.08}$
goods-n-mediumhst	31774	1.8687	$8.7^{+0.03}_{-0.03}$	$-0.77^{+0.05}_{-0.05}$
goods-n-mediumhst	32944	4.2812	$8.45^{+0.06}_{-0.07}$	$-1.05^{+0.07}_{-0.08}$
goods-n-mediumhst	33432	2.5917	$8.27^{+0.08}_{-0.11}$	$-1.25^{+0.09}_{-0.11}$
goods-n-mediumhst	33436	2.012	$8.35^{+0.07}_{-0.08}$	$-1.39^{+0.09}_{-0.12}$
goods-n-mediumhst	33991	1.7355	$8.65^{+0.04}_{-0.04}$	$-0.9^{+0.06}_{-0.07}$
goods-n-mediumhst	34067	1.7375	$8.37^{+0.08}_{-0.08}$	$-1.26^{+0.11}_{-0.15}$
goods-n-mediumhst	34155	1.7395	$8.31^{+0.08}_{-0.11}$	< -1.37
goods-n-mediumhst	34643	2.0492	$8.32^{+0.07}_{-0.08}$	< -1.46
goods-n-mediumhst	34958	2.3184	$8.38^{+0.06}_{-0.07}$	$-1.05^{+0.02}_{-0.02}$
goods-n-mediumhst	38428	6.7102	$8.13^{+0.12}_{-0.14}$	< -0.99
goods-n-mediumhst	38648	5.2654	$7.64^{+0.25}_{-0.23}$	< -0.99
goods-n-mediumhst	45651	2.2211	$8.37^{+0.07}_{-0.08}$	$-1.19^{+0.05}_{-0.06}$
goods-n-mediumjwst	16125	3.364	$8.3^{+0.09}_{-0.12}$	< -1.18
goods-n-mediumjwst	24438	2.4433	$8.52^{+0.05}_{-0.05}$	$-1.3^{+0.04}_{-0.04}$
goods-n-mediumjwst	25356	4.4096	$8.39^{+0.08}_{-0.1}$	< -1.06
goods-n-mediumjwst	26276	2.9751	$8.55^{+0.05}_{-0.05}$	$-0.69^{+0.04}_{-0.04}$
goods-n-mediumjwst	57605	2.5754	$8.51^{+0.07}_{-0.1}$	< -0.72
goods-n-mediumjwst	70173	2.9956	$8.18^{+0.08}_{-0.1}$	$-1.3^{+0.07}_{-0.08}$
goods-n-mediumjwst	82830	5.7969	$7.76^{+0.18}_{-0.16}$	< -0.49
goods-n-mediumjwst	10003617	2.9802	$7.72^{+0.14}_{-0.13}$	< -0.93
goods-s-deephst	17670	2.3427	$8.2^{+0.09}_{-0.1}$	< -1.3
goods-s-deephst	17824	2.6929	$8.03^{+0.11}_{-0.13}$	< -1.28
goods-s-deephst	10008071	2.227	$8.39^{+0.06}_{-0.06}$	$-1.29^{+0.02}_{-0.03}$
goods-s-deephst	10013545	4.035	$8.1^{+0.1}_{-0.11}$	< -1.54
goods-s-deephst	10016186	3.9279	$8.21^{+0.09}_{-0.12}$	< -1.3
goods-s-deephst	10016374	5.5029	$7.72^{+0.15}_{-0.14}$	< -0.72
goods-s-mediumhst	6227	2.6126	$8.46^{+0.05}_{-0.06}$	$-1.13^{+0.03}_{-0.04}$
goods-s-mediumhst	9335	3.7258	$8.03^{+0.16}_{-0.18}$	$-1.1^{+0.09}_{-0.11}$
goods-s-mediumhst	9669	4.0238	$8.09^{+0.11}_{-0.11}$	< -1.09
goods-s-mediumhst	9785	3.5481	$8.18^{+0.09}_{-0.11}$	$-1.25^{+0.08}_{-0.09}$
goods-s-mediumhst	9891	4.7727	$7.94^{+0.11}_{-0.12}$	< -1.04
goods-s-mediumhst	11491	3.7787	$8.73^{+0.03}_{-0.04}$	$-0.28^{+0.09}_{-0.11}$

Table C.2. (continued)

Tier	ID	z_{spec}	12+log(O/H)	log(N/O)
goods-s-mediumhst	11929	2.996	$8.36^{+0.06}_{-0.08}$	$-1.13^{+0.03}_{-0.03}$
goods-s-mediumhst	12102	3.4968	$7.98^{+0.12}_{-0.14}$	< -0.87
goods-s-mediumhst	13369	3.4119	$8.25^{+0.08}_{-0.09}$	$-1.03^{+0.03}_{-0.03}$
goods-s-mediumhst	13596	3.7314	$8.0^{+0.12}_{-0.13}$	$-1.2^{+0.08}_{-0.11}$
goods-s-mediumhst	13620	5.9173	$8.26^{+0.09}_{-0.10}$	< -1.07
goods-s-mediumhst	13638	5.8246	$8.21^{+0.12}_{-0.16}$	< -1.06
goods-s-mediumhst	13972	3.5998	$8.17^{+0.15}_{-0.2}$	< -0.92
goods-s-mediumhst	14133	5.9801	$7.63^{+0.22}_{-0.18}$	< -0.46
goods-s-mediumhst	15168	4.0453	$8.18^{+0.09}_{-0.1}$	$-1.42^{+0.09}_{-0.11}$
goods-s-mediumhst	15210	5.757	$8.19^{+0.1}_{-0.12}$	< -1.29
goods-s-mediumhst	15265	6.2594	$7.74^{+0.15}_{-0.12}$	< -0.56
goods-s-mediumhst	15270	4.0526	$8.2^{+0.08}_{-0.1}$	$-1.3^{+0.05}_{-0.06}$
goods-s-mediumhst	15353	4.7061	$8.57^{+0.29}_{-0.28}$	$-1.37^{+0.11}_{-0.14}$
goods-s-mediumhst	16375	4.4362	$8.35^{+0.07}_{-0.08}$	$-1.05^{+0.03}_{-0.03}$
goods-s-mediumhst	16385	4.0177	$8.37^{+0.07}_{-0.09}$	$-1.09^{+0.04}_{-0.05}$
goods-s-mediumhst	16402	4.7048	$8.27^{+0.07}_{-0.08}$	$-1.39^{+0.08}_{-0.11}$
goods-s-mediumhst	16431	5.9175	$7.68^{+0.13}_{-0.12}$	< -0.72
goods-s-mediumhst	17057	4.0171	$8.24^{+0.08}_{-0.09}$	$-1.57^{+0.11}_{-0.16}$
goods-s-mediumhst	17159	4.8534	$8.2^{+0.1}_{-0.11}$	$-0.85^{+0.03}_{-0.04}$
goods-s-mediumhst	17349	3.4914	$7.62^{+0.14}_{-0.12}$	$-0.87^{+0.12}_{-0.12}$
goods-s-mediumhst	17376	4.8678	$8.02^{+0.14}_{-0.16}$	$-0.94^{+0.16}_{-0.17}$
goods-s-mediumhst	17408	4.3653	$8.17^{+0.1}_{-0.11}$	< -1.12
goods-s-mediumhst	17509	6.8449	$7.87^{+0.13}_{-0.14}$	< -0.61
goods-s-mediumhst	35570	3.0632	$8.27^{+0.07}_{-0.08}$	$-1.39^{+0.04}_{-0.05}$
goods-s-mediumhst	42055	3.0864	$8.06^{+0.1}_{-0.12}$	$-1.29^{+0.06}_{-0.07}$
goods-s-mediumhst	43623	2.8526	$8.57^{+0.05}_{-0.06}$	< -1.14
goods-s-mediumhst	45788	2.3681	$8.21^{+0.1}_{-0.12}$	< -1.03
goods-s-mediumhst	47038	2.5631	$8.33^{+0.11}_{-0.14}$	< -1.0
goods-s-mediumhst	48826	1.7599	$8.52^{+0.04}_{-0.05}$	$-1.07^{+0.03}_{-0.04}$
goods-s-mediumhst	58656	4.7797	$7.96^{+0.11}_{-0.13}$	$-0.97^{+0.08}_{-0.1}$
goods-s-mediumhst	58658	5.3817	$7.97^{+0.12}_{-0.13}$	< -0.99
goods-s-mediumhst	58711	4.312	$8.03^{+0.14}_{-0.16}$	< -0.88
goods-s-mediumhst	58930	6.6281	$7.97^{+0.12}_{-0.14}$	< -0.8
goods-s-mediumjwst	51204	3.4718	$7.94^{+0.12}_{-0.13}$	$-1.09^{+0.13}_{-0.19}$
goods-s-mediumjwst	203195	1.7661	$8.39^{+0.06}_{-0.07}$	$-1.34^{+0.06}_{-0.07}$
goods-s-mediumjwst	257044	2.6647	$7.9^{+0.21}_{-0.21}$	< -0.89
goods-s-mediumjwst	10007081	2.689	$8.56^{+0.04}_{-0.05}$	$-1.12^{+0.04}_{-0.04}$
goods-s-mediumjwst	10007444	1.9054	$8.49^{+0.05}_{-0.06}$	$-1.39^{+0.04}_{-0.05}$
goods-s-mediumjwst	10012102	3.4971	$8.06^{+0.11}_{-0.13}$	< -1.06
goods-s-mediumjwst	10021915	1.7747	$8.32^{+0.08}_{-0.1}$	< -1.2
goods-s-mediumjwst	10042485	2.2108	$8.36^{+0.07}_{-0.08}$	$-1.4^{+0.1}_{-0.14}$
goods-s-mediumjwst	10057885	3.5544	$8.04^{+0.12}_{-0.15}$	< -1.09
goods-s-mediumjwst	10104771	3.0742	$7.73^{+0.22}_{-0.17}$	< -0.56

This paper has been typeset from a TeX/LaTeX file prepared by the author.